Journal of Medicinal Chemistry

pubs.acs.org/jmc

Article

Deciphering the Therapeutic Potential of Novel Pentyloxyamide-Based Class I, IIb HDAC Inhibitors against Therapy-Resistant Leukemia

Fabian Fischer,[○] Julian Schliehe-Diecks,[○] Jia-Wey Tu, Tanja Gangnus, Yu Lin Ho, Mara Hebeis, Leandro A. Alves Avelar, Katerina Scharov, Titus Watrin, Marie Kemkes, Pawel Stachura, Katharina Daugs, Lukas Biermann, Josefa Kremeyer, Nadine Horstick, Ingrid Span, Aleksandra A. Pandyra, Arndt Borkhardt, Holger Gohlke, Matthias U. Kassack, Bjoern B. Burckhardt, Sanil Bhatia,* and Thomas Kurz*

Cite This: *J. Med. Chem.* 2024, 67, 21223−21250

Read Online

ACCESS | Metrics & More | Article Recommendations | Supporting Information

ABSTRACT: Histone deacetylase inhibitors (HDACi) are established anticancer drugs, especially in hematological cancers. This study aimed to design, synthesize, and evaluate a set of HDACi featuring a pentyloxyamide connecting unit linker region and substituted phenylthiazole cap groups. A structural optimization program yielded HDACi with nanomolar inhibitory activity against histone deacetylase class I/IIb enzymes. The novel inhibitors (**4d** and **4m**) showed superior antileukemic activity compared to several approved HDACi. Furthermore, **4d** and **4m** displayed synergistic activity when combined with chemotherapeutics, decitabine, and clofarabine. In vitro pharmacokinetic studies showed the most promising profile for **4d** with intermediate microsomal stability, excellent plasma stability, and concentration-independent plasma protein binding. Additionally, **4d** demonstrated comparable in vivo pharmacokinetics to vorinostat. When administered in vivo, **4d** effectively inhibited the proliferation of leukemia cells without causing toxicity. Furthermore, the binding modes of **4d** and **4m** to the catalytic domain 2 of HDAC6 from *Danio rerio* were determined by X-ray crystallography.

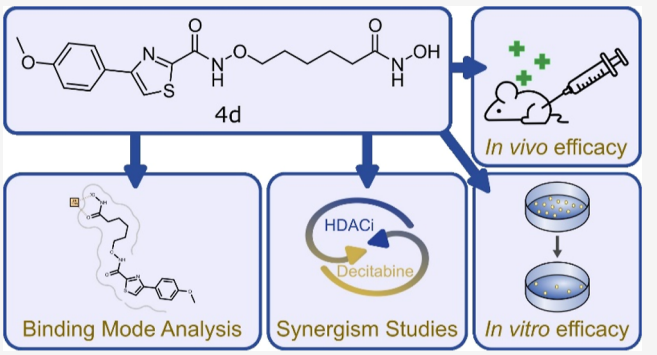

1. INTRODUCTION

Leukemia is characterized by genetic and epigenetic heterogeneity due to the presence of diverse molecular alterations, contributing to the formation of distinct subgroups and influencing the prognosis and therapeutic outcome of patients.[1−3] Leukemia is the most common cancer in children, with a 5 year-overall survival rate exceeding 85%.[4] However, approximately 20−25% of childhood leukemia patients experience relapsed or refractory leukemia; among those cases only around 15−50% of patients are able to achieve remission.[5] Another ongoing challenge in leukemia treatment is the therapy-related toxicity of routinely used drugs,[6,7] along with certain leukemia subtypes that continue to be linked to unfavorable outcomes.[8] In order to prevent long-term therapy-related health damage and to successfully treat therapy-refractory subtypes, new antileukemic drugs are urgently needed.

A possible target for new therapies is the characteristic perturbations of cancer cells in their epigenetic regulation.[9] Epigenetic dysregulation is common for all kinds of human cancer irrespective of solid tumors or hematological malignancies.[10] It has been argued that epigenetic disruption is the causative mechanism behind all hallmarks of cancer steering proliferation, growth suppressor evasion, or apoptosis of cancer cells.[11] Previous studies revealed that hematological malignant cells are especially sensitive to treatment with HDAC inhibitors (HDACi),[12] although the exact mechanism behind this observation remains elusive as it is not allocated to a single cause.[13] Today, all approved HDACi are approved for the therapy of hematological malignancies.[14] The epigenetic regulation of transcription is significantly governed by the acetylation status of histones.[15] This status is tightly regulated by the interplay of two families of enzymes that control the acetylation or deacetylation of ε-amino-groups of

Received: August 24, 2024
Revised: October 23, 2024
Accepted: October 30, 2024
Published: November 27, 2024

https://doi.org/10.1021/acs.jmedchem.4c02024
J. Med. Chem. 2024, 67, 21223−21250

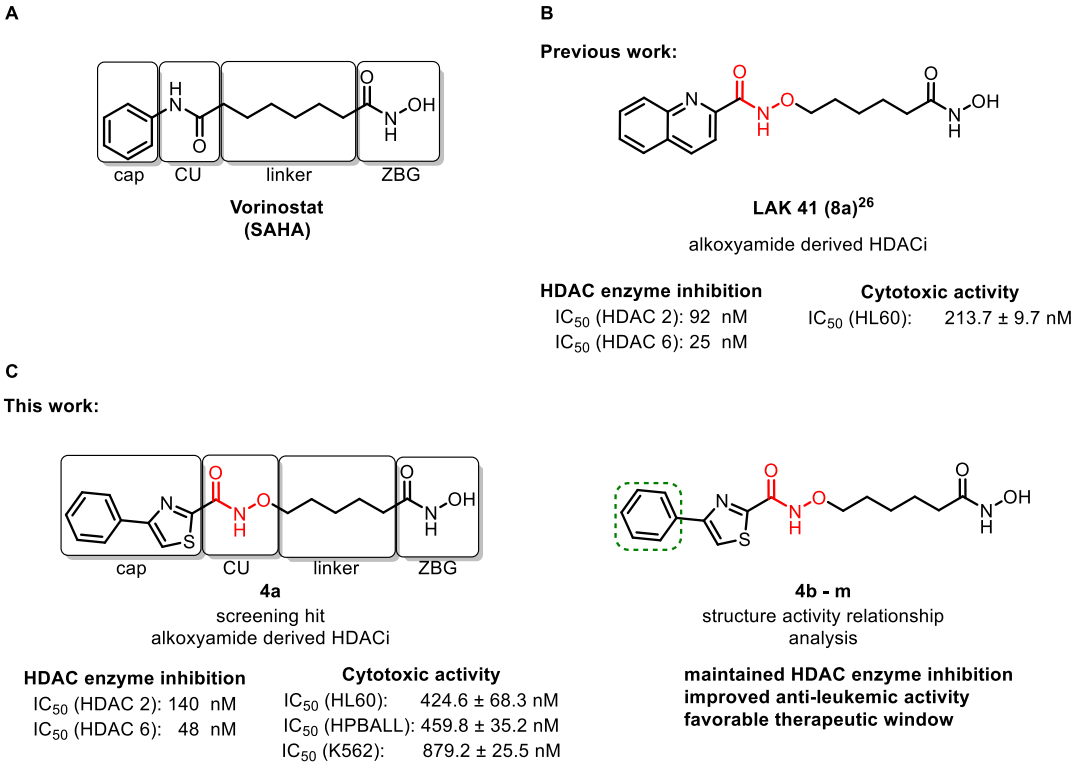

Figure 1. Development of novel pentyloxyamide-based HDACi (A) pharmacophore model of HDAC-inhibitors exemplified on vorinostat. CU = connecting unit and ZBG = zinc-binding-group. (B) Previously published pentyloxyamide-derived HDAC inhibitor.[26] (C) Initial screening hit **4a** showed nanomolar HDAC-isoenzyme inhibition and high nanomolar cytotoxic activity on three different leukemic cell lines. Derivatisation of the terminal phenyl moiety improved the antileukemic activity while retaining HDAC isoenzyme inhibition.

lysine residues: histone acetyltransferases acetylate the ε-amino group of lysine residues while HDAC remove acetyl groups from lysines.[16] HDAC enzymes are classified into four classes related to their homology toward yeast deacetylases.[17] Three of the four classes, namely class I, II, and IV HDAC enzymes, are zinc-dependent metalloenzymes. Class I consists of HDAC enzymes 1, 2, 3, and 8. Especially the nucleic HDAC enzymes 1, 2, and 3 are directly involved in the regulation of the acetylation status of histones.[18] Class IIb HDACs are formed by the cytosolic enzymes HDAC6 and 10. Substrates of HDAC6 are, among others, proteins that are found to be dysregulated in cancer like HSP90[19] or Ku70.[20]

In addition to their potent antileukemic effects used as mono treatment, HDACi are displaying strong synergistic effects in combination with a broad variety of anticancer drugs.[21] For instance, HDACi act synergistically with alkylating[22,23] and hypomethylating agents,[24] proteasome inhibitors,[25−27] and immunomodulating drugs.[28,29] In light of the promising results seen in preclinical studies, clinical trials are currently underway to investigate the potential of HDACi (vorinostat) in combination with the hypomethylating agent (azacytidine) for the treatment of pediatric or adult acute myeloid leukemia (AML) patients (NCT03843528 and NCT00392353). This provides the rationale for a systematic investigation of HDACi as synergistic combination partners for the therapy of resistant leukemic cells.

Our newly developed HDAC inhibitors, targeting class I and IIb, have demonstrated remarkable efficacy against different types of leukemic cells, including those resistant to standard therapies. Notably, these inhibitors exhibit a higher selectivity toward leukemic cells while minimizing damage to healthy cells, distinguishing them from several approved HDACi. Moreover, our most promising candidates (**4d** and **4m**) have displayed significant synergistic effects when combined with the approved chemotherapeutic agents, decitabine and clofarabine. Promising in vitro pharmacokinetic characteristics and in vivo activity encourage their further investigation.

2. RESULTS AND DISCUSSION

We screened our internal library for novel and easily accessible lead structures against three leukemic cell lines K562—(chronic myeloid leukemia or CML); HL60—(AML or AML); and HPBALL—(T-cell acute lymphoblastic leukemia or T-ALL) and identified HDACi **4a** as a hit compound. Strikingly, **4a** outperformed the approved HDACi, vorinostat, both in terms of the HDAC enzyme inhibitory activity and on cytotoxic activity on various leukemic cell lines. **4a** combines a phenylthiazole cap group that has been successfully deployed in the development of HDACi before[30−33] and an oxyamide group as a bioisosteric replacement for the common amide moiety[26,34] (Figure 1). Currently, the two clinically approved Mitogen-activated protein kinase (MEK) 1/2 inhibitors, binimetinib and selumetinib, are establishing the oxyamide group as a valuable structural motif in the field of anticancer drugs.[35,36] We have shown previously that HDACi with an oxyamide linker region are equally or even more potent than some approved HDACi with an amide connecting unit.[26,34] The oxyamide connecting unit extends the chemical space of amide bioisosters and may contribute to the recently emerging

https://doi.org/10.1021/acs.jmedchem.4c02024
J. Med. Chem. 2024, 67, 21223−21250

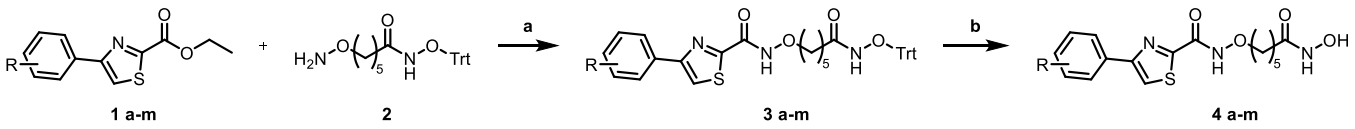

Figure 2. Reagents and conditions: (a) (1) 1M NaOH, THF, RT o.n., (2) HBTU, DIPEA, DMF, RT, o.n., and (b) TFA, Et_3SiH, DCM, RT, 30 min.

Table 1. Inhibition of Human HDAC2, 4, 6, and 8 by Compounds 4a−m and Reference Compounds Vorinostat, Panobinostat, and Tubastatin A

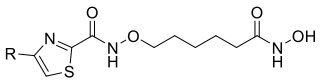

compound	R	IC_{50} (HDAC2) [μM]	IC_{50} (HDAC4) [μM]	IC_{50} (HDAC6) [μM]	IC_{50} (HDAC8) [μM]
4a		0.059 ± 0.012	> 100	0.075 ± 0.03	4.01 ± 0.9
4b		0.046 ± 0.009	> 100	0.026 ± 0.006	2.16 ± 0.3
4c		0.056 ± 0.013	> 100	0.026 ± 0.008	5.20 ± 1.0
4d		0.015 ± 0.004	> 100	0.038 ± 0.01	5.75 ± 0.9
4e		0.065 ± 0.008	> 100	0.051 ± 0.05	1.29 ± 0.3
4f		0.045 ± 0.011	> 100	0.047 ± 0.015	2.32 ± 0.3
4g		0.048 ± 0.012	> 100	0.045 ± 0.012	6.38 ± 1.6
4h		0.047 ± 0.008	> 100	0.081 ± 0.03	2.51 ± 0.3
4i		0.105 ± 0.016	> 100	0.049 ± 0.017	5.41 ± 0.3
4j		0.060 ± 0.03	> 100	0.064 ± 0.03	7.01 ± 1.9
4k		0.065 ± 0.03	> 100	0.108 ± 0.004	4.86 ± 0.5
4l		0.010 ± 0.003	> 100	0.030 ± 0.01	3.68 ± 0.5
4m		0.0045 ± 0.0007	> 100	0.064 ± 0.03	4.80 ± 1.6
Vorinostat	-	0.165 ± 0.006	47.8 ± 6.0	0.047 ± 0.003	5.85 ± 0.7
Panobinostat	-	N.D.	0.725 ± 0.06	N.D.	0.299 ± 0.07
Tubastatin	-	N.D.	N.D.	0.033 ± 0.017	N.D.

[a]All compounds were evaluated in duplicate in two independent experiments. Values represent the mean ± SEM. N.D. = not determined.

https://doi.org/10.1021/acs.jmedchem.4c02024
J. Med. Chem. 2024, 67, 21223−21250

Table 2. Inhibition of Human HDAC1, 2, 3, 4, 6, 8, and 11 by Compounds 4d and 4m and Reference Compounds Vorinostat, Panobinostat, and Tubastatin A

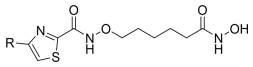

compound	R	IC_{50} (HDAC1) [μM]	IC_{50} (HDAC2) [μM]	IC_{50} (HDAC3) [μM]	IC_{50} (HDAC4) [μM]	IC_{50} (HDAC6) [μM]	IC_{50} (HDAC8) [μM]	IC_{50} (HDAC11) [μM]
4d		0.0045 ± 0.0010	0.015 ± 0.004	0.013 ± 0.002	> 100	0.038 ± 0.012	5.8 ± 0.8	26 ± 4
4m		0.012 ± 0.003	0.0045 ± 0.0007	0.048 ± 0.012	> 100	0.060 ± 0.03	4.8 ± 1.6	36 ± 7
Vorinostat	-	0.082 ± 0.018	0.16 ± 0.01	0.073 ± 0.010	47 ± 6	0.047 ± 0.003	5.9 ± 0.7	> 100
Panobinostat	-	0.0082 ± 0.0015	N.D.	0.014 ± 0.003	0.72 ± 0.06	N.D.	0.30 ± 0.07	2.9 ± 0.2
Tubastatin	-	N.D.	N.D.	N.D.	N.D.	0.033 ± 0.017	N.D.	N.D.

[a]All compounds were evaluated in duplicate in two independent experiments. Values represent the mean ± SEM. N.D. = not determined.

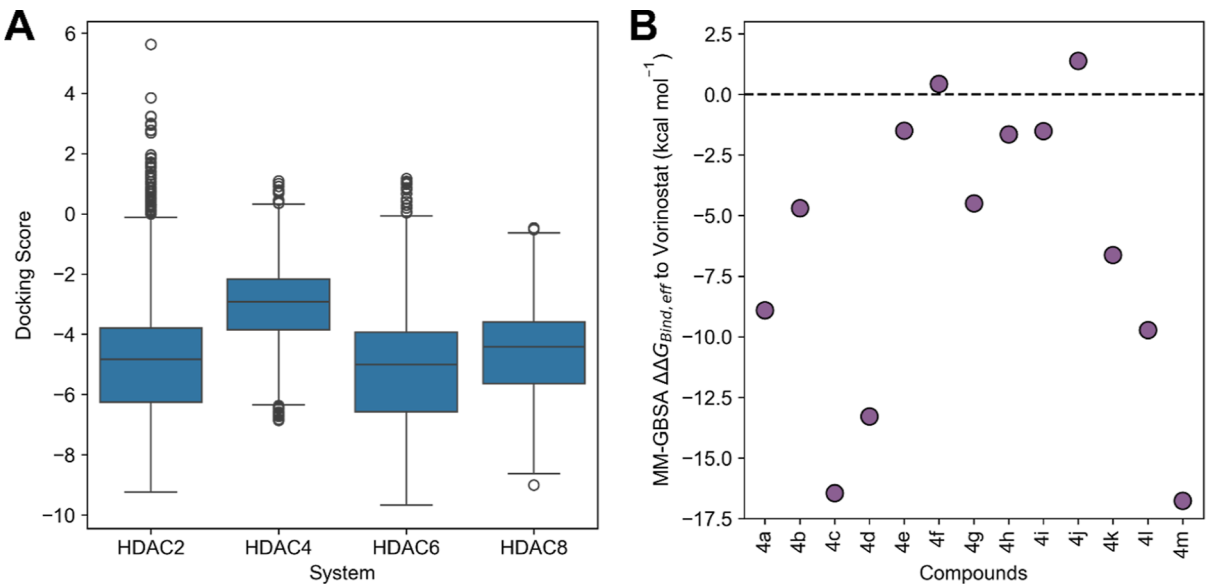

Figure 3. (A) Comparison of the docking results between the isoenzymes HDAC2, 4, 6, and 8 for compounds **4a**−**4m**. The results mirror the enzyme assay data in that the compounds on average show better inhibition of HDAC2, HDAC6, and HDAC8 than HDAC4. (B) MM-GBSA results of the best-docked pose of a compound in HDAC2. In line with the results of the enzyme assay, **4m** is predicted to have the best effective binding energy.

topic of hydroxylamine analogs to established amine moieties.[37,38]

As starting materials for a diverse set of phenylthiazole analogs were readily available, we aimed in this study to further develop **4a** into a new antileukemic lead structure by elucidating the structure−activity relationship of its terminal phenyl moiety.

2.1. Synthesis. The synthesis of the novel HDACi (**4a**−**m**) started with the saponification of phenylthiazole carboxylic esters (**1a**−**m**) followed by HBTU-mediated coupling reactions of the generated corresponding sodium salts with the hydroxylamine linker **2** containing the *O*-trityl-protected hydroxamic acid zinc binding group using a modified protocol of Goodreid et al.[39] (Figure 2). The coupling reactions for the construction of the pentyloxyamide moiety were performed utilizing the in situ generated sodium salts of the respective carboxylic acids as the corresponding acids of **1a**−**m** were prone to decarboxylation. The synthesis of the hydroxylamine linker **2** was previously published by our group.[26] Subsequent TFA and triethylsilane-mediated deprotection of the *O*-trityl-protected hydroxamates yielded the hydroxamic acids **4a**−**m**.

2.2. HDAC Enzyme Inhibition. All synthesized HDACi are nanomolar inhibitors of HDAC2, a representative of HDAC class I, and of HDAC6, a representative of HDAC class IIb. The HDAC enzyme inhibition profile did not differ remarkably among the improved analogs (Table 1). Derivate **4m** was the most potent HDAC2 inhibitor improving the IC_{50} of the parent compound **4a** (IC_{50} 0.140 μM) significantly by a factor of 13 (IC_{50} 0.0045 μM). Also, compounds **4d** (IC_{50} 0.015 μM) and **4l** (IC_{50} 0.010 μM) improved HDAC2 inhibition in comparison to **4a** by a factor of 4 or 6, respectively. Interestingly, HDAC6 inhibition was not improved to the same extent as HDAC2 inhibition. **4c** is the most active HDAC6 inhibitor in this series and exceeded the activity of the parent compound by a factor of about three (IC_{50} 0.026 μM). However, each newly synthesized HDAC inhibitor surpassed vorinostat in regards to HDAC2 inhibition and was similarly potent as tubastatin A in HDAC6 enzyme inhibition.

https://doi.org/10.1021/acs.jmedchem.4c02024
J. Med. Chem. 2024, 67, 21223−21250

Encouraged by the promising results of **4m** and **4d**, these compounds were subjected to an expanded HDAC isozyme analysis (Table 2), which demonstrated nanomolar inhibition of HDAC 1 and 3 but only weak HDAC11 inhibition.

2.3. Docking Studies. Molecular docking was performed to assess the binding affinities of the compounds **4a**−**4m** to human HDAC2, 4, 6, and 8 from a structural perspective. Binding affinities predicted with the Glide SP scoring function of the Schrödinger Suite[40] generally align with the enzyme assay results when considered on a per-isoform basis (Table 1, Figure 3): On average, **4a**−**4m** yield more favorable docking scores in HDAC2, HDAC6, and HDAC8 (−5.1 ± 1.8 kcal mol^{-1}, −5.3 ± 1.5 kcal mol^{-1}, and −4.7 ± 1.2 kcal mol^{-1}, respectively) than in HDAC4 (−3.0 ± 1.4 kcal mol^{-1}). Although predicting binding affinities with scoring functions requires caution when the differences are small,[41] this agreement mirrors that IC_{50} values for HDAC4 are one to two orders of magnitude larger than for the other isoforms. To support the results, Molecular Mechanics - Generalized Born Surface Area (MM-GBSA) computations were used to predict effective binding energies for the best-docked pose of each compound in HDAC2. The results identify **4m** as the compound with the highest binding affinity, which agrees with the experimental data. The other compounds cannot be expected to be ranked well due to the small value range (a factor of ∼2 except for **4d**, **4l**, which are predicted second and third best, qualitatively in line with the experimental data; **4c** is overpredicted; Table 1) and SEM values of up to ∼50% of the mean value.

The docking poses of **4m** and the unsubstituted compound **4a** (Figure 4) in human HDAC2 show an interaction of the hydroxamate moiety with the zinc ion, hydrogen bonds with D100 and Y304, and stacking interactions of the phenyl moiety with H29 close to the rim of the binding tunnel. The *p*-substitution of the phenyl ring with pyrrolidine in **4m** increases the interaction surface of the complex, allowing for additional apolar interactions. The entropic penalty for extending the ligand with the pyrrolidine moiety is likely small since free rotation about the *C*−*N* axis is already restricted in solution due to conjugation such that only a few degrees of freedom are lost upon binding.

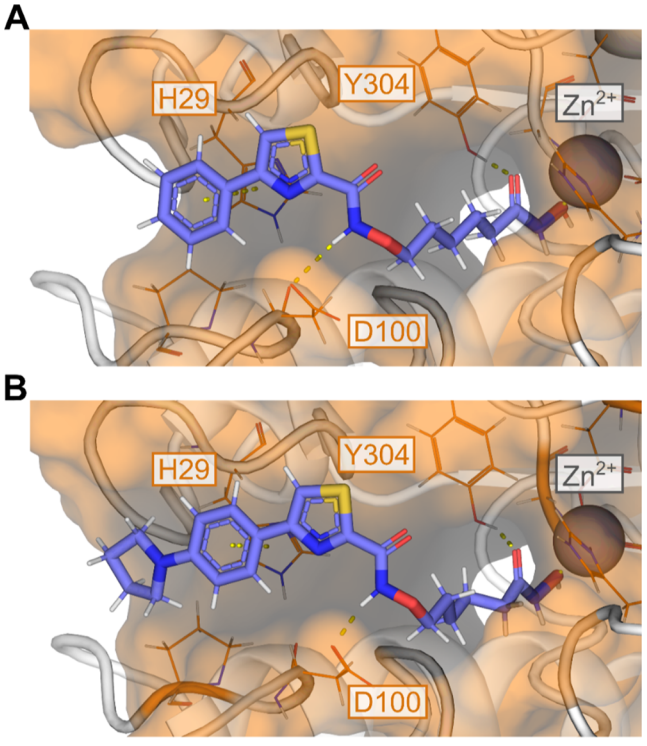

Figure 4. Predicted binding poses of compounds **4a** (A) and **4m** (B) to human HDAC2 (PDB-ID: 7KBG).[42]

2.4. Crystal Structures of 4d and 4m in Complex with HDAC6. To analyze the binding mode of **4d** and **4m** to HDAC6, both inhibitors were cocrystallized with the catalytic domain 2 (CD2) of HDAC6 from *Danio rerio* (zebrafish). This enzyme can be used as a model for human HDAC6 due to high structural similarity and high conservation of the active site.[43]

The crystal structures of CD2 from *Dr*HDAC6 bound to **4d** and **4m** were solved at 1.90 and 2.14 Å resolutions, respectively (Figure 5 and Supporting Information Table S1),

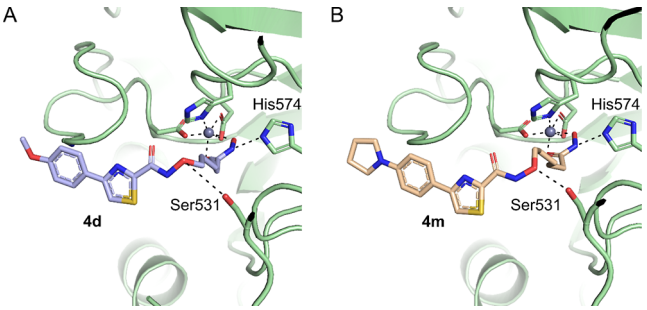

Figure 5. Crystal structures of (A) HDAC6−**4d** complex and (B) HDAC6−**4m** complex. The HDAC6 protein is shown as a cartoon and colored pale green. Close-up view of the active site with the ligands and the side chains of the amino acids coordinated to the zinc ion shown as a stick model and colored light blue (**4d**) and wheat (**4m**). The ligands and amino acid side chains are colored according to the element-specific color code. The zinc ion is shown as a sphere and colored gray. A figure displaying the simulated annealing omit map of the ligands is shown in the Supporting Information (Figure S1) (PDB ID: 9GGH and 9GGK).

providing, for the first time, insights into the binding mode of pentyloxyamide-based HDACi. The structures do not reveal pronounced conformational changes relative to the HDAC6 structure in the absence of any ligands (PDB ID: 5EEM).[44] The root-mean-square deviation (rmsd) between unliganded and **4d**-bound structures is 0.4 Å for 353 Cα atoms and between unliganded and **4m**-bound structures is 0.5 Å for 353 Cα atoms.

The inhibitors **4d** and **4m** bind in a similar conformation to *Dr*HDAC6 with the hydroxamate group coordinated to the zinc ion in the active site. The flexible pentyloxyamide connecting unit linker region is able to enter the narrow channel to the active site and enable a tight coordination to the zinc with O−Zn distances of 2.0 Å. The higher electron density observed in the simulated annealing omit map of the inhibitor shows that the sulfur atom of the thiazole group has the same orientation in both inhibitors, suggesting that only one conformation is adopted (Supporting Information Figure S1). Interestingly, the oxygen and nitrogen atoms of the oxyamide connecting unit of **4d** and **4m** are in a similar position despite not forming a specific interaction with the protein surface. In addition to the coordination of the hydroxamate group to the zinc ion, we observe two

https://doi.org/10.1021/acs.jmedchem.4c02024
J. Med. Chem. 2024, 67, 21223−21250

Table 3. Comparison of the IC_{50} of the Experimental Compounds in Three Different Leukemia Entities

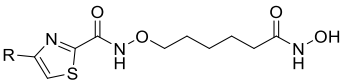

compound	R	IC_{50} (HL60) [nM]	IC_{50} (HPBALL) [nM]	IC_{50} (K562) [nM]
4a		424.6 ± 68.3	459.8 ± 35.2	879.2 ± 25.5
4b		332.1 ± 56.2	523.1 ± 58.2	993 ± 128.2
4c		670.7 ± 74.8	714.6 ± 55.2	1478.7 ± 53
4d		76.8 ± 8.2	110.6 ± 15.2	180.8 ± 55.7
4e		352.4 ± 25.5	359.9 ± 20	873.9 ± 238.4
4f		249.8 ± 84.5	421.2 ± 44.7	656.1 ± 264.7
4g		380.3 ± 36.8	465.3 ± 73.1	786.4 ± 230.9
4h		168.1 ± 104	355.9 ± 19.6	526.5 ± 28
4i		313.7 ± 96.5	403.8 ± 46.2	722 ± 164
4j		192.4 ± 22.4	279 ± 20.7	414.6 ± 38.8
4k		263.7 ± 70.7	446.4 ± 65.7	629.6 ± 69.6
4l		86 ± 10.4	119.4 ± 6.2	242.5 ± 52
4m		49.1 ± 5.4	100.1 ± 6	141.9 ± 13.2
Vorinostat	-	318.03 ± 36.7	823.53 ± 27	577.4 ± 119.8
Ricolinostat	-	2190.3 ± 24.9	2583.7 ± 71.16	2933 ± 79.5
CI994	-	1578.7 ± 92.5	4703.3 ± 117.2	5331.3 ± 948.17
Belinostat	-	157.7 ± 13.9	269.1 ± 5	217.9 ± 51.8

interactions with the HDAC6 protein. The imidazole ring of H574 interacts with the nitrogen atom in the hydroxamate group of the inhibitor, and the oxygen atom in the hydroxy group of S531 interacts with the bivalent oxygen atom of the oxyamide connecting unit. Notably, the predicted binding mode of **4m** to human HDAC2 differs from the conformation observed in the crystal structure of *Dr*HDAC6, which may be due to the differences in the sequence between human HDAC2 and zebrafish HDAC6. Taken together, the crystal structures of **4d** and **4m** in CD2 of *Dr*HDAC6 provide important insights into the binding mode of the novel pentyloxyamide-based HDACi.

2.5. High Throughput Drug Screening on Cytotoxicity of Novel HDACi. A HTDS[45] was conducted to evaluate the activity of 13 new synthesized HDACi across three leukemia cell lines: K562, HPBALL, and HL60 (Table 3). By representing the IC_{50} values of each HDACi through heatmaps and performing unsupervised clustering, three

https://doi.org/10.1021/acs.jmedchem.4c02024
J. Med. Chem. 2024, 67, 21223−21250

distinct clusters were identified (Supporting Information Figure S2). Compared to the lead inhibitor **4a**, the first cluster had similar activity against the three entities, while the second cluster consisted of HDACi with slightly lower IC_{50} and the third one showed significantly lower IC_{50} (~0.7 $\log_{10}$ fold change). In the HL60 cell line, which is the most sensitive, HDACi **4d**, **4m**, and **4l** showed IC_{50} values between 0.049 and 0.086 μM, whereas in the K562 cell line, the range was 0.141 to 0.242 nM. Throughout all three cell lines the inhibitor with the most potent anticancer activity is **4m**, followed by **4d** and **4l**.

2.6. Structure−Activity-Relationship Analysis. First, we modulated the electronic properties of the terminal phenyl ring by introducing a methoxy or fluorine substituent at the 1′, 2′, or 3′-position. Though the introduction of fluorine did not influence the antileukemic effect of the HDAC inhibitors significantly regardless of the ring position (**4e−g**), the introduction of a methoxy substituent at the 4′-position (**4d**) enhanced the cytotoxic activity against leukemia cells in comparison to the 2′ or the 3′ derivates (**4b**, **4c**).

Second, the replacement of the phenyl ring with thiophene was tolerated (**4h** and **4i**). Interestingly, the sulfur in the 2′-position (**4h**) proved to be beneficial for the antileukemic activity. However, the overall influence on the cytotoxic activity against leukemic cells remained rather small.

Third, we focused on the optimization of the substituent in 4′-position. The molecular docking studies suggested that the introduction of a larger substituent would favor additional apolar interactions with the HDAC2 enzyme. Correlating with the molecular docking studies, the pyrrolidine analog **4m** is a compound with strong antileukemic activity and low nanomolar inhibition of the HDAC2 enzyme. Further agreeing with that, extending the size of the cap group with a 2′-benzofuran moiety (**4l**) also enhanced the cytotoxic activity remarkably in comparison to **4a**. Overall, the introduction of larger substituents in 4′-position in combination with electron donating heteroatoms (**4d**, **4m**) and the 2′-substitued benzofuran (**4l**) improved the antileukemic activity in comparison to the unsubstituted compound **4a** remarkably (Figure 5). In addition, there is also a good correlation between the antileukemic activity and the inhibition of HDAC2 and 6.

2.7. Western Blot Analysis. The HDAC inhibitory effects of the three most promising derivatives (**4d**, **4l**, and **4m**) were next evaluated through cell-based assays using the HL60 cell line. Treatment of HL60 cells with compounds **4d**, **4l**, and **4m** resulted in notable α-tubulin acetylation (indicating effective inhibition of HDAC6), as determined by Western blot analysis. Vorinostat was utilized as a control for comparison (Figure 6). When evaluating HDAC class I inhibition, the optimized inhibitors displayed higher histone H3 acetylation levels compared to vorinostat. Furthermore, correlating with the H3 acetylation, we observed higher PARP cleavage (indicator of apoptosis induction) with **4d**, **4l** and **4m**, suggesting their enhanced effectiveness in comparison to vorinostat.

2.8. Selective Cytotoxicity of 4d and 4m against Leukemia Cells Surpasses Various Commercial HDAC Inhibitors. Following the confirmation of cellular HDAC inhibition by the promising new HDACi series, we selected two most potent HDACi (**4d** and **4m**) for an extended drug screening analysis. This analysis involved evaluating their

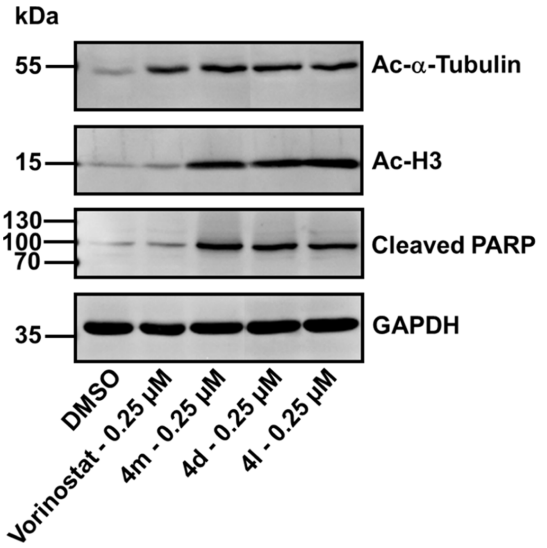

Figure 6. Western Blot analysis was conducted to assess the effects on HDAC inhibition markers (ac-H3 and ac-Tubulin) and the induction of apoptosis marker (cleaved PARP) following a 24 h treatment with **4d**, **4m**, and vorinostat (control) in HL60 leukemia cells (n = 3). A representative blot is shown here with GAPDH serving as the loading control.

effectiveness against 12 commercially available HDAC inhibitors using 7 leukemia cell lines (Figure 7A and Supporting Information Tables S2−S4) and 27 leukemia patient-derived xenograft (PDX) cells (Figure 7B and Supporting Information Tables S2−S4) across distinct therapy response subgroups. We incorporated healthy controls into our screens to determine whether **4d** and **4m** operate within a safe therapeutic window. These controls comprised $CD34^+$ hematopoietic stem and progenitor cells derived from cord blood and T-cells from healthy donors. By determining drug sensitivity scores (DSS) and generating selective or differential DSS (dDSS),[46] we obtained comparative data to evaluate their selectivity on the leukemia cells compared to the healthy controls. In comparative studies, both **4d** and **4m** demonstrated superior efficacy compared to clinically advanced HDAC inhibitors including tubastatin A, ricolinostat, CI994, romidepsin, and vorinostat. This was evidenced by their significantly elevated sDSS values when assayed against a panel of leukemia cell lines and PDX cells. Moreover, **4d** and **4m** consistently displayed selective antileukemic effects in the majority of tested leukemia cell types, suggesting their superiority over other examined HDACi. Additionally, standard chemotherapeutics used in leukemia treatment protocols, including cytarabine, idarubicin, daunorubicin, and azacitidine, were incorporated into the PDX drug screening analysis. Both **4d** and **4m** demonstrated significantly higher sDSS values, indicative of an improved therapeutic window and relatively similar cytotoxic profiles toward both chemotherapy-sensitive and chemotherapy-resistant subgroups (Figure 7B).

2.9. 4d and 4m Induce Cell Cycle Arrest and Apoptosis in Leukemia Cells. HDAC inhibition commonly leads to cell cycle arrest as an initial response, followed by the induction of apoptosis.[47,48] Analysis of the cell cycle demonstrated that treatment with **4d** in a concentration of 0.15 μM and **4m** at both concentrations significantly increased the proportion of HL60 cells in the G1 phase.

https://doi.org/10.1021/acs.jmedchem.4c02024
J. Med. Chem. 2024, 67, 21223−21250

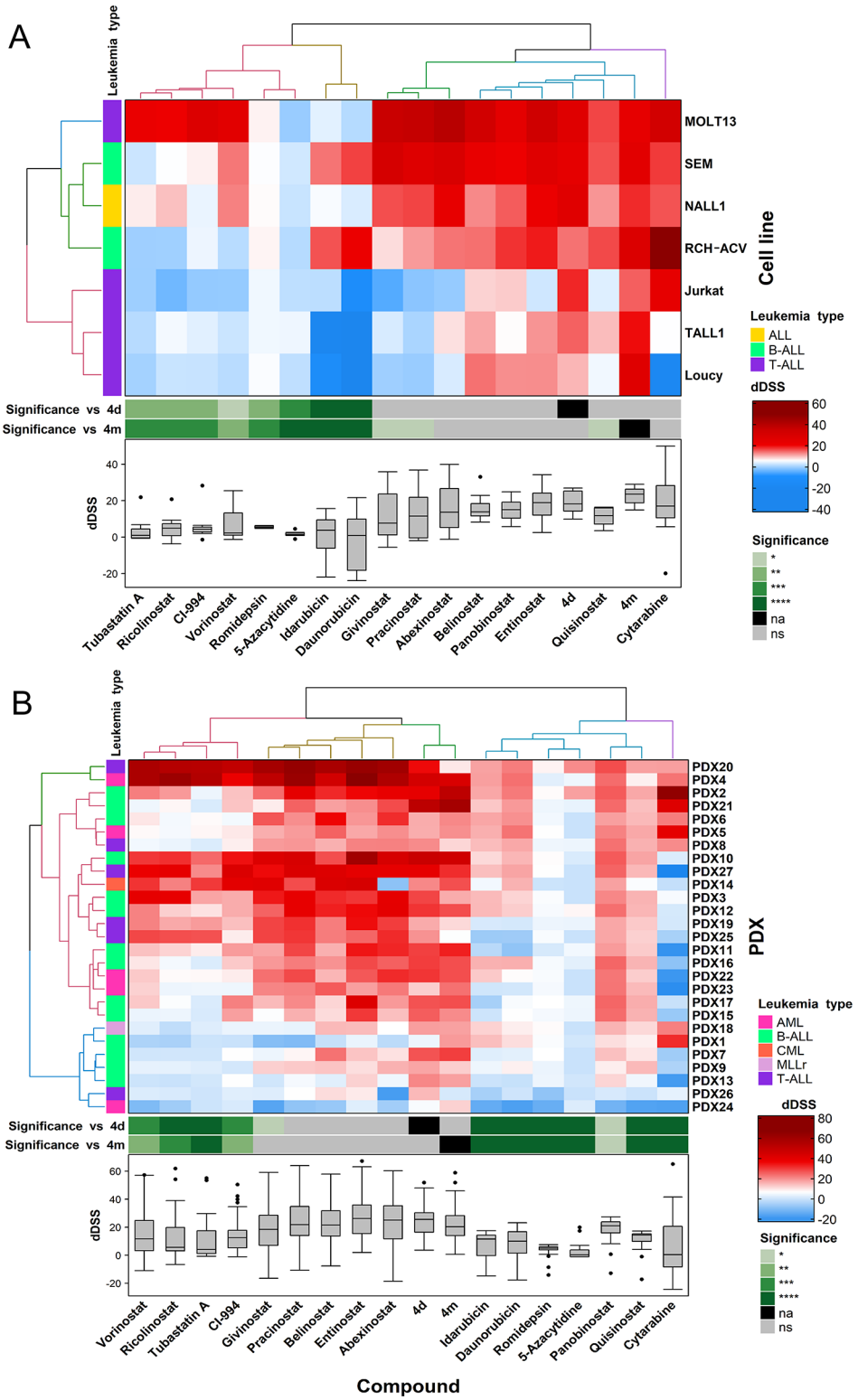

Figure 7. Unsupervised clustered heatmap displaying the differential drug sensitivity score (dDSS) of (A) leukemia cell lines and (B) PDX-grown leukemia cells. The statistical analysis was conducted using one-way ANOVA, $n = 1$. ALL = acute lymphoblastic leukemia, AML = acute myeloid leukemia, B-ALL = B-cell acute lymphoblastic leukemia, CML = chronic myeloid leukemia, MLLr = MLL rearranged leukemia, T-ALL = T-cell acute lymphoblastic leukemia, na = not applicable, ns = not significant, * = p(adj) > 0.05, ** = p(adj) > 0.01, *** = p(adj) > 0.001, and **** = p(adj) > 0.0001.

4d and **4m** reduced the number of cells in the S and G2/M phases significantly (Figure 8). Furthermore, an increased population of cells exhibited sub G1 labeling, indicating DNA fragmentation and confirming the induction of apoptosis. In comparison, **4m** exhibited greater potency than **4d** in inducing cell cycle arrest at the same concentration, which can be attributed to the lower IC_{50} value reported for **4m** as compared to **4d** (Table 3).

https://doi.org/10.1021/acs.jmedchem.4c02024
J. Med. Chem. 2024, 67, 21223−21250

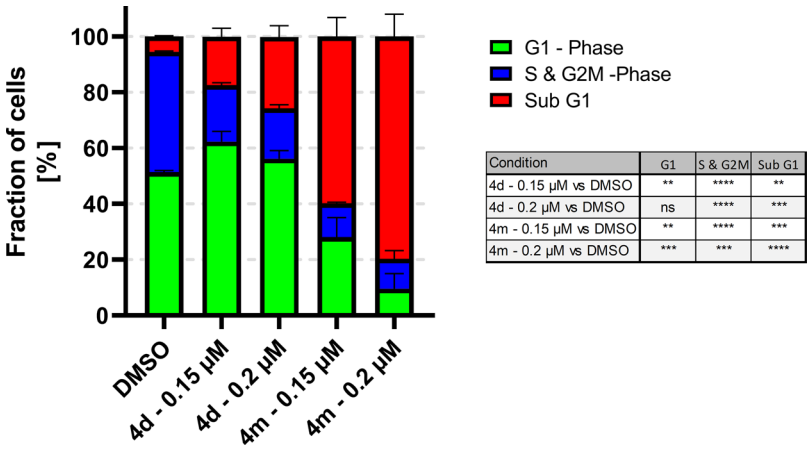

Condition	G1	S & G2M	Sub G1
4d - 0.15 µM vs DMSO	**	****	**
4d - 0.2 µM vs DMSO	ns	****	***
4m - 0.15 µM vs DMSO	**	****	***
4m - 0.2 µM vs DMSO	***	***	****

Figure 8. Bar graph depicting a cell cycle analysis via propidium iodide staining of HL60 leukemia cells treated with **4m** or **4d**, while the bar graphs displays statistical significance (unpaired student *t*-test, $n = 3$). ns = not significant, ** = p(adj) > 0.01, *** = p(adj) > 0.001, and **** = p(adj) > 0.0001.

To assess apoptosis induction by **4d** and **4m** further, we employed a trypan blue staining in conjunction with a caspase 3/7 assay on HL60 leukemia cells. As a control, we used the pan-caspase inhibitor Q-VD.[49] Treatment with **4d** or **4m** resulted in a significant reduction of viability ∼20% after 24 h and 70% after 48 h (Figure 9A). Q-VD reduced the loss of viability by 50%, suggesting that the cytotoxic effects triggered by both compounds are associated with apoptosis and are largely caspase-dependent. The caspase 3/7 assay further validated these findings, showing a marked increase in caspase activity after 48 h treatments with **4d** or **4m** (Figure 9B). Notably, Q-VD effectively negated this caspase 3/7 activity. In sum, the findings robustly indicate that both **4d** and **4m** induce apoptosis, leading to cytotoxic impacts on leukemia cells.

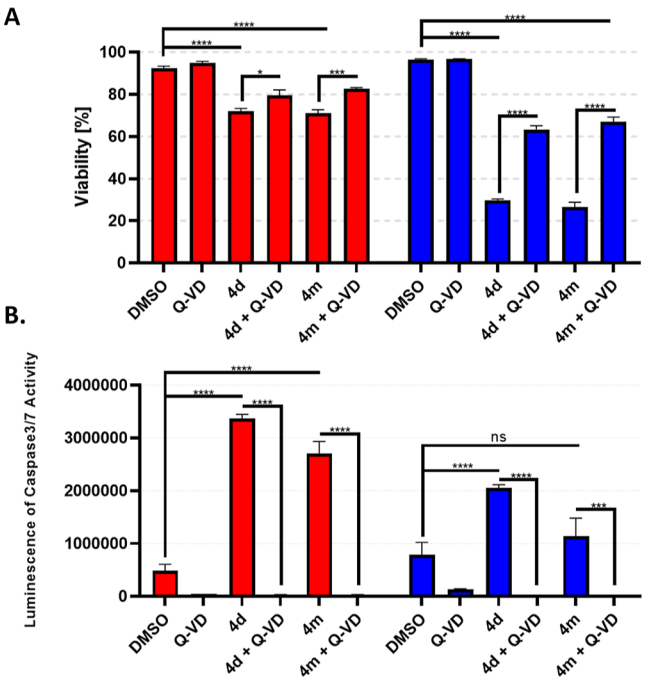

Figure 9. Bar diagram comparing the changes in (A) viability and (B) apoptosis induction via caspase 3/7 activity of HL60 leukemia cells treated with **4m** or **4d** and Q-VD (pan-Caspase inhibitor) via trypan blue or caspase3/7 assay, respectively. The statistical analysis was conducted using unpaired student *t*-test, $n = 3$. ns = not significant, * = p(adj) > 0.05, ** = p(adj) > 0.01, *** = p(adj) > 0.001, and **** = p(adj) > 0.0001.

2.10. 4d and 4m Synergize Effectively with the Standard Chemotherapy Drugs Decitabine and Clofarabine. Current clinical therapeutic strategies acknowledge the shortcomings of singular drug treatments, advocating for the utilization of synergistic drug combinations. These combinations aim to reduce cytotoxicity, exploit the unique susceptibilities of cancer cells, and avert drug resistance development. Therefore, we investigated potential synergistic drug combinations with the novel HDACi **4d** and **4m**. Decitabine, a first line chemotherapeutic, functions as a DNA methyltransferase inhibitor resulting in DNA hypomethylation. Synergistic drug effects between decitabine and HDACi have been well characterized, particularly in the context of AML.[50,51] Utilizing a matrix synergy screening method with the zero-interaction potency (ZIP) algorithm, we identified high ZIP synergy scores ranging from 60 to 80 across various concentration for both **4d** and **4m** when combined with decitabine (Figure 10A,B). Subsequently, we looked into the underlying mechanism of this drug synergy by evaluating the acetylation levels of histone H3 (Figure 10C). Although decitabine alone did not augment H3 acetylation, its combination with **4d** or **4m** showcased more pronounced bands compared to the individual HDACi treatment.

The combination ratio of decitabine to **4d** (5:1) was determined through synergy analysis, as this concentration ratio exhibited the highest synergistic interaction between them against AML cells. We have conducted additional combination experiments using a broad range of **4d** concentrations in conjunction with decitabine (Figure 10D). We included vorinostat as a positive control, maintaining the same concentrations as for **4d**. Notably, at equivalent concentrations, **4d** significantly increased actylated-H3 levels and cleaved PARP levels (a marker of apoptosis) compared to vorinostat in combination with decitabine (Figure 10E,F). Therefore, this enhanced effect on protein acetylation (Ac−H3) likely contributes to the observed synergistic cytotoxicity outcomes.

https://doi.org/10.1021/acs.jmedchem.4c02024
J. Med. Chem. 2024, 67, 21223−21250

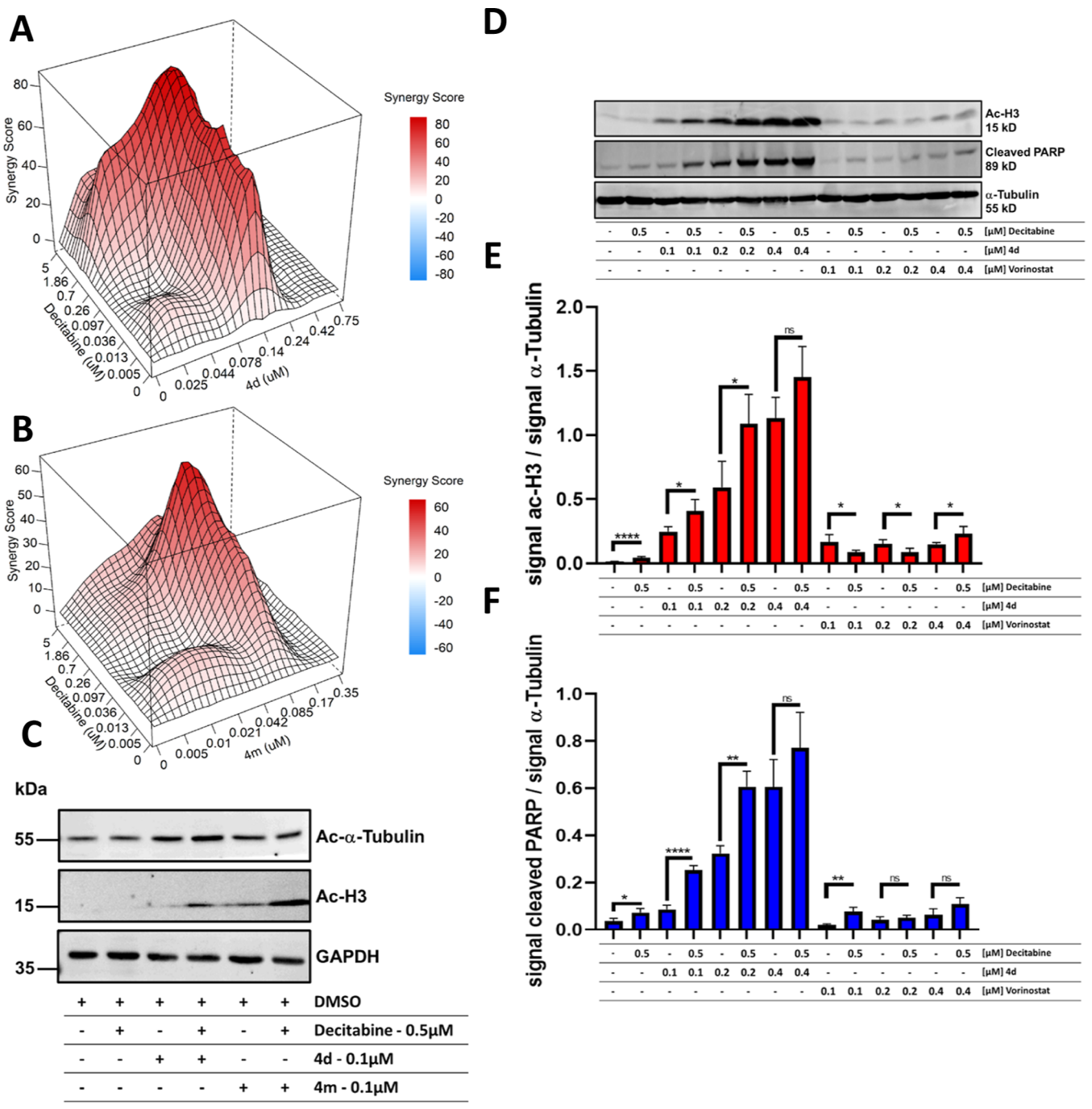

Figure 10. 3D synergy plots of HL60 cells treated with drug combinations for 72 h. The plots represent synergy scores from a combination matrix analyzed by the ZIP algorithm: (A) **4d** + decitabine and (B) **4m** + decitabine (n = 2). (C) Western blot analysis illustrating the differences in HDAC inhibition markers, ac-H3 and ac-Tubulin, in HL60 cells. The comparison is between solo treatment and combination treatments of either **4d** or **4m** with decitabine (n = 3) for 24 h. A representative blot is displayed with GAPDH as the loading control. (D) Western blot with increasing concentrations of **4d** and vorinostat combined with a fixed concentration of decitabine (n = 3). (E/F) Quantification of the signal of ac-H3 or cleaved PARP of D (unpaired student t-test, n = 3). ns = not significant, ** = p(adj) > 0.01, *** = p(adj) > 0.001, and **** = p(adj) > 0.0001.

The observed synergy of the epigenetic combination, which includes HDACi (**4d**) and DNMTi (Decitabine), has been corroborated by our studies and others, demonstrating significant synergistic activity against AML cells.[24,50−52] In fact, the safety, tolerability, and antileukemia activity of this combination have led to clinical trials involving AML patients.[53,54] Mechanistic insights suggest that the observed synergistic interaction is due to the crosstalk between DNA methylation and HDAC pathways. This mechanism involves a 5-methylcytosine-binding protein binding to gene promoters and recruiting HDACs.[55] In AML cells, this interaction is significant for the activation of tumor suppressor genes, including CDKN2B.[56] However, we acknowledge that the detailed mechanism underlying enhanced cytotoxicity upon combining HDAC and DNMT inhibitors is still unclear.

https://doi.org/10.1021/acs.jmedchem.4c02024
J. Med. Chem. 2024, 67, 21223−21250

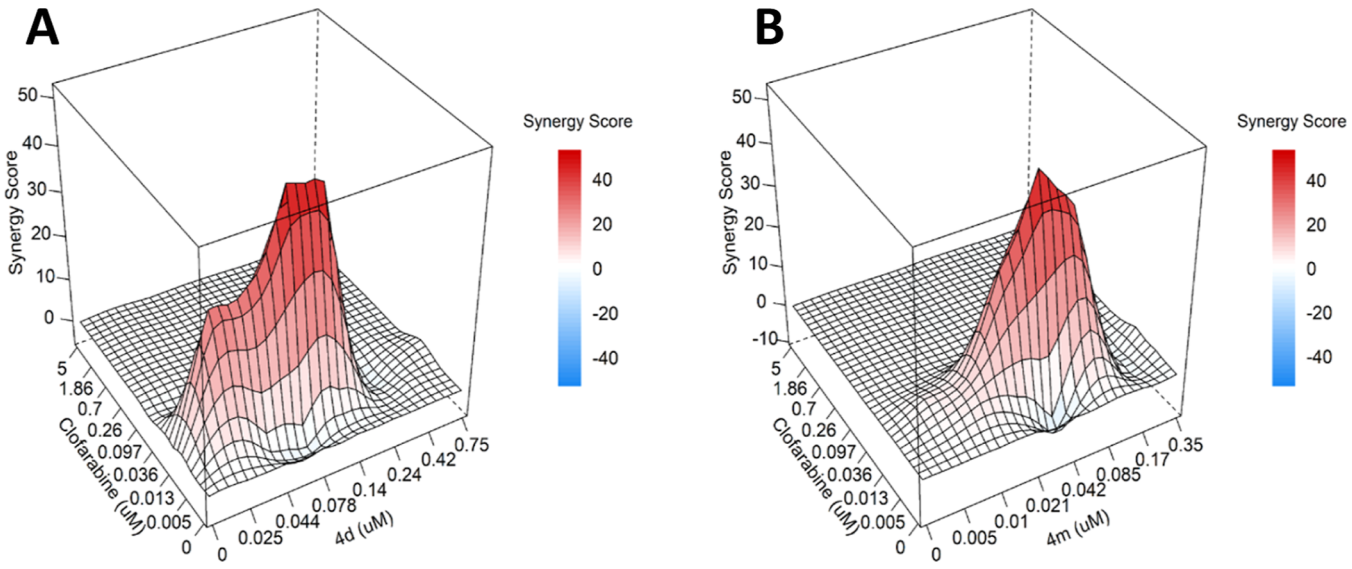

Figure 11. 3D synergy plots of HL60 cells treated with drug combinations for 72 h. The plots represent synergy scores from a combination matrix analyzed by the ZIP algorithm: (A) **4d** + clofarabine and (B) **4m** + clofarabine (n = 2).

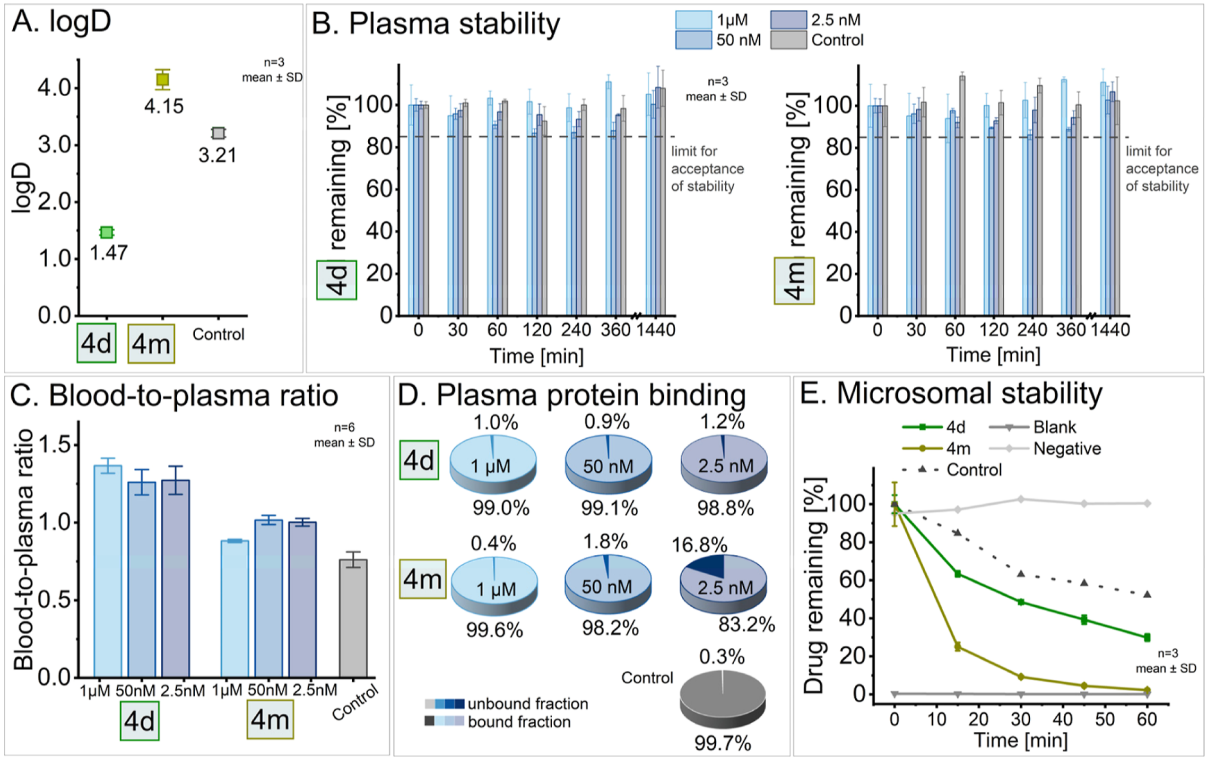

Figure 12. Overview of in vitro pharmacokinetics of **4d** and **4m**. (A) Interval plot of the determination of the coefficient of distribution (log D). Carvedilol was used as a control. (B) Stability of **4d** and **4m** in human plasma over 24 h at three different concentrations. A limit of −15% was set as acceptance criterium for stability according to bioanalytical guidelines. 4% bovine serum albumin (BSA) (absence of plasma enzymes) was used as a control spiked with a concentration of 50 nM of the drug. (C) Blood-to-plasma ratio of **4d** and **4m** for the three assessed concentration levels applying carvedilol as a control. (D) Plasma protein binding for **4d** and **4m** at three different concentration levels. The mean value of n = 3 is displayed. Itraconazol was used as a control. (E) Microsomal stability of **4d** and **4m** in HLMs. Propranolol was used as a control. The blank contains no drug, while the negative is free of HLMs. BSA: bovine serum albumin, HLM: HLMs, and SD: standard deviation.

HDAC inhibition contributes to increased DNA damage.[57] We examined the synergistic impact of combining **4d** and **4m** with clofarabine, a purine nucleoside analog and DNA synthesis inhibitor. In line with our previous observations, we found in a similar matrix synergy approach, ZIP synergy scores around 50 when **4d** and **4m** were administered in combination with clofarabine (Figure 11A,B).

These findings indicate that HDAC inhibitors **4d** and **4m** enhance the effectiveness of first line chemotherapeutics

https://doi.org/10.1021/acs.jmedchem.4c02024
J. Med. Chem. 2024, 67, 21223−21250

Table 4. Comparison of In Vitro Pharmacokinetic Data of 4d and 4m to Vorinostat[a]

	vorinostat	4d	4m
log D	1.46[63]	1.47 ± 0.05	4.15 ± 0.18
plasma stability/$t_{1/2}$	75 min[63]	>24 h	>24 h
$K_{B/P}$	2.0[64]	1.26 ± 0.16 (50 nM)	1.02 ± 0.06 (50 nM)
plasma protein binding	71%[65] (1.89 μM)	99.0% (1 μM)	99.6% (1 μM)
microsomal stability/$t_{1/2}$(clearance category)	60 min[66] (intermediate)	35.9 min[66] (intermediate)	11.2 min (high)

[a]$K_{B/P}$: blood-to-plasma ratio, log D: coefficient of distribution at pH 7.4, $t_{1/2}$: half-life.

Table 5. Pharmacokinetic Parameters (AUC_{last}, C_{max}, T_{max}, and $t_{1/2}$) Were Calculated According to a Noncompartmental Analysis (NCA) from the Blood Concentration of 4d Based on Actual Blood Sampling Time Pre-Dose and Post-Dose[a]

variable	mouse 1	mouse 2	mouse 3	mean [±SD]	vorinostat	
	intraperitoneal 10 mg/kg				per oral 50 mg/kg	
C_{max} (ng/mL)	1490	1030	1230	1250 [±232]	501[67]	580[68]
T_{max} (h)	0.25	0.25	0.25	0.25 [±0]	na[67]	0.08[68]
AUC_{last} (h·ng/mL)	523	396	480	466 [±65]	619[67]	347[68]
$t_{1/2}$ (h)	0.275	0.554	0.227	0.352 [±0.177]	0.75[67]	0.8[68]

[a]Na: not applicable.

decitabine and clofarabine potentially allowing for dose reduction and decreasing the likelihood of drug resistance.

2.11. 4d Shows Promising Human In Vitro Pharmacokinetics Superior to 4m. Determination of in vitro pharmacokinetic properties of new chemical entities is a key step in drug discovery and aids in nonclinical evaluation. To assess the initial ADME characteristics (absorption, distribution, metabolism, and elimination) of **4d** and **4m**, coefficient of distribution, plasma stability, blood-to-plasma ratio, microsomal stability, and plasma protein binding were investigated.

Good oral absorption can be assumed for the coefficient of distribution (log D) between 0 and 3.[58] The log D value was determined as 1.47 ± 0.05 for **4d** and 4.15 ± 0.18 for **4m** (Figure 12A), favoring **4d**. Carvedilol acted as a control and confirmed the assay validity (obtained: 3.21 vs in literature: 3.2).[59]

Further, in vitro plasma stability was determined, as instability is an indicator for rapid clearance or a short half-life ($t_{1/2}$), resulting in poor in vivo performance. **4d** and **4m** demonstrated excellent stability over the 24 h period monitored in human plasma at 37 °C (Figure 12B).

4m showed equal affinity to plasma and red blood cells, while **4d** tended toward higher distribution into red blood cells (Figure 12C), as determined by the blood-to-plasma ratio ($K_{B/P}$). One-way ANOVA confirmed no concentration dependency over the range of 2.5 nM to 1 μM for **4d** ($K_{B/P}$: 1.27 at 2.5 nM, 1.26 at 50 nM, and 1.37 at 1 μM), while for **4m** the $K_{B/P}$ at the highest concentration level investigated (1 μM) was significantly lower if compared to the lower concentration levels ($K_{B/P}$: 1.00 at 2.5 nM, 1.02 at 50 nM, and 0.88 at 1 μM). The control compound carvedilol validated the assay performance ($K_{B/P}$ obtained: 0.76 vs $K_{B/P}$ in literature: 0.76).[60]

Plasma protein binding was high for **4d** with a mean of 99.0% over the observed concentration range with no concentration-dependency. **4m** exhibited an atypical concentration-dependent plasma protein binding with lower binding for lower concentrations (Figure 12D). If proceeding in drug development, this phenomenon needs to be further investigated.[61] Itraconazol as control showed high plasma protein binding throughout all cavities confirming no leakage and being in line with values reported in the literature.[62]

While **4m** was extensively metabolized by hepatic enzymes, such as Cytochrome P450 and Uridine 5′-diphospho-glucuronosyltransferases, in Human liver microsomes (HLMs), **4d** showed moderate metabolism (Figure 12E). The half-life of **4d** was 35.9 min, with an intrinsic clearance of 38.6 μL/min/mg. When corrected for nonspecific protein binding in the incubation mixture, the unbound intrinsic clearance was determined as 54.7 μL/min/mg. The half-life of **4m** was substantially shorter with 11.2 min. While the corresponding intrinsic clearance resulted in 123.6 μL/min/mg, its unbound intrinsic clearance was 466.4 μL/min/mg.

Using the collected data, the in vivo hepatic clearance was estimated to be 0.39 L/min for **4d** and 8.18 L/min for **4m**. Assuming a hepatic blood flow of 1500 mL/min, **4d** can therefore be classified as a low hepatic extraction drug (calculated hepatic extraction ratio (E_h) < 0.3) and **4m** as high hepatic extraction drug (E_h > 0.7).

Finally, the collected in vitro pharmacokinetic data of **4d** and **4m** were compared to that of the approved drug vorinostat (Table 4). In comparison to vorinostat, **4d** appeared most promising for further pharmacokinetic investigation.

2.12. Preclinical Pharmacokinetic Study of 4d in Mice Showed Comparability to Vorinostat. Building on our human in vitro pharmacokinetic data, an in vivo pharmacokinetic study using **4d** was performed in three C57BL/6 mice. After intraperitoneal application of 10 mg/kg, a rapid onset of the compound was observed with a t_{max} of 0.25 h (mean) and C_{max} of 1250 ± 232 ng/mL (mean ± SD). Remarkably, dose adjusted overall exposure (AUC_{inf}/dose) of **4d** in mice was higher if compared to vorinostat (47 vs 12 h·kg·ng/mL/mg). Similar to vorinostat ($t_{1/2}$ = 0.75), **4d** was characterized by a short elimination half-life of 0.35 h (mean), indicating a substantial metabolism/elimination of **4d** in mice. A summary of pharmacokinetic data and a comparison with vorinostat is shown in Table 5.

2.13. 4d Suppresses In Vivo Growth of Myeloid Leukemia (MV4-11 and C1498) Cells. The pronounced cytotoxic effect of **4d** on leukemia cells, combined with the comparatively promising in vitro pharmacokinetic character-

https://doi.org/10.1021/acs.jmedchem.4c02024
J. Med. Chem. 2024, 67, 21223−21250

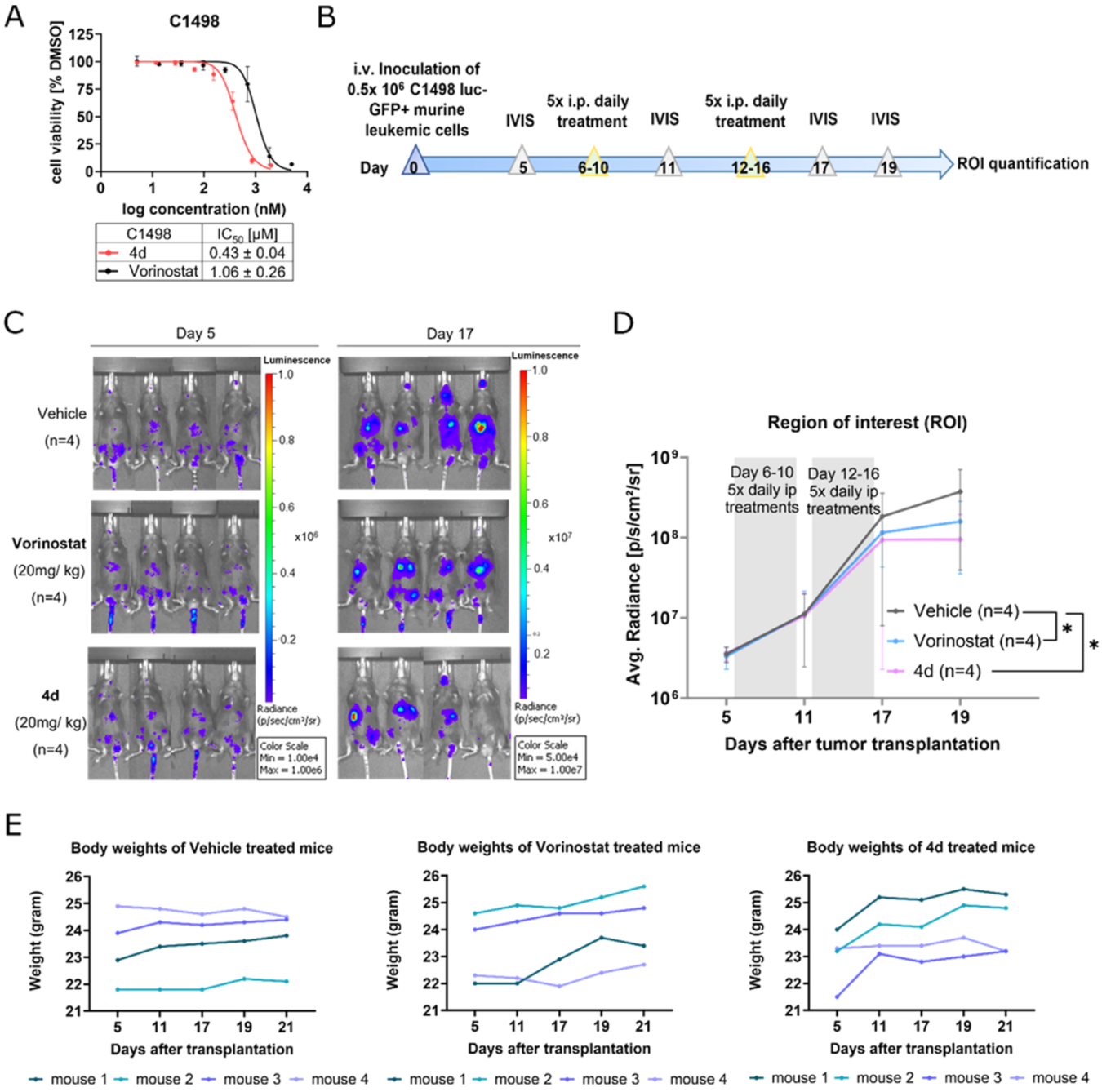

Figure 13. (A) Dose−response curve with IC_{50} value showing the inhibitory effect of vorinostat and compound **4d** on the proliferation of the C1498 cell line. The curve and IC_{50} values were generated with GraphPad Prism software by measuring the percentage of viable cells after 72 h incubation of cells with vorinostat and compound **4d** via CellTiter-Glo assay. Cell viability was normalized to DMSO (solvent)-treated controls. This curve and each point represent the results of the mean ± SD of biological and technical triplicates. (B) Schematic timeline of the experimental design. Each mouse received 0.5 × 10^6 C1498 luc-GFP^+ murine leukemic cells. After confirmation of tumor engraftment via monitoring the bioluminescence-based in vivo imaging system (IVIS) on day5, mice were grouped into three treatment groups, Vehicle (n = 4), Vorinostat (n = 4), and **4d** (n = 4). All mice received daily treatments accordingly via intraperitoneal injection. Tumor progression was examined by measuring bioluminescent signals with IVIS and ROI (p/s/cm^2/sr) quantification. (C) IVIS images of treated mice were taken on days 5 and 17. (D) ROI values at various time points, representing the measurement of leukemia cell growth. Statistical analysis was performed using a two-way mixed ANOVA with Greenhouse-Geisser correction. (E) Changes in body weight of each mouse from the three treatment groups before and after the treatment course.

istics of **4d**, prompted us to evaluate its effectiveness in a preclinical leukemic xenograft mouse (NSG) model using human AML cell line MV4-11. Initially, we determined the IC_{50} of **4d** in the MV4-11 cell line using the CellTiter-Glo assay, with vorinostat serving as a positive control, as described in prior methods. The dose−response curve and corresponding IC_{50} values were generated by applying a nonlinear regression algorithm to plot the log of inhibitor concentrations against normalized cell viability (Supporting Information Figure S3A). **4d** demonstrated an IC_{50} of 0.036 μM in MV4-11 cells, exhibiting over a 7-fold increase in potency compared to vorinostat. The in vivo experimental

https://doi.org/10.1021/acs.jmedchem.4c02024
J. Med. Chem. 2024, 67, 21223−21250

design is illustrated in Supporting Information Figure S3B. Briefly, mice were first intravenously (i.v.) injected with (0.5×10^6) human AML (MV4-11) cells, stably expressing luciferase-GFP for tracking in vivo transplantation. The in vivo growth of the leukemia cells was examined after 14 days of injection via bioluminescence measurement using in vivo imaging system (IVIS). Next, the leukemia bearing mice were distributed randomly to two groups. From day 16 onward, the mice were treated for 8 consecutive days with intraperitoneal injections of either with a vehicle control or **4d** (at a dose of 10 mg/kg). The IVIS images (Supporting Information Figure S3C) and the quantified region of interest (ROI) measurements during the treatment period indicated that the treatment with **4d** significantly ($p = 0.002$) suppresses the in vivo growth of MV4-11 leukemia cells as compared to the vehicle control group (Supporting Information Figure S3D). At day 42, which is 3 weeks after discontinuing the **4d** treatment, no differences in the growth of leukemia cells was observed between **4d** treated and vehicle group. Importantly, for measuring the potential signs of toxicity, such as body weight alterations, the **4d** treatment group exhibited a minor (not significant) reduction during and after the treatment course when compared to the vehicle control group (Supporting Information Figure S3E).

Next, given the growing evidence of immunomodulatory effects of HDAC inhibitors in cancer therapy,[69] we utilized an allograft leukemia model. In this model, leukemia is established by injecting (C57BL/6) derived murine AML (C1498) cells by intravenous injection in immunocompetent wildtpye (C57BL/6) mice.[70] Similarly, we initially determined the IC_{50} of **4d** in C1498 cells, with vorinostat serving as a positive control. Both **4d** and vorinostat affected C1498 cell growth in a concentration-dependent manner with IC_{50} of 0.425 and 1.06 μM, respectively (Figure 13A). Similar to human leukemia cells, exposure to **4d** or vorinostat increased actylated-H3 levels in murine C1498 leukemia cells (Supporting Information Figure S4). The in vivo experimental design is illustrated in Figure 13B. Briefly, leukemia was established by injecting (0.5×10^6) murine AML (C1498) cells, stably expressing luciferase-GFP by intravenous injection in C57BL/6 mice.[70] Confirmation of tumor engraftment was assessed on day 5 after injection of leukemia cells by measuring the luminescence signals in the mice following D-Luciferin intraperitoneal injection (Figure 13C). Starting on day 6, the mice were divided into three treatment groups and administered intraperitoneally with either vehicle, positive control vorinostat (20 mg/kg), or **4d** (20 mg/kg) for 2 weeks. Compared to the vehicle control group, both the vorinostat- ($p = 0.0249$) and **4d** ($p = 0.0326$)-treated groups exhibited significantly lower leukemia burden after the second treatment cycle, with this difference becoming more pronounced by day 19 (Figure 13D). Additionally, no significant differences in body weight were observed during the treatment course (Figure 13E). Additionally, for the target engagement studies, we isolated liver cells from mice 24 h post-treatment with **4d**. Consistent with our in vitro observations, the intracellular staining intensity of acetylhistone H3 in liver cells was markedly increased in the **4d**-treated mice, pointing toward target engagement inside the organ tissues (Supporting Information Figure S5).

3. CONCLUSIONS

We developed a novel pentyloxyamide-based HDACi with substituted phenylthiazole cap groups and evaluated their potential as novel antileukemic lead structures. The leading candidates from this series, **4d** and **4m**, exhibited nanomolar inhibition toward HDAC2 and HDAC6 and demonstrated cytotoxic effects against a wide range of therapy-sensitive and therapy-resistant leukemia cell lines as well as against patient-derived leukemia cells. In addition, the binding modes of both inhibitors were determined by X-ray crystallography, revealing specific interactions with the CD2 of HDAC6 from *D. rerio* (zebrafish).

Importantly, **4d** and **4m** exhibited comparable or even higher DSS than well-established and clinically used HDAC inhibitors, along with greater selectivity toward malignant cells relative to healthy controls. Considering the current reliance on combination therapies in modern cancer treatment, drugs that demonstrate synergistic interactions can significantly influence the therapeutic outcome, delay or prevent the development of resistance, and increase the treatable population of patients. In this regard, the combination of **4d** and **4m** with the routinely used chemotherapeutic agents clofarabine and decitabine exhibited a notable synergistic cytotoxic effect. The promising in vitro pharmacokinetic characteristics and first in vivo pharmacokinetic data support comprehensive in vivo investigation of **4d**. Notably, in vivo administration of **4d** effectively suppressed the growth of leukemia cells without inducing any observable signs of toxicity in mice. Overall, these findings position **4d** and **4m** as novel lead structures with potential for further preclinical development, as they not only demonstrate a therapeutic window but also promising antileukemic effects when used in combination with established antileukemic drugs. Current challenges, such as the improvable in vivo pharmacokinetics of HDAC inhibitors **4d** and **4m** will be addressed along with further structure−activity relationship (SAR) studies in a follow-up lead optimization program.

4. EXPERIMENTAL SECTION

4.1. Chemistry. Chemicals and solvents were purchased from commercial suppliers (Acros Organics, TCI, abcr, Alfa Aesar, Ambeed, BLDpharm, and Merck) and used without further purification. Dry solvents were purchased from Acros Organics. The reactions were monitored by thin-layer chromatography (TLC) using Macherey-Nagel precoated ALUGRAM Xtra SIL G/UV_{254} plates. Spots were visualized either by irradiation with ultraviolet light (254 nm) or staining in potassium permanganate solution. Hydroxamic acids were further stained using a 1% solution of iron(III) chloride in ethanol. Flash chromatography was performed on a CombiFlash RF 200 or a Büchi Pure C-810 Flash using RediSep Rf-columns using the solvent mixtures of *n*-hexane/ethyl acetate or dichloromethane/methanol according to the separation. Melting points (mp) analyses were performed using a Büchi M-565 melting point apparatus and are uncorrected. Proton (^1H) and carbon (^{13}C) NMR spectra were recorded on a Bruker Avance III 300 or 600 MHz using DMSO-d_6 as the solvent. Chemical shifts are given in parts per million (ppm) relative to the residual solvent peak for ^1H and ^{13}C NMR. Coupling constants, J, were reported in Hertz (Hz). High-resolution mass spectra (HRMS) analysis was performed on a UHR-QTOF maXis 4G, Bruker Daltonics, by electrospray ionization (ESI). Analytical HPLC analyses were carried out on an Knauer AZURA system equipped with AZURA 6.1L (pumps), AZURA column thermostat CT 2.1 and AZURA UVD 2.1L (UV-detector), and a Spark Holland B.V. OPTIMAS model 820 autosampler, or on a Agilent LC 1260 Infinity II system equipped

https://doi.org/10.1021/acs.jmedchem.4c02024
J. Med. Chem. 2024, 67, 21223−21250

with an G7116A Infinity II Multicolumn Thermostat, a G7104C Infinity II Flexible Pump a G7129C Infinity II Vialsampler and a G7114A Infinity II Variable Wavelength Detector. The separation took place on a Eurospher II 100 5 C18 (150 × 4 mm) column. UV absorption was detected at 254 nm. HPLC-grade water +0.1% TFA (solvent A) and HPLC-grade acetonitrile +0.1% TFA (solvent B) were used for elution at a flow rate of 1 mL/min. A linear gradient of 10% B to 100% B within 30 min was used. In the case of the *O*-trityl protected compounds **3a-m** HPLC-grade water (solvent A) and HPLC-grade acetonitrile (solvent B) were used for elution at a flow rate of 1 mL/min. A linear gradient of 10% B to 100% B within 30 min was used. All compounds are >95.0% pure by HPLC.

*4.1.1. General Procedure for the Preparation of Phenylthiazoles **1a**−**1m**.* The respective 2-bromoketone (1.0 equiv) and ethyl thiooxamate (1.0 equiv) were dissolved in ethanol (7 mL/mmol) and heated at 70 °C. If the TLC (eluent: ethyl acetate/*n*-hexane) showed incomplete conversion after 7 h of heating, the reaction was stirred at room temperature overnight. After evaporation of the solvent, the resulting residue was diluted with ethyl acetate and washed three times with 50 mL of saturated sodium bicarbonate solution and once with 50 mL of brine. The organic phase was dried over anhydrous sodium sulfate and filtrated, and the solvent was evaporated under reduced pressure. The crude product was purified using flash chromatography using ethyl acetate and *n*-hexane as the eluent (0−30% ethyl acetate) to yield phenylthiazoles **1a**−**m**.

*4.1.1.1. **1a** Ethyl 4-Phenylthiazole-2-carboxylate.* Synthesis according to general procedure A using phenacyl bromide (4.1 g, 20.0 mmol) afforded **1a** as a light yellow solid (3.3 g, 14.1 mmol, 71%). mp 36.9 °C, t_r 14.47 min, purity: 99.3%.

^{1}H NMR (300 MHz, DMSO-d_6): δ 1.36 (t, J = 7.1 Hz, 3H), 4.42 (q, J = 7.1 Hz, 2H), 7.36−7.44 (m, 1H), 7.45−7.53 (m, 2H), 7.98−8.00 (m, 1H), 8.02 (d, J = 1.5 Hz, 1H), 8.53 (s, 1H).

^{13}C NMR (75 MHz, DMSO-d_6): δ 14.1, 62.2, 121.0, 126.2, 128.7, 129.0, 133.2, 156.3, 157.5, 159.4.

HRMS (m/z): MH^+ calcd for $C_{12}H_{11}NO_2S$ 234.0583; found, 234.0584.

*4.1.1.2. **1b** Ethyl 4-(2-Methoxyphenyl)thiazole-2-carboxylate.* Synthesis according to general procedure A using 2-bromo-1-(2-methoxyphenyl)ethanone (2.3 g, 10,0 mmol) afforded **1b** as a white solid (2.0 g, 7.6 mmol, 76%). mp 70.3 °C, t_r 15.21 min purity: 99.1%.

^{1}H NMR (300 MHz, DMSO-d_6): δ 1.36 (t, J = 7.1 Hz, 3H), 3.94 (s, 3H), 4.41 (q, J = 7.1 Hz, 2H), 7.09 (ddd, J = 7.8, 7.3, 1.1 Hz, 1H), 7.18 (dd, J = 8.4, 1.1 Hz, 1H), 7.40 (ddd, J = 8.3, 7.3, 1.8 Hz, 1H), 8.13 (dd, J = 7.7, 1.8 Hz, 1H), 8.45 (s, 1H).

^{13}C NMR (75 MHz, DMSO-d_6): δ 14.1, 55.6, 62.1, 111.9, 120.7, 121.6, 124.2, 129.4, 129.9, 152.3, 155.8, 156.6, 159.5.

HRMS (m/z): MH^+ calcd for $C_{13}H_{13}NO_3S$ 264.0689; found, 264.0696.

*4.1.1.3. **1c** Ethyl 4-(3-Methoxyphenyl)thiazole-2-carboxylate.* Synthesis according to general procedure A using 3-methoxyphenacyl bromide (2.3 g, 10.0 mmol) afforded **1c** as a white solid (1.9 g, 7.4 mmol, 74%). mp 76.6 °C, t_r 14.36 min purity: 98.9%.

^{1}H NMR (300 MHz, DMSO-d_6): δ 1.36 (t, J = 7.1 Hz, 3H), 3.83 (s, 3H), 4.42 (q, J = 7.1 Hz, 2H), 6.98 (ddd, J = 8.2, 2.6, 1.0 Hz, 1H), 7.40 (ddd, J = 8.2, 7.7, 0.4 Hz, 1H), 7.51−7.62 (m, 2H), 8.56 (s, 1H).

^{13}C NMR (75 MHz, DMSO-d_6): δ 14.1, 55.2, 62.2, 111.6, 114.4, 118.6, 121.3, 130.1, 134.6, 156.1, 157.3, 159.3, 159.7.

HRMS (m/z): MH^+ calcd for $C_{13}H_{13}NO_3S$ 264.0689; found, 264.0693.

*4.1.1.4. **1d** Ethyl 4-(4-Methoxyphenyl)thiazole-2-carboxylate.* Synthesis according to general procedure A using 4-methoxyphenacyl bromide (2.3 g, 10.0 mmol) afforded **1d** as a white solid (1.9 g, 7.3 mmol, 73%). mp 150.5 °C, t_r 14.40 min purity: 97.7%.

^{1}H NMR (300 MHz, DMSO-d_6): δ 1.36 (t, J = 7.1 Hz, 3H), 3.81 (s, 3H), 4.41 (q, J = 7.1 Hz, 2H), 6.99−7.09 (m, 2H), 7.90−7.98 (m, 2H), 8.37 (s, 1H).

^{13}C NMR (75 MHz, DMSO-d_6): δ 14.1, 55.2, 62.1, 114.3, 119.0, 126.0, 127.7, 156.3, 157.2, 159.4, 159.7.

HRMS (m/z): MH^+ calcd for $C_{13}H_{13}NO_3S$ 264.0689; found, 264.0693.

*4.1.1.5. **1e** Ethyl 4-(2-Fluorophenyl)thiazole-2-carboxylate.* Synthesis according to general procedure A using 2-bromo-2′fluoroacetophenone (2.2 g, 10.0 mmol) afforded **1e** as a white solid (1.3 g, 5.2 mmol, 52%). mp 65.7 °C, t_r 15.25 min purity: 99.8%.

^{1}H NMR (300 MHz, DMSO-d_6): δ 1.36 (t, J = 7.1 Hz, 3H), 4.42 (q, J = 7.1 Hz, 2H), 7.31−7.43 (m, 2H), 7.48 (tdd, J = 7.2, 5.3, 2.7 Hz, 1H), 8.11 (td, J = 7.8, 1.7 Hz, 1H), 8.37 (d, J = 2.4 Hz, 1H).

^{13}C NMR (75 MHz, DMSO-d_6): δ 14.0, 62.3, 116.3 (d, J = 22.0 Hz), 121.0 (d, J = 11.5 Hz), 124.8−125.2 (m), 129.8 (d, J = 2.8 Hz), 130.6 (d, J = 8.7 Hz), 149.8 (d, J = 2.3 Hz), 157.1, 157.8, 159.3, 161.1.

HRMS (m/z): MH^+ calcd for $C_{12}H_{10}FNO_2S$ 252.0489; found, 252.0490.

*4.1.1.6. **1f** Ethyl 4-(3-Fluorophenyl)thiazole-2-carboxylate.* Synthesis according to general procedure A using 2-bromo-1-(3-fluorophenyl)ethan-1-one (2.2 g, 10.0 mmol) afforded **1f** as a white solid (1.6 g, 6.5 mmol, 65%). mp 66.0 °C, t_r 14.81 min purity: 99.7%.

^{1}H NMR (300 MHz, DMSO-d_6): δ 1.36 (t, J = 7.1 Hz, 3H), 4.42 (q, J = 7.1 Hz, 2H), 7.24 (dddd, J = 9.1, 8.3, 2.6, 1.0 Hz, 1H), 7.41−7.66 (m, 1H), 7.73−7.92 (m, 2H), 8.64 (s, 1H).

^{13}C NMR (75 MHz, DMSO-d_6): δ 14.1, 62.3, 112.8 (d, J = 23.2 Hz), 115.5 (d, J = 21.2 Hz), 121.1−123.0 (m), 131.1 (d, J = 8.4 Hz), 135.5 (d, J = 8.3 Hz), 154.8 (d, J = 2.9 Hz), 157.7, 159.3, 161.0, 164.2.

HRMS (m/z): MH^+ calcd for $C_{12}H_{10}FNO_2S$ 252.0489; found, 252.0489.

*4.1.1.7. **1g** Ethyl 4-(4-Fluorophenyl)thiazole-2-carboxylate.* Synthesis according to general procedure A using 2-bromo-1-(4-fluorophenyl)ethan-1-one (1.1 g, 5.0 mmol) afforded **1g** as a white solid (0.8 g, 3.3 mmol, 66%). mp 74.0 °C t_r 14.79 min purity: 99.9%.

^{1}H NMR (300 MHz, DMSO-d_6): δ 1.36 (t, J = 7.1 Hz, 3H), 4.41 (q, J = 7.1 Hz, 2H), 7.25−7.39 (m, 2H), 7.96−8.13 (m, 2H), 8.51 (s, 1H).

^{13}C NMR (126 MHz, DMSO-d_6): δ 13.9, 62.1, 115.7 (d, J = 21.7 Hz), 120.6, 128.3 (d, J = 8.3 Hz), 129.8 (d, J = 3.1 Hz), 155.2, 157.5, 159.2, 161.3, 163.2.

HRMS (m/z): MH^+ calcd for $C_{12}H_{10}FNO_2S$ 252.0489; found, 252.0494.

*4.1.1.8. **1h** Ethyl 4-(Thiophen-2-yl)thiazole-2-carboxylate.* Synthesis according to general procedure A using 2-bromo-1-(thiophen-2-yl)ethanone (2.1 g, 10.0 mmol) afforded **1h** as a black solid (1.3 g, 10.0 mmol, 54%). mp 53.4 °C t_r 13.81 min purity: 96.5%.

^{1}H NMR (300 MHz, DMSO-d_6): δ 1.35 (t, J = 7.1 Hz, 3H), 4.41 (q, J = 7.1 Hz, 2H), 7.16 (dd, J = 5.1, 3.6 Hz, 1H), 7.61 (dd, J = 5.1, 1.2 Hz, 1H), 7.68 (dd, J = 3.6, 1.2 Hz, 1H), 8.37 (s, 1H).

^{13}C NMR (75 MHz, DMSO-d_6): δ 14.1, 62.3, 119.3, 125.5, 126.9, 128.2, 136.8, 151.1, 157.4, 159.2.

HRMS (m/z): MH^+ calcd for $C_{10}H_9NO_2S_2$ 240.0147; found, 240.0149.

*4.1.1.9. **1i** Ethyl 4-(Thiophen-3-yl)thiazole-2-carboxylate.* Synthesis according to general procedure A using 3-(bromoacetyl)-thiophene (1.0 g, 4.7 mmol) afforded **1i** as a brown oil (0.7 g, 3.0 mmol, 63%). T_r 13.43 min purity: 99.0%.

^{1}H NMR (300 MHz, DMSO-d_6): δ 1.35 (t, J = 7.1 Hz, 3H), 4.41 (q, J = 7.1 Hz, 2H), 7.63−7.69 (m, 2H), 8.03 (dd, J = 2.6, 1.6 Hz, 1H), 8.36 (s, 1H).

^{13}C NMR (151 MHz, DMSO-d_6): δ 14.1, 62.2, 120.3, 123.3, 126.2, 127.4, 135.4, 152.6, 157.3, 159.4.

HRMS (m/z): MH^+ calcd for $C_{10}H_9NO_2S_2$ 240.0147; found, 240.0151.

*4.1.1.10. **1j** Ethyl 4-(p-Tolyl)thiazole-2-carboxylate.* Synthesis according to general procedure A using 2-bromo-1-(*p*-tolyl) (2.2 g, 10.0 mmol) afforded **1j** as a white solid (1.7 g, 6.9 mmol, 69%). mp 60.0 °C, t_r 15.59 min purity: 99.3%.

https://doi.org/10.1021/acs.jmedchem.4c02024
J. Med. Chem. 2024, 67, 21223−21250

^{1}H NMR (300 MHz, DMSO-d_6): δ 1.36 (t, J = 7.1 Hz, 3H), 2.35 (s, 3H), 4.41 (q, J = 7.1 Hz, 2H), 7.29 (dd, J = 7.9, 0.7 Hz, 2H), 7.84−7.94 (m, 2H), 8.45 (s, 1H).

^{13}C NMR (75 MHz, DMSO-d_6): δ 14.1, 20.8, 62.2, 120.1, 126.2, 129.5, 130.6, 138.2, 156.4, 157.3, 159.4.

HRMS (m/z): MH$^+$ calcd for $C_{13}H_{13}NO_2S$ 248.0740; found, 248.0744.

4.1.1.11. ***1k*** *Ethyl 4-(4-(Trifluoromethyl)phenyl)thiazole-2-carboxylate.* Synthesis according to general procedure A using 2-bromo-4′-(trifluoromethyl)acetophenone (2.8 g, 10.0 mmol) afforded **1k** as a white solid (2.3 g, 7.7 mmol, 77%). mp 134.3 °C, t_r 16.36 min purity: 96.4%.

^{1}H NMR (300 MHz, DMSO-d_6): δ 1.36 (t, J = 7.1 Hz, 3H), 4.43 (q, J = 7.1 Hz, 2H), 7.85 (d, J = 8.1 Hz, 2H), 8.23 (d, J = 8.0 Hz, 2H), 8.74 (s, 1H).

^{13}C NMR (75 MHz, DMSO-d_6): δ 14.1, 62.3, 123.3, 125.9 (d, J = 4.1 Hz), 126.9, 128.5, 128.9, 136.9, 154.5, 158.0, 159.3.

HRMS (m/z): MH$^+$ calcd for $C_{13}H_{10}F_3NO_2S$ 302.0457; found, 302.0465.

4.1.1.12. ***1l*** *Ethyl 4-(Benzofuran-2-yl)thiazole-2-carboxylate.* Synthesis according to general procedure A using 2-(bromoacetyl)-benzofuran (1.0 g, 4.1 mmol) afforded **1l** as a brown solid (0.5 g, 1.7 mmol, 42%). mp 128.6 °C, t_r 16.02 min purity: 99.4%.

^{1}H NMR (300 MHz, DMSO-d_6): δ 1.37 (t, J = 7.1 Hz, 3H), 4.43 (q, J = 7.1 Hz, 2H), 7.25−7.41 (m, 2H), 7.42 (d, J = 0.9 Hz, 1H), 7.69 (ddq, J = 17.4, 8.1, 0.8 Hz, 2H), 8.49 (s, 1H).

^{13}C NMR (151 MHz, DMSO-d_6): δ 14.1, 62.4, 104.2, 111.3, 121.8, 122.5, 123.5, 125.3, 128.2, 147.3, 150.3, 154.3, 158.7, 159.1.

HRMS (m/z): MH$^+$ calcd for $C_{14}H_{11}NO_3S$ 274.0532; found, 274.0534.

4.1.1.13. ***1m*** *Ethyl 4-(4-(Pyrrolidine-1-yl)phenyl)thiazole-2-carboxylate.* Synthesis according to general procedure A using 2-bromo-4′-(1-pyrrolidinyl)acetophenone (2.8 g, 10.0 mmol) afforded **1m** as a dark yellow solid (0.9 g, 2.9 mmol, 29%). mp 180.5 °C, t_r 15.15 min purity: 99.3%.

^{1}H NMR (300 MHz, DMSO-d_6): δ 1.35 (t, J = 7.1 Hz, 3H), 1.88−2.04 (m, 4H), 3.21−3.32 (m, 4H), 4.40 (q, J = 7.1 Hz, 2H), 6.54−6.67 (m, 2H), 7.75−7.87 (m, 2H), 8.16 (s, 1H).

^{13}C NMR (151 MHz, DMSO-d_6): δ 14.1, 25.0, 47.2, 62.0, 111.6, 116.5, 120.5, 127.3, 147.8, 156.7, 157.5, 159.5.

HRMS (m/z): MH$^+$ calcd for $C_{16}H_{18}N_2O_2S$ 303.1162; found, 303.1167.

4.1.1.14. 6-(Aminooxy)-N-(trityloxy)hexanamide. The synthesis of the linker **2** was performed after an adapted protocol of Avelar et al.[71]

4.1.1.15. 6-Bromo-N-(trityloxy)hexanamide. To a stirred solution of 6-bromohexanoic acid (7.4 g, 38 mmol, 1.0 equiv) in 100 mL THF, isobutyl chloroformate (IBCF) (5.8 mL, 45 mmol, 1.2 equiv) and *N*-methylmorpholine (NMM) (5.0 mL, 45 mmol, 1.2 equiv) were added at 10 °C. After stirring for 15 min *O*-tritylhydroxylamine (13 g, 38 mmol, 1.0 equiv) dissolved in 50 mL, THF was carefully added, and the reaction was left stirring at room temperature overnight. The precipitate was filtered off, the filtrate was evaporated, and the crude residue was dissolved in ethyl acetate and washed three times with 100 mL of saturated sodium bicarbonate solution and once with 100 mL of brine. The organic phase was dried over anhydrous sodium sulfate, filtrated, and evaporated. The crude product was recrystallized from ethyl acetate/n hexanes to yield **I** (14 g, 30 mmol, 80%) as a white solid. mp 128.0 °C, t_r 17.58 min purity: 99.6%.

^{1}H NMR (300 MHz, DMSO-d_6): δ 1.07 (dd, J = 15.6, 6.6 Hz, 1H), 1.14−1.28 (m, 1H), 1.64 (p, J = 6.9 Hz,1H), 1.79 (t, J = 7.2 Hz, 1H), 3.41 (t, J = 6.8 Hz, 2H), 7.33 (s, 8H), 10.18 (s, 1H) ^{13}C NMR (75 MHz, DMSO-d_6): δ 23.8, 26.9, 31.7, 31.9, 34.9, 91.7, 127.4, 127.5, 128.9, 142.4, 170.1.

HRMS (m/z): MNa$^+$ calcd for $C_{25}H_{26}BrNO_2$ 474.1039; found, 474.1041.

4.1.1.16. 6-((1,3-Dioxoisoindolin-2-yl)oxy)-N-(trityloxy)-hexanamide. **I** (7.1 g, 16 mmol, 1.0 equiv), *N*-hydroxyphthalimide (NHPI) (2.6 g, 16 mmol, 1.0 equiv), and triethylamine (4.5 mL, 31 mmol, 2.0 equiv) were suspended in 100 mL acetonitrile and refluxed for 12 h. The solvent was removed, the residue dissolved in ethyl acetate and extracted with saturated sodium bicarbonate solution until the aqueous phase did not show any left NHPI. The organic phase was dried over anhydrous sodium sulfate, filtrated, and evaporated. The crude product was recrystallized using ethyl acetate/n hexanes to yield **II** (6.2 g, 12 mmol, 74%) as a white solid. mp 142.0 °C, HPLC t_r 16.72 min purity: 96.9%.

^{1}H NMR (300 MHz, DMSO-d_6): δ 1.11 (d, J = 16.0 Hz, 2H), 1.18−1.30 (m, 2H), 1.52 (t, J = 7.4 Hz, 2H), 1.72−1.85 (m, 2H), 4.03 (t, J = 6.7 Hz, 2H), 7.32 (s, 15H), 7.86 (s, 4H), 10.19 (s, 1H) ^{13}C NMR (75 MHz, DMSO-d_6): δ 24.4, 27.3, 77.5, 91.7, 123.2, 127.4, 127.5, 128.6, 129.0, 134.7, 142.5, 163.3, 170.2.

HRMS (m/z): MH$^+$ calcd for $C_{33}H_{30}N_2O_5$ 535.2227; found, 535.2237.

4.1.1.17. Synthesis of 6-(Aminooxy)-N-(trityloxy)hexanamide. **II** (2.1 g, 4.0 mmol, 1.0 equiv) was dissolved in 40 mL dichloromethane; subsequently, hydrazine monohydrate (0.4 mL, 8 mmol, 2.0 equiv) was added, and the reaction was left stirring overnight. The precipitate was filtered off, and the filtrate was washed three times with 50 mL of saturated sodium bicarbonate solution and once with 50 mL of brine. The organic phase was dried over anhydrous sodium sulfate, filtrated, and evaporated to yield the **2** (1.5 g, 3.7 mmol, 94%) as a white wax, which was suitable to use without any further purification. HPLC: tr 13.17 min purity: 96.0%.

^{1}H NMR (300 MHz, DMSO-d_6): δ 0.98 (q, J = 8.5 Hz, 2H), 1.18 (t, J = 7.6 Hz, 2H), 1.32 (q, J = 7.0 Hz, 2H), 1.77 (t, J = 7.4 Hz, 2H), 3.40 (t, J = 6.7 Hz, 2H), 5.84 (s, 2H), 7.32 (s, 15H), 10.16 (s, 1H).

^{13}C NMR (75 MHz, DMSO-d_6): δ 24.7, 25.0, 27.7, 31.9, 74.7, 91.7, 127.4, 127.5, 128.9, 142.5, 170.2.

HRMS (m/z): MH$^+$ calcd for $C_{25}H_{28}N_2O_3$ 405.2173; found, 405.2172.

4.1.2. General Procedure for the Preparation of the O-Trityl-Protected Hydroxamates ***3a−m.*** The synthesis of the *O*-trityl-protected hydroxamates was performed after an adapted protocol of Goodreid et al.[39]

After solving the corresponding phenylthiazole (**1a−m**) (1.0 equiv) in tetrahydrofuran (15 mL/mmol), an equimolar amount of 1 M sodium hydroxide solution in water was added. The reaction was monitored via TLC (eluent ethyl acetate/*n*-hexane). After complete consumption of the starting material, the solvent was evaporated under reduced pressure, and the resulting solid was dried in a vacuum. The dried product was suspended in *N*,*N*-dimethylformamide (2.2 mL/mmol). HBTU (1.1 equiv) and DIPEA (1.1 equiv) were added, and the resulting suspension was left stirring until a clear solution was formed (usually after 1 h). To that solution **2** (1.1 equiv) solved in *N*,*N*-dimethylformamide (2.2 mL/mmol) was added, and the reaction was left stirring overnight. The solvent was removed under reduced pressure, the resulting product diluted with 50 mL dichloromethane and washed three times with 50 mL of saturated sodium bicarbonate solution and three times with 50 mL of brine. The organic layer was dried over anhydrous sodium sulfate, filtrated, and the solvent was removed under reduced pressure. The obtained crude product was purified via flash chromatography, unless otherwise stated, using *n*-hexane/ethyl acetate (0−100%) as the eluent to yield the *O*-trityl-protected hydroxamates **3a−m**.

4.1.2.1. ***3a*** *N-((6-Oxo-6-((trityloxy)amino)hexyl)oxy)-4-phenylthiazole-2-carboxamide.* Synthesis according to general procedure B using **2a** (114 mg, 0.5 mmol) afforded **3a** as a white solid (150 mg, 0.25 mmol, 51%). mp 130.0 °C, t_r 17.46 min purity: 99.6%.

^{1}H NMR (600 MHz, DMSO-d_6): δ 1.11 (dd, J = 14.8, 7.9 Hz, 2H), 1.25 (dq, J = 11.3, 5.4 Hz, 2H), 1.45−1.53 (m, 2H), 1.82 (t, J = 7.3 Hz, 2H), 3.86 (t, J = 6.6 Hz, 2H), 7.26−7.38 (m, 15H), 7.40 (t, J = 7.4 Hz, 1H), 7.49 (t, J = 7.7 Hz, 2H), 8.07 (d, J = 7.3 Hz, 2H), 8.44 (s, 1H), 10.21 (s, 1H), 12.15 (s, 1H).

https://doi.org/10.1021/acs.jmedchem.4c02024
J. Med. Chem. 2024, 67, 21223−21250

^{13}C NMR (151 MHz, DMSO-d_6): δ 25.0, 25.2, 27.8, 32.4, 76.0, 92.2, 119.8, 126.8, 127.9, 128.0, 129.1, 129.3, 129.4, 133.8, 142.9, 155.9, 157.1, 162.0, 170.7.

HRMS (m/z): MNa^+ calcd for $C_{35}H_{33}N_3O_4S$ 614.2084; found, 614.2092.

4.1.2.2. ***3b*** *4-(2-Methoxyphenyl)-N-((6-oxo-6-((trityloxy)amino)-hexyl)oxy)thiazole-2-carboxamide.* Synthesis according to general procedure B using **2b** (0.8 g, 3.0 mmol) afforded **3b** as a white solid (1.7 g, 2.2 mmol, 74%). mp 190.6 °C, t_r 17.66 min purity: 98.8%.

^{1}H NMR (300 MHz, DMSO-d_6): δ 1.04−1.17 (m, 2H), 1.18−1.31 (m, 2H), 1.48 (t, J = 7.8 Hz, 2H), 1.80 (t, J = 7.0 Hz, 2H), 3.84 (t, J = 6.7 Hz, 2H), 3.94 (s, 3H), 7.03−7.13 (m, 1H), 7.17 (d, J = 8.4 Hz, 1H), 7.33 (s, 16H), 8.29−8.37 (m, 2H), 10.19 (s, 1H), 12.12 (s, 1H).

^{13}C NMR (75 MHz, DMSO-d_6): δ 24.5, 24.7, 27.3, 31.9, 55.6, 75.5, 91.7, 111.7, 120.4, 121.7, 122.6, 127.4, 127.5, 129.0, 129.7, 129.8, 142.4, 151.4, 156.6, 159.8, 170.2.

HRMS (m/z): MH^+ calcd for $C_{36}H_{35}N_3O_5S$ 622.2370; found, 622.2373.

4.1.2.3. ***3c*** *4-(3-Methoxyphenyl)-N-((6-oxo-6-((trityloxy)amino)-hexyl)oxy)thiazole-2-carboxamide.* Synthesis according to general procedure B using **2c** (0.8 g, 3.0 mmol) afforded **3c** as a white solid (1.2 g, 1.9 mmol, 62%). mp 142.8 °C, t_r 17.36 min purity: 99.3%.

^{1}H NMR (300 MHz, DMSO-d_6): δ 12.15 (s, 1H), 10.20 (s, 1H), 8.46 (s, 1H), 7.73−7.58 (m, 2H), 7.33 (d, J = 4.6 Hz, 16H), 6.96 (dd, J = 8.2, 2.6 Hz, 1H), 3.84 (d, J = 5.5 Hz, 5H), 1.81 (t, J = 6.9 Hz, 2H), 1.59−1.40 (m, 2H), 1.24 (s, 2H), 1.19−1.01 (m, 2H).

^{13}C NMR (75 MHz, DMSO-d_6): δ 24.5, 24.7, 27.3, 31.9, 55.2, 75.5, 91.7, 111.9, 114.2, 118.6, 119.6, 127.4, 127.5, 129.0, 129.9, 134.7, 142.4, 155.3, 156.5, 159.7, 161.4, 170.2.

HRMS (m/z): MH^+ calcd for $C_{36}H_{35}N_3O_5S$ 622.2370; found, 622.2373.

4.1.2.4. ***3d*** *4-(4-Methoxyphenyl)-N-((6-oxo-6-((trityloxy)amino)-hexyl)oxy)thiazole-2-carboxamide.* Synthesis according to general procedure B using **2d** (263 mg, 1.0 mmol) afforded **3d** as a white solid (150 mg, 0.24 mmol, 24%). mp 195.4 °C, t_r 17.34 min purity: 98.2%.

^{1}H NMR (300 MHz, DMSO-d_6): δ 1.11 (q, J = 7.7 Hz, 2H), 1.16−1.33 (m, 2H), 1.48 (p, J = 7.0 Hz, 2H), 1.81 (t, J = 7.3 Hz, 2H), 3.83 (d, J = 10.2 Hz, 5H), 6.99−7.08 (m, 2H), 7.33 (d, J = 4.7 Hz, 15H), 7.95−8.04 (m, 2H), 8.27 (s, 1H), 10.20 (s, 1H), 12.11 (s, 1H).

^{13}C NMR (75 MHz, DMSO-d_6): δ 24.5, 24.7, 27.3, 31.9, 55.2, 75.5, 91.7, 114.2, 117.3, 126.2, 127.4, 127.5, 127.7, 129.0, 142.5, 155.4, 156.6, 159.6, 161.3, 170.2.

HRMS (m/z): MNa^+ calcd for $C_{36}H_{35}N_3O_5S$ 644.2189; found, 644.2196.

4.1.2.5. ***3e*** *4-(2-Fluorophenyl)-N-((6-oxo-6-((trityloxy)amino)-hexyl)oxy)thiazole-2-carboxamide.* Synthesis according to general procedure B using **2e** (0.8 g, 3.0 mmol) afforded **3e** as a white solid (1.3 g, 2.1 mmol, 70%). mp 159.2 °C, t_r 17.87 min purity: 98.6%.

^{1}H NMR (300 MHz, DMSO-d_6): δ 1.00−1.18 (m, 2H), 1.24 (s, 2H), 1.47 (d, J = 8.2 Hz, 2H), 1.80 (t, J = 7.1 Hz, 2H), 3.85 (t, J = 6.6 Hz, 2H), 7.33 (s, 16H), 7.46 (dt, J = 7.9, 5.4 Hz, 1H), 8.21−8.34 (m, 2H), 10.19 (s, 1H), 12.18 (s, 1H).

^{13}C NMR (75 MHz, DMSO-d_6): δ 24.5, 24.7, 27.3, 31.9, 75.5, 91.7, 116.2 (d, J = 22.0 Hz), 121.0 (d, J = 11.5 Hz), 123.5 (d, J = 13.5 Hz), 124.8 (d, J = 3.4 Hz), 127.4, 127.5, 129.0, 130.1, 130.5 (d, J = 8.8 Hz), 142.5, 148.9, 156.4, 157.9, 161.2, 170.2.

HRMS (m/z): MH^+ calcd for $C_{35}H_{32}FN_3O_4S$ 610.2170; found, 610.2163.

4.1.2.6. ***3f*** *4-(3-Fluorophenyl)-N-((6-oxo-6-((trityloxy)amino)-hexyl)oxy)thiazole-2-carboxamide.* Synthesis according to general procedure B using **2f** (0.8 g, 3.0 mmol) afforded **3f** as a white solid (0.6 g, 1.0 mmol, 34%). mp 142.8 °C, t_r 17.85 min purity: 99.1%.

^{1}H NMR (300 MHz, DMSO-d_6): δ 1.11 (d, J = 7.2 Hz, 2H), 1.23 (d, J = 7.0 Hz, 2H), 1.48 (t, J = 7.3 Hz, 2H), 1.80 (t, J = 7.1 Hz, 2H), 3.85 (t, J = 6.6 Hz, 2H), 7.17−7.41 (m, 16H), 7.53 (td, J = 8.2, 6.2 Hz, 1H), 7.88−7.97 (m, 2H), 8.55 (s, 1H), 10.19 (s, 1H), 12.16 (s, 1H).

^{13}C NMR (75 MHz, DMSO-d_6): δ 24.7, 27.3, 75.6, 91.8, 113.3, 115.3 (d, J = 21.5 Hz), 120.6, 122.3, 127.4, 127.5, 129.0, 130.9 (d, J = 9.1 Hz), 135.7 (d, J = 8.4 Hz), 142.5, 154.0, 156.4, 161.7.

HRMS (m/z): MH^+ calcd for $C_{35}H_{32}FN_3O_4S$ 610.2170; found, 610.2173.

4.1.2.7. ***3g*** *4-(4-Fluorophenyl)-N-((6-oxo-6-((trityloxy)amino)-hexyl)oxy)thiazole-2-carboxamide.* Synthesis according to general procedure B using **2g** (253 mg, 1.0 mmol) afforded **3g** as a white solid (313 mg, 0.5 mmol, 51%). mp 163.0 °C, t_r 17.57 min purity: 99.6%.

^{1}H NMR (300 MHz, DMSO-d_6): δ 1.11 (d, J = 7.3 Hz, 2H), 1.24 (s, 2H), 1.40−1.55 (m, 2H), 1.79 (d, J = 7.5 Hz, 2H), 3.84 (t, J = 6.6 Hz, 2H), 7.24−7.41 (m, 17H), 8.06−8.15 (m, 2H), 8.41 (s, 1H), 10.18 (s, 1H), 12.13 (s, 1H).

^{13}C NMR (75 MHz, DMSO-d_6): δ 24.5, 24.7, 27.3, 31.9, 75.5, 91.7, 115.7 (d, J = 21.7 Hz), 119.1, 127.4, 127.5, 128.4 (d, J = 8.3 Hz), 128.9, 130.0 (d, J = 2.9 Hz), 142.4, 154.4, 156.5, 160.6, 161.6, 163.9, 170.2.

HRMS (m/z): MH^+ calcd for $C_{35}H_{32}FN_3O_4S$ 610.2170; found, 610.2180.

4.1.2.8. ***3h*** *N-((6-Oxo-6-((trityloxy)amino)hexyl)oxy)-4-(thiophen-2-yl)thiazole-2-carboxamide.* Synthesis according to general procedure B using **2h** (0.7 g, 3.0 mmol) afforded **3h** as a white solid (1.6 g, 2.6 mmol, 88%). mp 174.6 °C, t_r 17.23 min purity: 98.1%.

^{1}H NMR (600 MHz, DMSO-d_6): δ 1.09 (p, J = 7.9 Hz, 2H), 1.24 (p, J = 7.5 Hz, 2H), 1.47 (p, J = 7.0 Hz, 2H), 1.80 (q, J = 7.9 Hz, 2H), 3.84 (t, J = 6.6 Hz, 2H), 7.15 (dd, J = 5.0, 3.6 Hz, 1H), 7.25−7.38 (m, 15H), 7.58−7.62 (m, 1H), 7.64−7.68 (m, 1H), 8.25 (s, 1H), 10.19 (s, 1H), 12.09 (s, 1H).

^{13}C NMR (151 MHz, DMSO-d_6): δ 24.5, 24.7, 27.3, 31.9, 75.4, 91.7, 118.0, 125.4, 126.8, 127.4, 127.5, 128.1, 129.0, 136.8, 142.5, 150.3, 156.4, 161.8, 170.2.

HRMS (m/z) MH^+ calcd for $C_{33}H_{31}N_3O_4S_2$ 598.1829, found 598.1832.

4.1.2.9. ***3i*** *N-((6-Oxo-6-((trityloxy)amino)hexyl)oxy)-4-(thiophen-3-yl)thiazole-2-carboxamide.* Synthesis according to general procedure B using **2i** (665 mg, 2.8 mmol) afforded **3i** after recrystallization in *n*-hexane/ethyl acetate as a white solid (1.5 g, 2.6 mmol, 92%). mp 214.7 °C, t_r 16.91 min purity: 96.9%.

^{1}H NMR (300 MHz, DMSO-d_6): δ 1.10 (d, J = 7.2 Hz, 2H), 1.23 (d, J = 6.8 Hz, 2H), 1.46 (d, J = 7.2 Hz, 2H), 1.79 (d, J = 7.5 Hz, 2H), 3.84 (t, J = 6.6 Hz, 2H), 7.33 (d, J = 4.3 Hz, 15H), 7.62−7.73 (m, 2H), 8.01 (dd, J = 2.8, 1.5 Hz, 1H), 8.25 (s, 1H), 10.19 (s, 1H), 12.09 (s, 1H).

^{13}C NMR (126 MHz, DMSO-d_6): δ 24.9, 25.1, 27.7, 32.3, 75.9, 92.2, 119.0, 123.3, 126.7, 127.6, 127.8, 127.9, 129.3, 136.1, 142.9, 152.1, 157.0, 161.8, 170.6.

HRMS (m/z): MH^+ calcd for $C_{33}H_{31}N_3O_4S_2$ 598.1829; found, 598.1836.

4.1.2.10. ***3j*** *N-((6-Oxo-6-((trityloxy)amino)hexyl)oxy)-4-(p-tolyl)-thiazole-2-carboxamide.* Synthesis according to general procedure B using **2j** (742 mg, 3.0 mmol) afforded **3j** as a white solid (313 mg, 0.5 mmol, 17%). mp 163.2 °C, t_r 17.93 min purity: 95.1%.

^{1}H NMR (300 MHz, DMSO-d_6): δ 1.10 (d, J = 6.4 Hz, 2H), 1.23 (s, 2H), 1.46 (d, J = 7.7 Hz, 3H), 1.79 (d, J = 7.6 Hz, 2H), 2.35 (s, 3H), 3.84 (t, J = 6.6 Hz, 2H), 7.24−7.41 (m, 17H), 7.95 (d, J = 8.1 Hz, 2H), 8.36 (s, 1H), 10.19 (s, 1H), 12.11 (s, 1H).

^{13}C NMR (75 MHz, DMSO-d_6): δ 20.9, 24.5, 24.7, 27.3, 31.9, 75.5, 91.7, 118.5, 126.2, 127.4, 127.5, 129.0, 129.4, 130.7, 138.0, 142.5, 156.6, 161.4, 170.2.

HRMS (m/z): MNa^+ calcd for $C_{36}H_{35}N_3O_4S$ 628.2240; found, 628.2244.

4.1.2.11. ***3k*** *N-((6-Oxo-6-((trityloxy)amino)hexyl)oxy)-4-(4-(trifluoromethyl)phenyl)thiazole-2-carboxamide.* Synthesis according to general procedure B using **2k** (904 mg, 3.0 mmol) afforded **3k** as a white solid (499 mg, 0.8 mmol, 25%). mp 182.5 °C, t_r 19.44 min purity: 99.8%.

^{1}H NMR (300 MHz, DMSO-d_6): δ 1.11 (q, J = 7.7 Hz, 2H), 1.25 (t, J = 7.3 Hz, 2H), 1.48 (t, J = 7.4 Hz, 2H), 1.81 (t, J = 7.0 Hz, 2H), 3.85 (t, J = 6.6 Hz, 2H), 7.33 (s, 15H), 7.86 (d, J = 8.2

https://doi.org/10.1021/acs.jmedchem.4c02024
J. Med. Chem. 2024, 67, 21223−21250

Hz, 2H), 8.29 (d, J = 8.1 Hz, 2H), 8.66 (s, 1H), 10.19 (s, 1H), 12.22 (s, 1H).

^{13}C NMR (75 MHz, DMSO-d_6): δ 24.4, 24.6, 27.2, 31.7, 75.4, 91.6, 121.6, 125.7, 126.8, 127.3, 127.4, 128.8, 137.0, 142.3, 153.6, 156.3, 162.0, 170.1.

HRMS (m/z): MNa^+ calcd for $C_{36}H_{32}F_3N_3O_4S$ 682.1958; found, 682.1966.

4.1.2.12. ***3l*** *4-(Benzofuran-2-yl)-N-((6-oxo-6-((trityloxy)amino)-hexyl)oxy)thiazole-2-carboxamide.* Synthesis according to general procedure B using **2l** (547 mg, 2.0 mmol) afforded **3l** after recrystallization in dichlorormethane/ethyl acetate as a light brown solid (408 mg, 0.7 mmol, 32%). mp 200.7 °C, t_r 18.46 min purity: 97.9%.

^{1}H NMR (300 MHz, DMSO-d_6): δ 1.03−1.19 (m, 2H), 1.14−1.34 (m, 3H), 1.42−1.56 (m, 2H), 1.74−1.87 (m, 2H), 3.85 (t, J = 6.6 Hz, 2H), 7.20−7.43 (m, 18H), 7.63−7.69 (m, 1H), 7.74 (dd, J = 7.3, 1.4 Hz, 1H), 8.42 (s, 1H), 10.19 (s, 1H), 12.24 (s, 1H).

^{13}C NMR (75 MHz, DMSO-d_6): δ 24.5, 24.7, 27.3, 31.9, 75.5, 91.7, 104.0, 111.2, 121.2, 121.8, 123.5, 125.3, 127.4, 127.5, 128.1, 129.0, 142.5, 146.5, 150.5, 154.3, 156.3, 163.1, 170.2.

HRMS (m/z): MH^+ calcd for $C_{37}H_{33}N_3O_5S$ 532.2214; found, 632.2211.

4.1.2.13. ***3m*** *N-((6-Oxo-6-((trityloxy)amino)hexyl)oxy)-4-(4-(pyrrolidin-1-yl)phenyl)thiazole-2-carboxamide.* Synthesis according to general procedure B using **2m** (907 mg, 3.0 mmol) afforded **3m**, after flash chromatography with dichloromethane/30% methanol in dichloromethane as a eluent, as a yellow solid (487 mg, 0.7 mmol, 25%). mp 192.1 °C, t_r 20.03 min purity: 95.3%.

^{1}H NMR (300 MHz, DMSO-d_6): δ 1.05−1.17 (m, 2H), 1.18−1.30 (m, 2H), 1.43−1.53 (m, 2H), 1.79 (d, J = 7.2 Hz, 2H), 1.92−2.02 (m, 4H), 3.27 (q, J = 5.1 Hz, 4H), 3.84 (t, J = 6.6 Hz, 2H), 6.56−6.64 (m, 2H), 7.31 (q, J = 5.1 Hz, 15H), 7.81−7.91 (m, 2H), 8.05 (s, 1H), 10.20 (s, 1H), 12.05 (s, 1H).

^{13}C NMR (75 MHz, DMSO-d_6): δ 24.5, 24.7, 25.0, 26.3, 27.3, 31.9, 47.3, 75.5, 91.7, 111.5, 114.7, 120.7, 127.4, 127.5, 129.0, 142.5, 147.8, 156.6, 156.8, 170.2.

HRMS (m/z): MH^+ calcd for $C_{39}H_{40}N_4O_4S$ 661.2843; found, 661.2838.

4.1.2.14. General Procedure for the Preparation of the Hydroxamates ***4a−4m.*** *O*-trityl-protected hydroxamate (**4a−m**) was dissolved in DCM (30 mL/mmol). Et_3SiH (10 equiv) and TFA (10 equiv) were added successively, and the reaction was left stirring for 30 min at room temperature. After that time, the reaction mixture was purified via flash chromatography using dichloromethane and 30% methanol in dichloromethane as eluents to yield hydroxamic acids **4a−m**.

4.1.2.15. ***4a*** *N-((6-(Hydroxyamino)-6-oxohexyl)oxy)-4-phenylthiazole-2-carboxamide.* Synthesis according to general procedure C using **3a** (296 mg, 0.5 mmol) afforded **4a** as a colorless wax (240 mg, 0.41 mmol, 81%). t_r 9.32 min purity: 95.1%.

^{1}H NMR (600 MHz, DMSO-d_6): δ 1.38 (qd, J = 9.0, 6.2 Hz, 2H), 1.55 (p, J = 7.5 Hz, 2H), 1.62 (p, J = 6.8 Hz, 2H), 1.98 (t, J = 7.4 Hz, 2H), 3.94 (t, J = 6.5 Hz, 2H), 7.40 (t, J = 7.3 Hz, 1H), 7.49 (t, J = 7.7 Hz, 2H), 8.07 (d, J = 7.4 Hz, 2H), 8.43 (s, 1H), 8.68 (s, 1H), 10.37 (s, 1H), 12.18 (s, 1H).

^{13}C NMR (151 MHz, DMSO-d_6): δ 25.3, 25.5, 27.8, 32.7, 76.1, 119.8, 126.8, 129.1, 129.3, 133.8, 155.9, 157.1, 162.0, 169.5.

HRMS (m/z): MH^+ calcd for $C_{16}H_{19}N_3O_4S$ 349.1096; found, 350.1170.

4.1.2.16. ***4b*** *N-((6-(Hydroxyamino)-6-oxohexyl)oxy)-4-(2-methoxyphenyl)thiazole-2-carboxamide.* Synthesis according to general procedure C using **3b** (622 mg, 1.0 mmol) afforded **4b** as a white solid (284 mg, 0.75 mmol, 75%). mp 137.4 °C, t_r 9.84 min, purity: 99.6%.

^{1}H NMR (300 MHz, DMSO-d_6): δ 1.26−1.47 (m, 2H), 1.58 (dp, J = 22.2, 7.0 Hz, 4H), 1.97 (t, J = 7.3 Hz, 2H), 3.93 (d, J = 4.0 Hz, 5H), 7.08 (td, J = 7.5, 1.1 Hz, 1H), 7.17 (dd, J = 8.4, 1.1 Hz, 1H), 7.39 (ddd, J = 8.4, 7.3, 1.8 Hz, 1H), 8.31 (dd, J = 7.8, 1.8 Hz, 1H), 8.35 (s, 1H), 8.67 (s, 1H), 10.35 (s, 1H), 12.14 (s, 1H).

^{13}C NMR (75 MHz, DMSO-d_6): δ 24.9, 25.0, 27.4, 32.2, 55.6, 75.6, 111.8, 120.5, 121.7, 122.6, 129.8, 129.8, 151.4, 156.6, 156.7, 159.8, 169.0.

HRMS (m/z): MH^+ calcd for $C_{17}H_{21}N_3O_5S$ 380.1275; found, 380.1272.

4.1.2.17. ***4c*** *N-((6-(Hydroxyamino)-6-oxohexyl)oxy)-4-(3-methoxyphenyl)thiazole-2-carboxamide.* Synthesis according to general procedure C using **3c** (622 mg, 1.0 mmol) afforded **4c** as a yellow wax (253 mg, 0.67 mmol, 67%). t_r 9.53 min purity 99.9%.

^{1}H NMR (300 MHz, DMSO-d_6): δ 1.38 (ddd, J = 12.4, 6.0, 3.2 Hz, 2H), 1.58 (dp, J = 22.5, 7.0 Hz, 4H), 1.97 (t, J = 7.3 Hz, 2H), 3.84 (s, 3H), 3.93 (t, J = 6.4 Hz, 2H), 6.96 (ddd, J = 8.3, 2.6, 1.0 Hz, 1H), 7.39 (t, J = 7.9 Hz, 1H), 7.57−7.72 (m, 2H), 8.46 (s, 1H), 8.67 (d, J = 1.8 Hz, 1H), 10.35 (s, 1H), 12.17 (s, 1H).

^{13}C NMR (75 MHz, DMSO-d_6): δ 24.9, 25.0, 27.4, 32.2, 55.3, 75.6, 111.9, 114.2, 118.6, 119.6, 129.9, 134.7, 155.3, 156.5, 159.7, 161.3, 169.0.

HRMS (m/z): MH^+ calcd for $C_{17}H_{21}N_3O_5S$ 380.1275; found, 380.1276.

4.1.2.18. ***4d*** *N-((6-(Hydroxyamino)-6-oxohexyl)oxy)-4-(4-methoxyphenyl)thiazole-2-carboxamide.* Synthesis according to general procedure C using **3d** (1.8 g, 3.0 mmol) afforded **4d** as a white solid (603 mg, 1.59 mmol, 53%). mp 151.1 °C, t_r 9.46 min purity 98.1%.

^{1}H NMR (300 MHz, DMSO-d_6): δ 1.38 (q, J = 8.1 Hz, 2H), 1.58 (dp, J = 22.1, 7.0 Hz, 4H), 1.97 (t, J = 7.3 Hz, 2H), 3.81 (s, 3H), 3.92 (t, J = 6.4 Hz, 2H), 6.92−7.18 (m, 2H), 7.85−8.13 (m, 2H), 8.27 (s, 1H), 8.67 (d, J = 1.8 Hz, 1H), 10.35 (d, J = 1.9 Hz, 1H), 12.13 (s, 1H).

^{13}C NMR (75 MHz, DMSO-d_6): δ 24.9, 25.0, 27.4, 32.2, 55.2, 75.6, 114.2, 117.3, 126.2, 127.7, 155.4, 156.6, 159.6, 161.3, 169.0.

HRMS (m/z): MH^+ calcd for $C_{17}H_{21}N_3O_5S$ 380.1275; found, 380.1277.

4.1.2.19. ***4e*** *4-(2-Fluorophenyl)-N-((6-(hydroxyamino)-6-oxohexyl)oxy)thiazole-2-carboxamide.* Synthesis according to general procedure C using **3e** (610 mg, 1.0 mmol) afforded **4e** as an orange wax (221 mg, 0.6 mmol, 60%). t_r 9.93 min purity 99.2%.

^{1}H NMR (300 MHz, DMSO-d_6): δ 1.28−1.46 (m, 2H), 1.58 (dp, J = 22.5, 7.0 Hz, 4H), 1.97 (t, J = 7.3 Hz, 2H), 3.93 (t, J = 6.4 Hz, 2H), 7.28−7.41 (m, 2H), 7.41−7.52 (m, 1H), 8.21−8.36 (m, 2H), 8.67 (d, J = 1.8 Hz, 1H), 10.35 (d, J = 1.8 Hz, 1H), 12.21 (s, 1H).

^{13}C NMR (126 MHz, DMSO-d_6): δ 24.7, 24.9, 27.3, 32.1, 75.5, 116.1 (d, J = 22.0 Hz), 121.0 (d, J = 11.5 Hz), 123.2 (d, J = 13.4 Hz), 124.7 (d, J = 3.4 Hz), 130.0 (d, J = 2.8 Hz), 130.3 (d, J = 8.7 Hz), 148.9, 156.4, 158.4, 160.4, 161.0, 168.9.

HRMS (m/z): MH^+ calcd for $C_{16}H_{18}FN_3O_4So$ 368.1075; found, 368.1067.

4.1.2.20. ***4f*** *4-(3-Fluorophenyl)-N-((6-(hydroxyamino)-6-oxohexyl)oxy)thiazole-2-carboxamide.* Synthesis according to general procedure C using **3f** (505 mg, 0.8 mmol) afforded **4f** as a colorless wax (258 mg, 0.7 mmol, 85%). t_r 9.89 min purity 95.9%.

^{1}H NMR (300 MHz, DMSO-d_6): δ 1.30−1.48 (m, 2H), 1.46−1.70 (m, 4H), 1.97 (t, J = 7.3 Hz, 2H), 3.93 (t, J = 6.5 Hz, 2H), 7.23 (td, J = 8.6, 2.5 Hz, 1H), 7.53 (td, J = 8.1, 6.1 Hz, 1H), 7.87−7.99 (m, 2H), 8.54 (s, 1H), 8.67 (s, 1H), 10.36 (s, 1H), 12.18 (s, 1H).

^{13}C NMR (75 MHz, DMSO-d_6): δ 24.9, 25.0, 27.4, 32.2, 75.6, 113.1 (d, J = 23.6 Hz), 115.3 (d, J = 20.7 Hz), 120.5, 122.3, 130.9 (d, J = 8.5 Hz), 135.8, 154.0, 156.4, 161.0, 161.7, 164.3, 169.0.

HRMS (m/z): MH^+ calcd for $C_{16}H_{18}FN_3O_4S$ 368.1075; found, 368.1081.

4.1.2.21. ***4g*** *4-(4-Fluorophenyl)-N-((6-(hydroxyamino)-6-oxohexyl)oxy)thiazole-2-carboxamide.* Synthesis according to general procedure C using **3g** (260 mg, 0.4 mmol) afforded **4g** as a white solid (99 mg, 0.3 mmol, 63%). mp 170.7 °C, t_r 9.65 min purity 98.5%.

^{1}H NMR (300 MHz, DMSO-d_6): δ 1.38 (q, J = 7.8 Hz, 2H), 1.45−1.67 (m, 4H), 1.97 (t, J = 7.2 Hz, 2H), 3.92 (t, J = 6.4 Hz, 2H), 7.26−7.39 (m, 2H), 8.03−8.16 (m, 2H), 8.41 (s, 1H), 8.68 (s, 1H), 10.36 (s, 1H), 12.17 (s, 1H).

https://doi.org/10.1021/acs.jmedchem.4c02024
J. Med. Chem. 2024, 67, 21223−21250

^{13}C NMR (75 MHz, DMSO-d_6): δ 24.9, 25.0, 27.4, 32.2, 75.6, 115.7 (d, J = 21.6 Hz), 119.1, 128.5 (d, J = 8.3 Hz), 130.0 (d, J = 3.0 Hz), 154.4, 156.5, 160.6, 161.6, 163.9, 169.0.

HRMS (m/z): MH$^+$ calcd for $C_{16}H_{18}FN_3O_4S$ 368.1075; found, 368.1074.

4.1.2.22. ***4h*** *N-((6-(Hydroxyamino)-6-oxohexyl)oxy)-4-(thiophen-2-yl)thiazole-2-carboxamide.* Synthesis according to general procedure C using **3h** (598 mg, 1.0 mmol) afforded **4h** as a white solid (226 mg, 0.6 mmol, 63%). mp 123.4 °C, t_r 8.87 min purity 98.8%.

^{1}H NMR (300 MHz, DMSO-d_6): δ 1.28−1.47 (m, 2H), 1.44−1.75 (m, 4H), 1.97 (t, J = 7.3 Hz, 2H), 3.92 (t, J = 6.4 Hz, 2H), 7.15 (dd, J = 5.1, 3.6 Hz, 1H), 7.54−7.71 (m, 2H), 8.25 (s, 1H), 8.67 (s, 1H), 10.35 (s, 1H), 12.12 (s, 1H).

^{13}C NMR (75 MHz, DMSO-d_6): δ 24.9, 25.0, 27.4, 32.2, 75.5, 118.0, 125.4, 126.8, 128.1, 136.8, 150.3, 156.4, 161.8, 169.0.

HRMS (m/z): MH$^+$ calcd for $C_{14}H_{17}N_3O_4S_2$ 356.0733; found, 356.0735.

4.1.2.23. ***4i*** *N-((6-(Hydroxyamino)-6-oxohexyl)oxy)-4-(thiophen-3-yl)thiazole-2-carboxamide.* Synthesis according to general procedure C using **3i** (598 mg, 1.0 mmol) afforded **4i** as a white solid (198 mg, 0.6 mmol, 56%). mp 140.4 °C, t_r 8.79 min purity 98.6%.

^{1}H NMR (300 MHz, DMSO-d_6): δ 1.38 (tt, J = 11.3, 6.3 Hz, 2H), 1.58 (dp, J = 22.1, 7.0 Hz, 4H), 1.97 (t, J = 7.3 Hz, 2H), 3.92 (t, J = 6.4 Hz, 2H), 7.42−7.81 (m, 2H), 8.01 (dd, J = 2.7, 1.6 Hz, 1H), 8.25 (s, 1H), 8.67 (s, 1H), 10.35 (s, 1H), 12.12 (s, 1H).

^{13}C NMR (75 MHz, DMSO-d_6): δ 24.8, 25.0, 27.3, 32.1, 75.5, 118.7, 122.9, 126.3, 127.3, 135.7, 151.7, 156.5, 161.4, 169.0.

HRMS (m/z): MH$^+$ calcd for $C_{14}H_{17}N_3O_4S_2$ 356.0733; found, 356.0734.

4.1.2.24. ***4j*** *N-((6-(Hydroxyamino)-6-oxohexyl)oxy)-4-(p-tolyl)-thiazole-2-carboxamide.* Synthesis according to general procedure C using **3j** (606 mg, 1.0 mmol) afforded **4j** as a white solid (212 mg, 0.6 mmol, 58%). mp 134.3 °C, t_r 10.20 min purity 97.8%.

^{1}H NMR (600 MHz, DMSO-d_6): δ 1.37 (tt, J = 9.5, 6.2 Hz, 2H), 1.54 (p, J = 7.5 Hz, 2H), 1.61 (p, J = 6.7 Hz, 2H), 1.97 (t, J = 7.4 Hz, 2H), 2.35 (s, 3H), 3.92 (t, J = 6.5 Hz, 2H), 7.22−7.34 (m, 2H), 7.90−8.00 (m, 2H), 8.35 (s, 1H), 8.67 (s, 1H), 10.35 (s, 1H), 12.14 (s, 1H).

^{13}C NMR (151 MHz, DMSO-d_6): δ 20.9, 25.0, 25.0 (d, J = 9.3 Hz), 27.4, 32.2, 75.6, 118.5, 126.2, 129.4, 130.7, 138.0, 155.6, 156.6, 161.4, 169.0.

HRMS (m/z): MH$^+$ calcd for $C_{17}H_{21}N_3O_4S$ 364.1326; found, 364.1330.

4.1.2.25. ***4k*** *N-((6-(Hydroxyamino)-6-oxohexyl)oxy)-4-(4-(trifluoromethyl)phenyl)thiazole-2-carboxamide.* Synthesis according to general procedure C using **3k** (382 mg, 0.6 mmol) afforded **4k** as a light brown solid (134 mg, 0.3 mmol, 56%). mp 127.2 °C, t_r 11.278 min purity 98.5%.

^{1}H NMR (300 MHz, DMSO-d_6): δ 1.37 (qd, J = 8.7, 5.5 Hz, 2H), 1.48−1.68 (m, 4H), 1.97 (t, J = 7.3 Hz, 2H), 3.93 (t, J = 6.4 Hz, 2H), 7.86 (d, J = 8.2 Hz, 2H), 8.23−8.33 (m, 2H), 8.66 (s, 2H), 10.36 (s, 1H), 12.25 (s, 1H).

^{13}C NMR (75 MHz, DMSO-d_6): δ 24.9, 25.0, 27.4, 32.2, 75.6, 121.7, 122.4, 125.8 (d, J = 3.2 Hz), 126.0, 126.9, 127.9−129.4 (m), 137.1, 153.7, 156.4, 162.1, 169.0.

HRMS (m/z): MH$^+$ calcd for $C_{17}H_{18}F_3N_3O_4S$ 418.1043; found, 418.1041.

4.1.2.26. ***4l*** *4-(Benzofuran-2-yl)-N-((6-(hydroxyamino)-6-oxohexyl)oxy)thiazole-2-carboxamide.* Synthesis according to general procedure C using **3l** (316 mg, 0.5 mmol) afforded **4l** as a off-white solid (112 mg, 0.3 mmol, 58%). Yield 58%, mp 150.4 °C, t_r 10.70 min purity 99.3%.

^{1}H NMR (300 MHz, DMSO-d_6): δ 1.18−1.45 (m, 2H), 1.58 (dp, J = 22.2, 7.0 Hz, 4H), 1.97 (t, J = 7.3 Hz, 2H), 3.93 (t, J = 6.4 Hz, 2H), 7.25−7.43 (m, 3H), 7.66 (dq, J = 8.2, 0.9 Hz, 1H), 7.70−7.78 (m, 1H), 8.42 (s, 1H), 8.67 (d, J = 1.8 Hz, 1H), 10.35 (d, J = 1.8 Hz, 1H), 12.27 (s, 1H).

^{13}C NMR (75 MHz, DMSO-d_6): δ 24.9, 25.0, 27.4, 32.2, 75.6, 104.1, 111.2, 121.3, 121.8, 123.5, 125.3, 128.1, 146.5, 150.5, 154.3, 156.3, 163.1, 169.0.

HRMS (m/z): MH$^+$ calcd for $C_{18}H_{19}N_3O_5S$ 390.1118; found, 390.1117.

4.1.2.27. ***4m*** *N-((6-(Hydroxyamino)-6-oxohexyl)oxy)-4-(4-(pyrrolidin-1-yl)phenyl)thiazole-2-carboxamide.* Synthesis according to general procedure C using **3m** (500 mg, 0.8 mmol) afforded as **4m** a yellow solid (93 mg, 0.2 mmol, 29%). mp 136.2 °C, t_r 9.29 min purity 98.9%.

^{1}H NMR (300 MHz, DMSO-d_6): δ 1.28−1.47 (m, 2H), 1.58 (dp, J = 21.9, 6.9 Hz, 4H), 1.86−2.07 (m, 6H), 3.23−3.34 (m, 4H), 3.92 (t, J = 6.4 Hz, 2H), 6.48−6.81 (m, 2H), 7.75−8.01 (m, 2H), 8.05 (s, 1H), 8.67 (s, 1H), 10.35 (s, 1H), 12.07 (s, 1H).

^{13}C NMR (151 MHz, DMSO-d_6): δ 24.9, 25.0, 25.0, 27.4, 32.2, 47.3, 48.6, 75.5, 111.5, 114.7, 120.7, 127.4, 147.8, 156.6, 156.8, 160.8, 169.0.

HRMS (m/z): MH$^+$ calcd for $C_{20}H_{26}N_4O_4S$ 419.1748; found, 419.1746.

4.2. Biological Evaluation. *4.2.1. Enzyme Assay.* HDAC1, 2, 3, 4, 6, and 8 human recombinant enzymes were purchased from Reaction Biology Corp. (Malvern, PA). HDAC 11 was purchased from Sigma-Aldrich (Saint Louis, MO). The HDAC activity assay of HDAC1 (catalog no. KDA-21-365), 2 (catalog no. KDA-21-277), 3 (catalog no. KDA-22-278), 4 (catalog no. KDA-21-279), 6 (catalog no. KDA-21-213), 8 (catalog no. KDA-21-481), and 11 (catalog no. SRP0113) was performed in 96-well plates (Corning Incorporated, New York City, NY). Briefly, 20 ng of HDAC1, 2, 3, and 8, 2 ng of HDAC4, 17.5 ng of HDAC6, and 30 ng of HDAC11 per reaction were used. Recombinant enzymes were diluted in assay buffer (50 mM Tris−HCl, pH 8.0, 137 mM NaCl, 2.7 mM KCl, 1 mM MgCl2, and 1 mg/mL BSA). 80 μL of this dilution was incubated with 10 μL of different concentrations of inhibitors in assay buffer. After a 5 min incubation step, the reaction was started with 10 μL of 400 μM (HDAC1), 300 μM (HDAC2), 500 μM (HDAC3), 150 μM (HDAC6) Boc-Lys(Ac)-AMC (Bachem, Bubendorf, Switzerland) or 100 μM (HDAC4), 60 μM (HDAC8), 500 μM (HDAC11) Boc-Lys(TFA)-AMC (Bachem, Bubendorf, Switzerland). The reaction was stopped after 90 min by adding 100 μL stop solution 16 mg/mL trypsin, 8 μM vorinostat for HDAC1, 2, and 3, 8 μM panobinostat for HDAC4, 8, and 11, and 4 μM tubastatin for HDAC6 in 50 mM Tris−HCl, pH 8.0, and 100 mM NaCl. Fifteen min after the addition of the stop solution, the fluorescence intensity was measured at an excitation of 355 nm and emission of 460 nm in a NOVOstar microplate reader (BMG Lab-Tech, Ortenburg, Germany).

4.2.2. Cell Culture. All leukemic cell lines were cultured at 37 °C with 5% CO_2 in RPMI 1640 GlutaMax medium supplemented with 10−20% fetal bovine serum (FBS), depending on the recommendation of the German collection of microorganisms and cell culture (DSMZ). PDX samples were generated by (intravenously) injecting leukemia cells, isolated from patients into immune-deficient *NOD.Cg-Prkdcscid Il2rgtm1Wjl/SzJ* or NSG mice aged 8−12 weeks.[45,72] The transplanted leukemia cells were isolated from the spleen or the bone marrow of the mice. If the proportion of human cells was below 90%, a mouse cell depletion kit (Miltenyi Biotec) was used to enrich the human cells. Subsequently, leukemia cells (≥90% human) derived from the bone marrow and spleen of the mice were utilized to conduct a short-term ex vivo drug sensitivity assay. PDX cells were short-term cultured in RPMI 1640 GlutaMax with 15% FBS, 0.1 mM 2- Mercaptoethanol, 1 mM Sodium Pyruvate, and Gentamicin 0.5 μg/mL. All animal experiments were conducted in accordance with the regulatory guidelines of the official committee at LANUV (Akt. 81-02.04.2017.A441), under the authorization of the animal research institute (ZETT) at the Heinrich Heine University Düsseldorf. Patient samples were received after obtaining informed consent in accordance with the Declaration of Helsinki. The experiments were approved by the ethics committee of the medical faculty of the Heinrich Heine University (Study no.: 2019-566).

https://doi.org/10.1021/acs.jmedchem.4c02024
J. Med. Chem. 2024, 67, 21223−21250

4.2.3. High Throughput Drug Screening. All compounds were used in 10 mM stock solutions and dissolved in DMSO.[45] Drug screening plates were preprinted with the Tecan D300e in 384 or 1536 well plates. To avoid plate effects, all plates were randomized, and all wells were further on normalized to the highest DMSO volume on the plate. Plates were stored at −80 °C and thawed 1 h prior to the experiment. Cells concentration and viability was determined via the Vi-CELL BLU cell counter. Only if cells exceeded 90% viability they were deemed acceptable for seeding. Cell lines were seeded at a concentration of 0.04×10^6 cells/mL in 384 well plates or at 0.5×10^6 cells/mL in 1536 well plates, while PDX samples were seeded in 1536 well plates at 1.5×10^6 cells/mL via the Multidrop reagent dispenser. The seeded plates were incubated for 72 h and subsequently evaluated via CellTiter-Glo. A Tecan Spark microplate reader was used to measure the emerging luminescence.

Initial IC_{50} determination of all experimental compounds was done in 11 concentrations (from 0.005 to 25 μM) three times with the three cell lines, K562 (CML), HL60 (AML), and HPBALL (T-ALL). The viability was determined in relation to the DMSO controls, and IC_{50} was calculated via Prism (log(inhibitor) vs normalized response − Variable slope). Screening with commercially available inhibitors was done in 6 concentration from 0.005−25 μM. Viability and inhibition curves were determined in the same way. DSS was calculated via the R package *DSS*. The dDSS was calculated by subtracting the DSS value of five healthy controls from the leukemia value. Significance was calculated by comparing all dDSS values of two drugs in a one-way Anova test. Heatmaps were generated via the complex heatmap package.

4.2.4. Synergy Drug Screening. Drug synergy was investigated by a matrix screening approach. Plates were designed by combining each concentration of drug A with each concentration of drug B. All drugs were printed in 8 concentrations on 384 well plates. (**4d**: 0.025−0.75 μM, **4m**: 0.005−0.35 μM, decitabine and clofarabine 0.005−5 μM). HL60 were seeded with a concentration of 0.1×10^6 cells/ml and afterward processed by the previously described protocol.[26] After the viability calculation, ZIP scores were generated through the "SynergyFinder" package.

4.2.5. Immunoblotting. Leukemia cells were treated with the indicated concentrations for 24 h. Afterward, the cells were collected and washed three times with cold PBS and, in the end, snap frozen with liquid nitrogen. Cells were lysed in Pierce RIPA buffer (with cOmplete Protease Inhibitor cocktail, PhosSTOP & Dithiothreitol), and DNA was removed via high speed centrifugation. The protein concentration was determined via the BCA assay. Protein lysates were diluted via 5× laemmli buffer and denatured at 95 °C for 5 min. Into every pocket of a 10% acryl amid gel, a volume with 20 μg of protein was added. SDS-Page were run for 90 min at 100 mV in 1× running buffer. The proteins were transferred with 1× transfer buffer with 10% methanol onto nitrocellulose membranes at 100 mV for 90 min.

The membranes were blocked with 3% BSA in Tris buffered saline with Tween for 1 h. The membranes were incubated overnight at 4 °C with primary antibodies, including antiacetyl-α-tubulin (catalog no. 5335), antiacetyl-histone H3 (catalog no. 9677S), anticleaved PARP (catalog no. 9541), and anti-GAPDH (catalog no. 97166), following the manufacturer's guidelines (Cell Signaling Technology). Signals were quantified via ImageJ and divided by the signal of the housekeeper.

4.2.6. Caspase 3/7 and Trypan Blue Assay. At a concentration of 0.25 μM, either **4d** or **4m** was introduced to wells containing HL60 leukemia cells. Additionally, compounds were coadministered with a caspase inhibitor Q-VD at a concentration of 10 μM in separate wells. Control conditions encompassed wells treated solely with DMSO or exclusively with Q-VD. Each experimental condition was executed in quadruplicate. Following a 24 or 48 h incubation period, the cells underwent treatment with a Caspase 3/7 Kit (Promega), and luminescence was quantified using the Tecan Spark microplate reader. In parallel, the identical cell solutions was dispensed into 24-well plates, and cell enumeration was conducted employing the Vi-CELL BLU (Beckman Coulter) cell counter after 24 or 48 h.

4.2.7. Cell Cycle Analysis. HL60 cells were plated in a concentration of 0.1×10^6 cells/ml in 12 well plates with a volume of 1.5 mL. Both **4d** and **4m** were added to the cultures at 0.15 or 0.20 μM. After 24 h of incubation, the cells were centrifuged and incubated with 0.2 mL Nicoletti assay buffer (0.1% trisodium citrate dehydrate, 0.1% Triton X-100, 50 μg/mL propidium iodide, 0.5 mg/mL RNase A). The solution was incubated 15 min at 4 °C and afterward measured via CytoFLEX (Beckman Coulter).

4.3. Molecular Modeling Studies. *4.3.1. Molecular Docking.* The cryo-EM structures of HDAC2 (PDB-ID: 7KBG),[42] HDAC4 (PDB-ID: 2VQM),[73] and HDAC8 (PDB-ID: 1T69)[74] were prepared for molecular docking using the Protein Preparation Wizard as implemented in the Maestro GUI of the Schrödinger Suite version 2024-1. Protonation states for Asp, Glu, His, and Lys, tautomers for His, and chi flips for Asp, Glu, and His were calculated at pH 7.0 ± 2.0 using the PROPKA[75] implementation within Maestro. A restrained energy minimization was performed focusing only on hydrogen atoms. Three-dimensional structures of the ligands **4a**−**4m** and vorinostat were generated and prepared using the LigPrep module in Maestro. Docking studies were performed with Glide (Schrödinger Release 2024-1) using the Glide XP docking protocol,[40] generating 75 poses for each ligand.

4.3.2. Effective Binding Energy Computations. To estimate relative affinities of compounds **4d** and **4m**, the best scoring pose of each ligand in HDAC2 was postprocessed using the MM-GBSA method in Prime with the VSGB 2.1 solvation model.[76] Side-chain flexibility of the protein was considered for all residues within 8 Å of the ligand pose.

4.4. Structure Determination. *4.4.1. Protein Preparation.* CD2 from *Dr*HDAC6 was recombinantly expressed using His_6-MBP-TEV-HDAC-pET28a(+) vector and purified as previously described with minor modifications.[77] Briefly, HDAC6 was expressed using the *Escherichia coli* strain BL21(DE3) grown in 2× yeast extract tryptone media (2YT) supplemented with 0.02 M glucose and kanamycin (50 mg/mL). Expression was induced at an optical density at 600 nm (OD_{600}) of 1.5 with 0.1 mM isopropyl-β-D-1-thiogalactopyranoside (IPTG) along with the addition of 0.2 mM zinc sulfate. Cultures were then incubated at 20 °C overnight and harvested by centrifugation.

To isolate the protein, cells were resuspended in wash buffer (50 mM K_2HPO_4/KH_2PO_4 pH 8.0, 300 mM NaCl, 5% Glycerol, 1 mM TCEP) and lysed by sonication. The crude lysate was clarified by centrifugation and then applied to a Protino Ni-NTA 5 mL column (Macherey-Nagel, Düren, Germany) using an ÄKTA Go system (Cytiva, Marlborough, Massachusetts, United States). The His_6-MBP-TEV-HDAC6 fusion protein was eluted using 150 mM imidazole. The fractions containing protein were combined, and the buffer exchanged with wash buffer. To remove the maltose binding protein and the affinity tag from the fusion protein TEV cleavage was performed. TEV cleavage was performed by adding the protease in a ratio of 1:10 in a buffer containing 1 mM DTT and 0.5 mM EDTA at 4 °C overnight. Subsequently, the solution was applied to an HisTrap Excel 5 mL column (Cytiva). Fractions were collected while washing the column with 10 mM imidazole. The volume of the combined fractions was reduced, and the solution loaded onto an HiLoad 16/600 Superdex 75 pg column (Cytiva). The column was washed with buffer (50 mM HEPES, 100 mM KCl and 5% Glycerol, pH 7.5). The purity of the target protein was monitored throughout using SDS-PAGE.

4.4.2. Crystallization. All HDAC6−inhibitor complexes were crystallized in sitting drops by the vapor diffusion method at 18 °C. For cocrystallization of the inhibitors with HDAC6, the protein solution (14.7 mg/mL in 50 mM HEPES, 100 mM KCl, and 5% Glycerol, pH 7.5) was incubated with 2 mM inhibitor. Then, 1 μL of the HDAC6−inhibitor complex solution was mixed with 1 μL of a reservoir solution. The structure of the HDAC6−**4d** complex was determined from a crystal obtained in 0.1 M sodium acetate, pH 8.7, 0.1 M sodium formiate, and 28% PEG3350. The structure of

https://doi.org/10.1021/acs.jmedchem.4c02024
J. Med. Chem. 2024, 67, 21223−21250

the HDAC6−**4m** complex was determined from a crystal obtained in 0.1 M sodium acetate, pH 8.7, 0.1 M sodium formiate, and 22% PEG3350. Crystals were harvested after 6 weeks and flash frozen in liquid nitrogen using a 50% aqueous PEG3350 solution as the cryoprotectant.

4.4.3. Data Collection and Structure Determination. X-ray diffraction data was collected at 100 K using synchrotron radiation on beamline MASSIF-3 (ID30A-3) at the European Synchrotron Radiation Facility, Grenoble, France.[78,79] The data was processed using XDS,[80] molecular replacement, and structure refinement were performed using CCP4i2.[81] Data reduction was performed with AIMLESS,[82] and molecular replacement was performed using Phaser[83] with the coordinates of CD2 of HDAC6 from *D. rerio* in complex with trichostatin A (TSA) (PDB ID: 5WGI).[77] Model building and refinement were performed with Coot[84] and Refmac.[85] PyMOL[86] was used to prepare the figures and to calculate the root-mean-square deviation (RMSD) of the Cα atoms using the align command with the number of cycles set to 0, thus, not including outlier rejection. The atomic coordinates have been deposited with the Protein Data Bank, Research Collaboratory for Structural Bioinformatics at Rutgers University (PDB ID: 9GGH and 9GGK). Authors will release the atomic coordinates upon article publication.

4.5. In Vitro Pharmacokinetics. *4.5.1. LC−MS/MS Method.* For the determination of in vitro pharmacokinetics of **4d** and **4m**, a tailored liquid chromatography coupled with tandem mass spectrometry (LC−MS/MS) assay was developed. Chromatographic separation was performed using a Luna Pentafluorophenyl (PFP (2)) column (100.0 × 2.0 mm; 3 μm; Phenomenex Ltd., Aschaffenburg, Germany). For the mobile phase, 0.1% FA in water (v/v) and 0.1% FA in methanol (v/v, B) were applied. Gradient separation at a flow rate of 0.4 mL/min was used, involving the following steps: 0.0−1.5 min: 5% B, 1.5−2.5 min: 5%−20% B, 2.5−4.5 min: 20%−95% B, 4.5.−7.5 min: 95% B, and 7.5−8.0 min: 95%−5% B. The injection volume was set to 20 μL, and the column oven was maintained at 60 °C. A TSQ Quantum Ultra triple quadrupole mass spectrometer (Thermo Fisher Scientific, Waltham, Massachusetts) with an ESI interface was used for the mass spectrometric detection. A spray voltage of 4000 V and a capillary temperature of 300 °C were applied. The vaporizer temperature was maintained at 380 °C, the sheath gas at 50 au, aux gas pressure at 5 au and ion sweep gas at 1.0 au. Argon was utilized as the collision gas with a pressure of 1.6 mTorr. **4j** was used as the internal standard for **4d** and **4m**, while deuterated standards were used for the control compounds in the respective in vitro pharmacokinetic assays. The following multiple reaction monitoring transitions with their collision energy and tube lens voltage (TL) were monitored in the positive ion mode: **4d**: 380.23 → 175.0 mass-to-charge ratio (m/z) (CE: 40 V, TL: 96 V), **4m**: 419.19 → 229.1 m/z (CE: 26 V, TL: 100 V), 4j: 364.15 → 217.1 m/z (CE: 17 V, TL: 158 V), Carvedilol: 407.04 → 224.07 m/z (CE: 22 V, TL: 150 V), Carvedilol d5 CE: 412.28 → 229.1 m/z (CE: 23 V, TL: 116 V), Propranolol 260.0 → 155.0 m/z (CE: 24 V, TL: 86 V), Propranolol d7 267.18 → 116.12 m/z (CE: 20 V, TL: 88 V), Itraconazol 705.4 → 392.18 m/z (CE: 34 V, TL: 154 V), Itraconazol d4 709.6 → 396.23 m/z (CE: 36 V, TL: 165 V).

4.5.2. Distribution Coefficient (log D). The log D determination was based on the shake flask method optimized for mass spectrometric analysis.[87] The distribution of test compounds was investigated between buffer presaturated octanol and octanol-presaturated 0.1 M potassium phosphate buffer pH 7.4. A 10 mM solution of the test compounds in DMSO and the control carvedilol were diluted 1:100 in buffer. A 200 μL aliquot was directly taken and 1:1 diluted in acetonitrile (v/v, standard). To the residual buffer volume, octanol was added in different v/v ratios: 1:0.1, 1:0.01, 3:0.01, and 5:0.01. Samples were shaken for 1 h to reach equilibrium before the two phases were separated by centrifugation at 13.200g for 10 min. Determinations were performed in triplicate for each compound from the aqueous phase. For the calculation of log D, the buffer/octanol v/v ratio was used in which the amount of drug was most similar in order to obtain the most precise measurement. The log D was then calculated by the following eq 1:

Calculation of log D. A_{St}: area ratio standard, A_w: area ratio after partition, V_w: volume aqueous phase, and V_o: volume octanol.

$$\log D = \log\left(\left(\frac{A_{St}}{A_w} - 1\right)\frac{V_w}{V_o}\right) \quad (1)$$

4.5.3. Plasma Stability. Ex vivo plasma stability was studied in fresh human plasma at 37 °C. Plasma was prewarmed to 37 °C, and reactions were started by spiking **4d** and **4m** to the plasma to a final concentration of 1 μM, 50 nM, and 2.5 nM. Sample aliquots of 100 μL were taken at 0, 30, 60, 120, 240, and 360 min and after 24 h. Each aliquot was mixed with 300 μL ice-cold acetonitrile containing the internal standards and directly vortexed, followed by 15 min shaking at 800 rpm at room temperature. Then, samples were centrifuged for 5 min at 13.200g. 300 μL of the supernatant was evaporated to dryness under heated nitrogen stream at 50 °C. Samples were stored at 4 °C, until completion of the assay and reconstituted in 100 μL 50/50 acetontitrile/water (v/v). This customized sample preparation protocol was characterized by good recoveries of 104.7 ± 6.7% for **4d** and 104.5 ± 6.6% for **4m** and low matrix effects of less than 11% for both compounds. The assay was conducted in triplicate. As a control, the compounds were incubated in 4% BSA to identify potential enzyme-related degradation in plasma. In vitro plasma half-life ($t_{1/2}$) was calculated by $t_{1/2} = \ln 2/k_e$, where k_e is the slope in the linear fit of the natural logarithm of the fraction remaining of the parent compound vs incubation time.

4.5.4. Blood-To-Plasma Ratio. The blood-to-plasma ratio ($K_{B/P}$) was determined to investigate the drug binding to erythrocytes. Therefore, freshly drawn whole blood was spiked to a final concentration of 1 μM, 50 nM, and 2.5 nM and cautiously shaken to avoid lysis and incubated at 37 °C for 30 min. Spiked whole blood was centrifuged at room temperature for 10 min at 2,000g, and the obtained plasma was used for analysis. Additionally, plasma was directly spiked to a final concentration of 1 μM, 50 nM, and 2.5 nM and also incubated for 30 min at 37 °C (reference plasma; not considering distribution into the red blood fraction). 100 μL of reference plasma and of plasma separated from spiked whole blood were precipitated with 300 μL of ice-cold acetonitrile containing 3.33 ng/mL of the internal standards. Following immediate vortexing, samples were shaken for 15 min at 800 rpm at room temperature. Subsequently, samples were centrifuged for 5 min at 13,200g and 300 μL of the supernatant was evaporated to dryness under a heated nitrogen stream at 50 °C. The residue was reconstituted in 100 μL 50/50 acetonitrile/water (v/v). Whole blood and plasma of two donors (male and female) in three independent replicates were used for the analysis. Carvedilol was used as a control compound with known $K_{B/P}$. The hematocrit was determined volumetrically. The blood-to-plasma-ratios were calculated according to eqs 2 and 3:[88,89]

Calculation of the Red blood cell partitioning coefficient. H: hematocrit; $K_{e/p}$: red blood cell partition coefficient, pref: reference plasma; and p: plasma separated from spiked whole blood.

$$K_{e/p} = \frac{1}{H} x \left(\frac{\text{Area ratio}_{pRef}}{\text{Area ratio}_{p}} - 1\right) + 1 \quad (2)$$

Calculation of the Blood-to-plasma ratio ($K_{e/p}$). H: hematocrit; $K_{e/p}$: red blood cell partition coefficient.

$$K_{b/p} = (K_{e/p} \times H) + (1 - H) \quad (3)$$

4.5.5. Plasma Protein Binding. Plasma protein binding was determined using equilibrium dialysis. A 20% ethanol regenerated dialysis membrane with a molecular weight cutoff of 6 kDa (Reichelt Chemietechnik GmbH + Co, Heidelberg, Germany) was placed into a 96-well dialysis apparatus to obtain two chambers. 150 μL of plasma spiked to a final concentration of 1 μM, 50 nM, and 2.5 nM

https://doi.org/10.1021/acs.jmedchem.4c02024
J. Med. Chem. 2024, 67, 21223−21250

of the test compounds and 150 μL of 0.9% saline were added to the respective sides of the 96-well dialysis plate; wells were sealed and the plate was placed into an incubator at 37 °C to dialyze for 24 h. Following 24 h of incubation, 100 μL of plasma were removed, directly precipitated with ice-cold acetonitrile containing the internal standards, and prepared as described above. 100 μL of methanol with internal standards was added to the saline at the acceptor chamber to keep the compounds dissolved before taking the respective aliquot. Plasma protein binding was analyzed in three independent replicates and itraconazole was used as a control in each chamber to account for potential leaking of the dialysis membrane. Plasma protein binding was calculated according to eq 4, where f_b is the fraction bound, c_{te} is the total plasma drug concentration at equilibrium, c_f is the free drug concentration of the acceptor side, V_{pi} is the initial plasma volume, and V_{pe} is the equilibrium plasma volume.[90]

Calculation of drug fraction bound.

$$f_b\ [\%] = \frac{(c_{te} - c_f) \times \frac{V_{pe}}{V_{pi}}}{\left[(c_{te} - c_f) \times \frac{V_{pe}}{V_{pi}}\right] + c_f} \times 100 \tag{4}$$

To determine plasma protein binding >99% more accurately, the dilution method was applied.[91] For this purpose, a 1:10 and a 1:20 dilution of plasma in 0.9% saline was additionally used as the donor. The diluted plasma was spiked to a final concentration of 1 μM, 50 nM, and 2.5 nM of **4d** and **4m** and incubated with 0.9% saline in the acceptor chamber for 24 h at 37 °C. Sample purification was performed as for the classical approach. Calibration curves from 1:10 and 1:20 diluted plasma were used to determine the corresponding donor concentrations. Plasma protein binding was analyzed in triplicates. As a control, the plasma protein binding of itraconazole was determined. Plasma protein binding was calculated according to eqs 5, 6, and 7 where f_u is the fraction unbound and D is the dilution level of the plasma.

Calculation of diluted fraction unbound. $f_{u,d}$: free fraction from diluted plasma.

$$f_{u,d}\ [\%] = \left(1 - \frac{(c_{te} - c_f) \times \frac{V_{pe}}{V_{pi}}}{\left[(c_{te} - c_f) \times \frac{V_{pe}}{V_{pi}}\right] + c_f}\right) \times 100 \tag{5}$$

Calculation of undiluted fraction unbound. D: plasma dilution factor, f_u: fraction unbound, $f_{u,d}$: fraction unbound from diluted plasma.

$$\text{Undiluted } f_u = \frac{\frac{1}{D}}{\left[\left(\frac{1}{f_{u,d}}\right) - 1\right] + \frac{1}{D}} \tag{6}$$

Calculation of undiluted fraction bound.

$$\text{Undiluted } f_b\ [\%] = (1 - f_u) \times 100 \tag{7}$$

4.5.6. Microsomal Stability. HLMs were used to determine microsomal stability using the cosolvent method. For this purpose, 905 μL of 0.1 M potassium phosphate buffer pH 7.4 and 25 μL of 20 mg/mL pooled (from 150 donors) HLMs (Corning, New York, USA) were added and gently inverted for mixing. 10 μL of a 100 μM working solution for **4d**, **4m**, and the control compound propranolol in acetonitrile/DMSO 80/20 (v/v) was added and gently inverted for three times. 47 μL of this mix was aliquoted into three reaction tubes per time point. To start the reaction, 3 μL of a freshly prepared mix of 125 μL NADPH Regenerating System Solution A and 25 μL NADPH Regenerating System Solution B (Corning, New York, USA) was added. The tubes were incubated at 37 °C and 300 rpm, and reactions were stopped at the time points 0, 15, 30, 45, and 60 min by adding 150 μL of ice-cold acetonitrile (containing 100 ng/mL of the internal standards). Each sample was directly vortexed and placed on ice. Following, samples were centrifuged at 13,200*g* for 10 min, and the supernatant was diluted 1:10 with acetonitrile/water 50/50 (v/v). A negative control (no HLMs) and a blank (no analytes) were used as controls besides propranolol. First-order kinetics was used to calculate half-life ($t_{1/2}$) and intrinsic clearance (Cl_{int}) (eqs 8 and 9).

Calculation of half-life ($t_{1/2}$). k_e: elimination rate constant.

$$t_{1/2} = \frac{\ln 2}{k_e} \tag{8}$$

Calculation of intrinsic clearance. $t_{1/2}$: half-life.

$$Cl_{int}\ [\mu L/\text{min}/\text{mg protein}] = \frac{\ln(2)}{t_{1/2}} \times \frac{\text{volume of incubation } [\mu L]}{\text{protein amount in incubation } [mg]} \tag{9}$$

The elimination rate constant (k_e) was determined as the negative slope of the plotted natural logarithm of the test compound peak area ratio versus time.

To correct for nonspecific binding in the HLM incubation, plasma protein binding of **4d** and **4m** to HLMs was determined by equilibrium dialysis. The procedure was conducted as described above, replacing plasma by a 0.5 mg/mL HLM mixture (no NADPH). The unbound intrinsic clearance, which is solely influenced by the activity of metabolizing enzymes, was calculated (eq 10).

Calculation of unbound intrinsic clearance. Cl_{int}: intrinsic clearance and f_{umic}: unbound fraction microsomal incubation.

$$\text{Unbound } Cl_{int} = \frac{CL_{int}}{f_{u_{mic}}} \tag{10}$$

4.5.7. In Vitro–In Vivo Extrapolation of Hepatic Clearance. The in vivo hepatic clearance of **4d** and **4m** was estimated using the in vitro determined $K_{B/P}$, unbound intrinsic clearance, and plasma protein binding at 50 nM according to eq 11. A hepatic blood flow of 1500 mL/min was used for calculation, displaying the normal value in the healthy male.[92] In addition, the hepatic extraction ratio was calculated according to eq 12. Drugs with an extraction ratio <0.3 were classified as low hepatic extraction drugs, 0.3–0.7 as intermediate hepatic extraction drugs, and >0.7 as high hepatic extraction drugs.

Calculation of hepatic clearance. Cl_H: hepatic clearance, $Cl_{int,u}$: unbound intrinsic clearance, f_u: fraction unbound in plasma, $K_{B/P}$, blood-to-plasma ratio, and Q_H: hepatic blood flow.

$$Cl_H = Q_H \times \frac{\frac{f_u}{K_{B/P}} \times Cl_{int,u}}{Q_H + \frac{f_u}{K_{B/P}} \times Cl_{int,u}} \tag{11}$$

Calculation of the hepatic extraction ratio (E_H). Cl_H: hepatic clearance and Q_H: hepatic blood flow.

$$E_H = \frac{Cl_H}{Q_H} \tag{12}$$

4.5.7.1. Preclinical Pharmacokinetic Study and Assessment. The pharmacokinetics of **4d** were assessed (by Pharmacelsus GmbH) following a single intraperitoneal dose (10 mg/kg) in C57BL/6 mice. Blood samples were collected from the tail vein of C57BL/6 mice at 0.25, 0.5, 1, 2, 4, 7, and 24 h post dose. The pharmacokinetic parameters were calculated based on the concentration time profiles of three mice using a standard NCA method. The maximum concentration (C_{max}) and the time to reach C_{max} (t_{max}) were directly acquired from the concentration–time curves. The apparent elimination half-life ($t_{1/2}$) was calculated as $0.693/\lambda z$, where λz was the elimination rate constant calculated by linear regression of the terminal linear portion of the ln-concentration–time curve. The area under the plasma concentration–time curve (AUC) from time 0 to the last time point (AUC_{last}) was calculated

https://doi.org/10.1021/acs.jmedchem.4c02024
J. Med. Chem. 2024, 67, 21223–21250

using the linear trapezoidal rule method. The AUC from 0 to infinity (AUC_{inf}) was calculated as AUC_{last} + Ct/λz, where Ct is the last measurable concentration. Oral clearance (CL/F) was calculated as dose/AUC_{inf}, and apparent volume of distribution (V_d/F) was obtained by dividing CL/F by λz.

4.5.7.2. Animal Experiment. The periclinal animal experiments were conducted to evaluate the therapeutic efficacy of **4d** on two in vivo leukemic mouse models encompassing cell line -derived xenograft (CDX) and mouse tumor allografts.

A CDX model was constructed by transplanting MV4-11 (DSMZ, no. ACC 102), a human AML cell line, into immunodeficient mice. MV4-11 cells were maintained in RPMI 1640 medium supplemented with 20% FBS. Luc-GFP-expressing MV4-11 cells were generated by lentiviral transduction with the luciferase reporter gene.[93] MV4-11 cells were maintained in RPMI 1640 medium supplemented with 20% FBS. MV4-11 GFP-Luc (0.5×10^6) cells were intravenously injected into 6 to 8 weeks old immunodeficient NSG mice (NOD.Cg-Prkdcscid Il2rgtm1Wjl/SzJ, Jackson laboratory). Engraftments of the leukemia cells was verified by the in vivo imaging system (IVIS Spectrum In Vivo Imaging System, PerkinElmer) 14 days after injection. The leukemia bearing mice were randomly divided to two treatment groups (4 mice/group), vehicle control (10% DMSO$^+$ 18% PEG300 + 5% TWEEN 20$^+$ 68% dH_2O), and compound **4d** (10 mg/kg). Starting from day 16, a total of 8 daily doses were administered through intraperitoneal (i.p.) injections.

A murine cell line-derived syngeneic model was constructed by transplanting C1498 (ATCC, TIB-49), an AML cell line that originated from a female C57BL/6 mouse, into immunocompetent mice.[70] C1498 cells were maintained in RPMI 1640 medium supplemented with 20% FBS. Luc-GFP-expressing C1498 cells were generated according to methods described above. C1498 GFP-Luc (0.5×10^6) cells were intravenously injected into 6 weeks old male C57BL/6J mice (Janvier). Verification of leukemic engraftments was done with IVIS imaging 5 days after tumor inoculation. The tumor-bearing mice were randomly divided into three treatment groups (4 mice/group), namely vehicle control, vorinostat (HDACi) (20 mg/kg), and compound **4d** (20 mg/kg). From day 6 to 10, daily treatments were administered i.p. for 5 consecutive days, followed by an IVIS imaging on day 11 and another successive 5 day treatment course. Body weight from each mouse was recorded every day. Treatment efficacy and tumor progression were monitored by means of IVIS and quantification of ROI values (radiance, p/s/cm^2/sr). The animal experiments were conducted in accordance with the regulatory guidelines of the official committee at LANUV, under the authorization of the animal research institute (ZETT) at the Heinrich Heine University Düsseldorf.

4.5.7.3. Flow Cytometry. In order to investigate changes in intracellular expression levels of histone 3 acetylation upon compound **4d** treatment, C1498 tumor-bearing C57B6/LJ mice were treated with vehicle or **4d** (20 mg/kg). For preparation of mice liver cells, liver tissue of vehicle or **4d** (20 mg/kg) treated mice were excised 12 h post treatment administration. The liver cells were isolated by smashing and filtering the liver tissue through a 40 μm cell strainer filter (Greiner cat. no. 542040). Erythrocyte lysis was performed by washing the cells once in ammonium chloride isotonic buffer. The liver cells acquired from both vehicle control or **4d** treated mice were harvested and fixed with fixation/permeabilization concentrate (Invitrogen cat. no. 00-5123-43) for 30 min at room temperature in the dark and were washed with permeabilization buffer (Invitrogen cat. no. 00-8333-56). Afterward, the cells were stained with Acetyl-Histone H3 (Lys9) antibody (Cell signaling, cat. no. 9649) for 3 h at room temperature in the dark. After incubation, the cells were washed again with the permeabilization buffer and stained with the 1:300 diluted Cyanine3 Donkey antirabbit IgG antibody (BioLegend, cat. no. 406402), and were then suspended in FACS buffer (PBS, 1% FCS, 5 mM EDTA) for flow cytometric analysis. Flow cytometry was performed by utilizing the Beckman Coulter CytoFLEX Cytometer, and the results were analyzed with FlowJo software.

■ ASSOCIATED CONTENT

Supporting Information

The Supporting Information is available free of charge at https://pubs.acs.org/doi/10.1021/acs.jmedchem.4c02024.

Simulated annealing omit map of **4d** and **4m** in the CD2 of *D. rerio* HDAC6 data collection and refinement statistics, comparison of the cytotoxic data of compounds **4a**−**4m** in a heatmap format effectiveness of **4d** in a MV4-11 leukemia xenograft mouse model, Western blot showing induction of ac-H3 in the C1498 cell line Histogram plot of ac-H3 intracellular staining in liver cells from C1498 tumor bearing mice, and NMR spectra and HPLC traces of synthesized compounds Raw IC_{50}, DSS, and dDSS values (PDF)

Molecular formular strings (CSV)

Atomic coordinates of HDAC2_4a_noH (PDB)

Atomic coordinates of HDAC2_4m_noH (PDB)

■ AUTHOR INFORMATION

Corresponding Authors

Sanil Bhatia − *Department of Pediatric Oncology, Hematology and Clinical Immunology, Medical Faculty, Heinrich Heine University Düsseldorf, 40225 Düsseldorf, Germany*; orcid.org/0000-0001-6494-7744; Phone: (+49) 211 81 04896; Email: sanil.bhatia@med.uni-duesseldorf.de; Fax: (+49) 211 81 16436

Thomas Kurz − *Institute of Pharmaceutical und Medicinal Chemistry, Heinrich Heine University Düsseldorf, 40225 Düsseldorf, Germany*; orcid.org/0000-0002-9474-4224; Phone: (+49) 211 81 14894; Email: thomas.kurz@hhu.de

Authors

Fabian Fischer − *Institute of Pharmaceutical und Medicinal Chemistry, Heinrich Heine University Düsseldorf, 40225 Düsseldorf, Germany*

Julian Schliehe-Diecks − *Department of Pediatric Oncology, Hematology and Clinical Immunology, Medical Faculty, Heinrich Heine University Düsseldorf, 40225 Düsseldorf, Germany*

Jia-Wey Tu − *Department of Pediatric Oncology, Hematology and Clinical Immunology, Medical Faculty, Heinrich Heine University Düsseldorf, 40225 Düsseldorf, Germany*

Tanja Gangnus − *Individualized Pharmacotherapy, Institute of Pharmaceutical and Medicinal Chemistry, University of Münster, 48149 Münster, Germany*; orcid.org/0009-0005-7573-6631

Yu Lin Ho − *Institute of Pharmaceutical und Medicinal Chemistry, Heinrich Heine University Düsseldorf, 40225 Düsseldorf, Germany*

Mara Hebeis − *Bioinorganic Chemistry, Friedrich-Alexander-Universität Erlangen-Nürnberg, 91058 Erlangen, Germany*

Leandro A. Alves Avelar − *Institute of Pharmaceutical und Medicinal Chemistry, Heinrich Heine University Düsseldorf, 40225 Düsseldorf, Germany*

Katerina Scharov − *Department of Pediatric Oncology, Hematology and Clinical Immunology, Medical Faculty, Heinrich Heine University Düsseldorf, 40225 Düsseldorf, Germany*

Titus Watrin − *Department of Pediatric Oncology, Hematology and Clinical Immunology, Medical Faculty,*

Heinrich Heine University Düsseldorf, 40225 Düsseldorf, Germany; orcid.org/0009-0003-2665-9639

Marie Kemkes − *Department of Pediatric Oncology, Hematology and Clinical Immunology, Medical Faculty, Heinrich Heine University Düsseldorf, 40225 Düsseldorf, Germany*

Pawel Stachura − *Department of Pediatric Oncology, Hematology and Clinical Immunology, Medical Faculty, Heinrich Heine University Düsseldorf, 40225 Düsseldorf, Germany; Department of Molecular Medicine II, Medical Faculty, Heinrich Heine University, 40225 Düsseldorf, Germany*

Katharina Daugs − *Department of Pediatric Oncology, Hematology and Clinical Immunology, Medical Faculty, Heinrich Heine University Düsseldorf, 40225 Düsseldorf, Germany*

Lukas Biermann − *Institute of Pharmaceutical und Medicinal Chemistry, Heinrich Heine University Düsseldorf, 40225 Düsseldorf, Germany*

Josefa Kremeyer − *Institute of Pharmaceutical und Medicinal Chemistry, Heinrich Heine University Düsseldorf, 40225 Düsseldorf, Germany*

Nadine Horstick − *Institute of Pharmaceutical und Medicinal Chemistry, Heinrich Heine University Düsseldorf, 40225 Düsseldorf, Germany*

Ingrid Span − *Bioinorganic Chemistry, Friedrich-Alexander-Universität Erlangen-Nürnberg, 91058 Erlangen, Germany;* orcid.org/0000-0002-2892-4825

Aleksandra A. Pandyra − *Department of Pediatric Oncology, Hematology and Clinical Immunology, Medical Faculty, Heinrich Heine University Düsseldorf, 40225 Düsseldorf, Germany; Institute of Clinical Chemistry and Clinical Pharmacology, University Hospital Bonn, 53127 Bonn, Germany; German Center for Infection Research (DZIF), 53127 Bonn, Germany*

Arndt Borkhardt − *Department of Pediatric Oncology, Hematology and Clinical Immunology, Medical Faculty, Heinrich Heine University Düsseldorf, 40225 Düsseldorf, Germany*

Holger Gohlke − *Institute of Pharmaceutical und Medicinal Chemistry, Heinrich Heine University Düsseldorf, 40225 Düsseldorf, Germany; Institute of Bio- and Geosciences (IBG-4: Bioinformatics), Forschungszentrum Jülich, 52425 Jülich, Germany;* orcid.org/0000-0001-8613-1447

Matthias U. Kassack − *Institute of Pharmaceutical und Medicinal Chemistry, Heinrich Heine University Düsseldorf, 40225 Düsseldorf, Germany;* orcid.org/0000-0002-9094-8481

Bjoern B. Burckhardt − *Individualized Pharmacotherapy, Institute of Pharmaceutical and Medicinal Chemistry, University of Münster, 48149 Münster, Germany;* orcid.org/0000-0002-1782-9937

Complete contact information is available at: https://pubs.acs.org/10.1021/acs.jmedchem.4c02024

Author Contributions

○F.F. and J.S.-D. contributed equally to this work. F.F. and J.S.-D. share first authorship. S.B. and T.K. contributed equally to this work as senior authors. F.F. and L.A.A.A. synthesized all intermediates and target compounds. J.K. contributed to the characterization of all intermediates and target compounds. M.H. and I.S. performed X-ray crystallography. J.S.-D., J.-W.T., K.S., M.K., P.S., A.A.P., and T.W. performed the biological evaluation. L.B. and N.H. provided the HDAC enzyme data. T.G. and B.B.B. performed the bioanalytical determination and evaluation of in vitro and in vivo pharmacokinetics. Y.L.H. performed molecular modeling, Y.L.H. and H.G. analyzed the results. A.B., H.G., M.U.K., B.B.B., S.B., and T.K. acquired funding and provided resources. F.F., J.S-D., S.B., and T.K. designed the study. The manuscript was written through the contributions of all authors. All authors have given approval to the final version.

Funding

This work was funded by the Deutsche Forschungsgemeinschaft (DFG, German Research Foundation) 270650915 (Research Training Group GRK 2158). S.B. additionally acknowledges financial support from Elterninitiative Kinderkrebsklinik e.V and Deutsche Forschungsgemeinschaft (DFG, German Research Foundation) BH 162/4-1 (528968169). A.B. acknowledges the financial support from the Katharina-Hardt Foundation, the Christiane and Claudia Hempel Foundation, and Löwenstern e.V. M.U.K. acknowledges financial support from the Deutsche Forschungsgemeinschaft (DFG, German Research Foundation) KA 1942/2-1.

Notes

The authors declare no competing financial interest.

■ ACKNOWLEDGMENTS

F.F., L.A.A.A., and T.K. thank the CeMSA@HHU (Center for Molecular and Structural Analytics @ Heinrich Heine University) for recording the mass-spectrometric and the NMR-spectroscopic data. We are grateful for computational support and infrastructure provided by the "Zentrum für Informations-und Medientechnologie" (ZIM) at the Heinrich Heine University Düsseldorf and the computing time provided by the John von Neumann Institute for Computing (NIC) to HG on the supercomputer JUWELS at the Jülich Supercomputing Centre (JSC) (user IDs: VSK33). We further thank Pharmacelsus for performing the preclinical in vivo study in mice. We acknowledge the European Synchrotron Radiation Facility (ESRF) for provision of synchrotron radiation facilities under proposal number mx2499 and we would like to thank Lindsay McGregor for assistance and support in using beamline ID30A-3 / MASSIF-3.

■ ABBREVIATIONS

AML, acute myeloid leukemia; AUC_{inf}, area under the curve from 0 to infinity; AUC_{last}, area under the curve from 0 to the time of the last quantifiable concentration; BCP-ALL, B cell precursor acute lymphoblastic leukemia; BSA, bovine serum albumin; CE, collision energy; CL/F, apparent total body clearance following extravascular administration; C_{max} (ng/mL), maximum observed concentration; CML, chronic myeloid leukemia; dDSS, differential DSS; DSMZ, german collection of microorganisms and cell culture; DSS, drug sensitivity scores; ESI, electrospray ionization; FBS, fetal bovine serum; HAT, histone acetyltransferases; HBTU, *O*-(benzotrialzol-1-yl)-*N, N,N′,N′*,-tetramethyluroniumhexafluorophosphat; HDAC, histone deacetylases; HDACi, HDAC inhibitors; HLM, human liver microsomes; HRMS, high-resolution mass spectra; HSCs, hematopoietic stem cells; HTDS, high throughput drug screening; Hz, Hertz; $K_{B/P}$, blood-to-plasma ratio; mp, melting points; MRM, multiple

reaction monitoring; PDX, patient-derived xenograft; ppm, parts per million; $t_{1/2}$, Terminal elimination half-life or apparent terminal elimination half-life; T-ALL, T cell acute lymphoblastic leukemia; TBST, tris buffered saline with Tween; TFA, trifluoroacetic acid; TL, Tube lens; TLC, thin-layer chromatography; tmax (h), time to reach the maximum concentration; V_z/F, apparent volume of distribution following extravascular administration; Λz, first order terminal elimination rate constant; ZIP, zero interaction potency

REFERENCES

(1) Cordo', V.; van der Zwet, J. C. G.; Canté-Barrett, K.; Pieters, R.; Meijerink, J. P. P. T-Cell Acute Lymphoblastic Leukemia: A Roadmap to Targeted Therapies. *Blood cancer Discovery* **2021**, *2* (1), 19−31.

(2) Ratti, S.; Lonetti, A.; Follo, M. Y.; Paganelli, F.; Martelli, A. M.; Chiarini, F.; Evangelisti, C. B-All Complexity: Is Targeted Therapy Still a Valuable Approach for Pediatric Patients? *Cancers* **2020**, *12* (12), 3498.

(3) Rooij, J. D. E. d.; Michel Zwaan, C.; van den Heuvel-Eibrink, M. Pediatric AML: From Biology to Clinical Management. *J. Clin. Med.* **2015**, *4* (1), 127−149.

(4) Pui, C. H.; Yang, J. J.; Hunger, S. P.; Pieters, R.; Schrappe, M.; Biondi, A.; Vora, A.; Baruchel, A.; Silverman, L. B.; Schmiegelow, K.; Escherich, G.; Horibe, K.; Benoit, Y. C. M.; Izraeli, S.; Yeoh, A. E. J.; Liang, D. C.; Downing, J. R.; Evans, W. E.; Relling, M. V.; Mullighan, C. G. Childhood Acute Lymphoblastic Leukemia: Progress through Collaboration. *J. Clin. Oncol.* **2015**, *33* (27), 2938−2948.

(5) Nguyen, K.; Devidas, M.; Cheng, S. C.; La, M.; Raetz, E. A.; Carroll, W. L.; Winick, N. J.; Hunger, S. P.; Gaynon, P. S.; Loh, M. L. Factors Influencing Survival after Relapse from Acute Lymphoblastic Leukemia: A Children's Oncology Group Study. *Leukemia* **2008**, *22* (12), 2142−2150.

(6) Schmiegelow, K.; Müller, K.; Mogensen, S. S.; Mogensen, P. R.; Wolthers, B. O.; Stoltze, U. K.; Tuckuviene, R.; Frandsen, T. Non-Infectious Chemotherapy-Associated Acute Toxicities during Childhood Acute Lymphoblastic Leukemia Therapy. *F1000Res.* **2017**, *6*, 444.

(7) O'Connor, D.; Bate, J.; Wade, R.; Clack, R.; Dhir, S.; Hough, R.; Vora, A.; Goulden, N.; Samarasinghe, S. Infection-Related Mortality in Children with Acute Lymphoblastic Leukemia: An Analysis of Infectious Deaths on UKALL2003. *Blood* **2014**, *124* (7), 1056−1061.

(8) Gu, Z.; Churchman, M. L.; Roberts, K. G.; Moore, I.; Zhou, X.; Nakitandwe, J.; Hagiwara, K.; Pelletier, S.; Gingras, S.; Berns, H.; Payne-Turner, D.; Hill, A.; Iacobucci, I.; Shi, L.; Pounds, S.; Cheng, C.; Pei, D.; Qu, C.; Newman, S.; Devidas, M.; Dai, Y.; Reshmi, S. C.; Gastier-Foster, J.; Raetz, E. A.; Borowitz, M. J.; Wood, B. L.; Carroll, W. L.; Zweidler-McKay, P. A.; Rabin, K. R.; Mattano, L. A.; Maloney, K. W.; Rambaldi, A.; Spinelli, O.; Radich, J. P.; Minden, M. D.; Rowe, J. M.; Luger, S.; Litzow, M. R.; Tallman, M. S.; Racevskis, J.; Zhang, Y.; Bhatia, R.; Kohlschmidt, J.; Mrózek, K.; Bloomfield, C. D.; Stock, W.; Kornblau, S.; Kantarjian, H. M.; Konopleva, M.; Evans, W. E.; Jeha, S.; Pui, C. H.; Yang, J.; Paietta, E.; Downing, J. R.; Relling, M. V.; Zhang, J.; Loh, M. L.; Hunger, S. P.; Mullighan, C. G. PAX5-Driven Subtypes of B-Progenitor Acute Lymphoblastic Leukemia. *Nat. Genet.* **2019**, *51* (2), 296−307.

(9) Cheng, Y.; He, C.; Wang, M.; Ma, X.; Mo, F.; Yang, S.; Han, J.; Wei, X. Targeting Epigenetic Regulators for Cancer Therapy: Mechanisms and Advances in Clinical Trials. *Signal Transduction Targeted Ther.* **2019**, *4* (1), 62.

(10) Gopi, L. K.; Kidder, B. L. Integrative Pan Cancer Analysis Reveals Epigenomic Variation in Cancer Type and Cell Specific Chromatin Domains. *Nat. Commun.* **2021**, *12* (1), 1419.

(11) Timp, W.; Feinberg, A. P. Cancer as a Dysregulated Epigenome Allowing Cellular Growth Advantage at the Expense of the Host. *Nat. Rev. Cancer* **2013**, *13* (7), 497−510.

(12) Zeng, H.; Qu, J.; Jin, N.; Xu, J.; Lin, C.; Chen, Y.; Yang, X.; He, X.; Tang, S.; Lan, X.; Yang, X.; Chen, Z.; Huang, M.; Ding, J.; Geng, M. Feedback Activation of Leukemia Inhibitory Factor Receptor Limits Response to Histone Deacetylase Inhibitors in Breast Cancer. *Cancer Cell* **2016**, *30* (3), 459−473.

(13) Ceccacci, E.; Minucci, S. Inhibition of Histone Deacetylases in Cancer Therapy: Lessons from Leukaemia. *Br. J. Cancer* **2016**, *114* (6), 605−611.

(14) Bondarev, A. D.; Attwood, M. M.; Jonsson, J.; Chubarev, V. N.; Tarasov, V. V.; Schiöth, H. B. Recent Developments of HDAC Inhibitors: Emerging Indications and Novel Molecules. *Br. J. Clin. Pharmacol.* **2021**, *87* (12), 4577−4597.

(15) Shvedunova, M.; Akhtar, A. Modulation of Cellular Processes by Histone and Non-Histone Protein Acetylation. *Nat. Rev. Mol. Cell Biol.* **2022**, *23* (5), 329−349.

(16) Yang, X. J.; Seto, E. HATs and HDACs: From Structure, Function and Regulation to Novel Strategies for Therapy and Prevention. *Oncogene* **2007**, *26* (37), 5310−5318.

(17) Park, S. Y.; Kim, J. S. A Short Guide to Histone Deacetylases Including Recent Progress on Class II Enzymes. *Exp. Mol. Med.* **2020**, *52* (2), 204−212.

(18) Ho, T. C. S.; Chan, A. H. Y.; Ganesan, A. Thirty Years of HDAC Inhibitors: 2020 Insight and Hindsight. *J. Med. Chem.* **2020**, *63*, 12460−12484.

(19) Liu, P.; Xiao, J.; Wang, Y.; Song, X.; Huang, L.; Ren, Z.; Kitazato, K.; Wang, Y. Posttranslational Modification and beyond: Interplay between Histone Deacetylase 6 and Heat-Shock Protein 90. *Mol. Med.* **2021**, *27* (1), 110.

(20) Kerr, E.; Holohan, C.; McLaughlin, K. M.; Majkut, J.; Dolan, S.; Redmond, K.; Riley, J.; McLaughlin, K.; Stasik, I.; Crudden, M.; Van Schaeybroeck, S.; Fenning, C.; O'Connor, R.; Kiely, P.; Sgobba, M.; Haigh, D.; Johnston, P. G.; Longley, D. B. Identification of an Acetylation-Dependant Ku70/FLIP Complex That Regulates FLIP Expression and HDAC Inhibitor-Induced Apoptosis. *Cell Death Differ.* **2012**, *19* (8), 1317−1327.

(21) Zhou, M.; Yuan, M.; Zhang, M.; Lei, C.; Aras, O.; Zhang, X.; An, F. Combining Histone Deacetylase Inhibitors (HDACis) with Other Therapies for Cancer Therapy. *Eur. J. Med. Chem.* **2021**, *226*, 113825.

(22) Diyabalanage, H. V. K.; Granda, M. L.; Hooker, J. M. Combination Therapy: Histone Deacetylase Inhibitors and Platinum-Based Chemotherapeutics for Cancer. *Cancer Lett.* **2013**, *329* (1), 1−8.

(23) Stenzel, K.; Hamacher, A.; Hansen, F. K.; Gertzen, C. G. W.; Senger, J.; Marquardt, V.; Marek, L.; Marek, M.; Romier, C.; Remke, M.; Jung, M.; Gohlke, H.; Kassack, M. U.; Kurz, T. Alkoxyurea-Based Histone Deacetylase Inhibitors Increase Cisplatin Potency in Chemoresistant Cancer Cell Lines. *J. Med. Chem.* **2017**, *60* (13), 5334−5348.

(24) Reßing, N.; Schliehe-Diecks, J.; Watson, P. R.; Sönnichsen, M.; Cragin, A. D.; Schöler, A.; Yang, J.; Schäker-Hübner, L.; Borkhardt, A.; Christianson, D. W.; Bhatia, S.; Hansen, F. K. Development of Fluorinated Peptoid-Based Histone Deacetylase (HDAC) Inhibitors for Therapy-Resistant Acute Leukemia. *J. Med. Chem.* **2022**, *65* (22), 15457−15472.

(25) Laporte, A. N.; Barrott, J. J.; Yao, R. J.; Poulin, N. M.; Brodin, B. A.; Jones, K. B.; Underhill, T. M.; Nielsen, T. O. HDAC and Proteasome Inhibitors Synergize to Activate Pro-Apoptotic Factors in Synovial Sarcoma. *PLoS One* **2017**, *12* (1), No. e0169407.

(26) Avelar, L. A. A.; Schrenk, C.; Sönnichsen, M.; Hamacher, A.; Hansen, F. K.; Schliehe-Diecks, J.; Borkhardt, A.; Bhatia, S.; Kassack, M. U.; Kurz, T. Synergistic Induction of Apoptosis in Resistant Head and Neck Carcinoma and Leukemia by Alkoxyamide-Based Histone Deacetylase Inhibitors. *Eur. J. Med. Chem.* **2021**, *211*, 113095.

(27) Bhatia, S.; Krieger, V.; Groll, M.; Osko, J. D.; Reßing, N.; Ahlert, H.; Borkhardt, A.; Kurz, T.; Christianson, D. W.; Hauer, J.; Hansen, F. K. Discovery of the First-in-Class Dual Histone

https://doi.org/10.1021/acs.jmedchem.4c02024
J. Med. Chem. 2024, 67, 21223−21250

Deacetylase-Proteasome Inhibitor. *J. Med. Chem.* **2018**, *61* (22), 10299−10309.
(28) Hideshima, T.; Cottini, F.; Ohguchi, H.; Jakubikova, J.; Gorgun, G.; Mimura, N.; Tai, Y. T.; Munshi, N. C.; Richardson, P. G.; Anderson, K. C. Rational Combination Treatment with Histone Deacetylase Inhibitors and Immunomodulatory Drugs in Multiple Myeloma. *Blood Cancer J.* **2015**, *5* (5), No. e312.
(29) Knox, T.; Sahakian, E.; Banik, D.; Hadley, M.; Palmer, E.; Noonepalle, S.; Kim, J.; Powers, J.; Gracia-Hernandez, M.; Oliveira, V.; Cheng, F.; Chen, J.; Barinka, C.; Pinilla-Ibarz, J.; Lee, N. H.; Kozikowski, A.; Villagra, A. Selective HDAC6 Inhibitors Improve Anti-PD-1 Immune Checkpoint Blockade Therapy by Decreasing the Anti-Inflammatory Phenotype of Macrophages and down-Regulation of Immunosuppressive Proteins in Tumor Cells. *Sci. Rep.* **2019**, *9* (1), 6136.
(30) Kozikowski, A. P.; Chen, Y.; Gaysin, A. M.; Savoy, D. N.; Billadeau, D. D.; Kim, K. H. Chemistry, Biology, and QSAR Studies of Substituted Biaryl Hydroxamates and Mercaptoacetamides as HDAC Inhibitors - Nanomolar-Potency Inhibitors of Pancreatic Cancer Cell Growth. *ChemMedChem* **2008**, *3* (3), 487−501.
(31) Curtin, M.; Glaser, K. Histone Deacetylase Inhibitors: The Abbott Experience. *Curr. Med. Chem.* **2003**, *10* (22), 2373−2392.
(32) Mo, H.; Zhang, R.; Chen, Y.; Li, S. T.; Wang, Y.; Zou, W.; Lin, Q.; Zhao, D. G.; Du, Y.; Zhang, K.; Ma, Y. Y. Synthesis and Anticancer Activity of Novel Histone Deacetylase Inhibitors That Inhibit Autophagy and Induce Apoptosis. *Eur. J. Med. Chem.* **2022**, *243* (August), 114705.
(33) Peng, X.; Li, L.; Chen, J.; Ren, Y.; Liu, J.; Yu, Z.; Cao, H.; Chen, J. Discovery of Novel Histone Deacetylase 6 (HDAC6) Inhibitors with Enhanced Antitumor Immunity of Anti-PD-L1 Immunotherapy in Melanoma. *J. Med. Chem.* **2022**, *65* (3), 2434−2457.
(34) Asfaha, Y.; Schrenk, C.; Alves Avelar, L. A.; Lange, F.; Wang, C.; Bandolik, J. J.; Hamacher, A.; Kassack, M. U.; Kurz, T. Novel Alkoxyamide-Based Histone Deacetylase Inhibitors Reverse Cisplatin Resistance in Chemoresistant Cancer Cells. *Bioorg. Med. Chem.* **2020**, *28* (1), 115108.
(35) Tran, B.; Cohen, M. S. The Discovery and Development of Binimetinib for the Treatment of Melanoma. *Expert Opin. Drug Discovery* **2020**, *15* (7), 745−754.
(36) Markham, A.; Keam, S. J. Selumetinib: First Approval. *Drugs* **2020**, *80* (9), 931−937.
(37) Lassalas, P.; Gay, B.; Lasfargeas, C.; James, M. J.; Tran, V.; Vijayendran, K. G.; Brunden, K. R.; Kozlowski, M. C.; Thomas, C. J.; Smith, A. B.; Huryn, D. M.; Ballatore, C. Structure Property Relationships of Carboxylic Acid Isosteres. *J. Med. Chem.* **2016**, *59* (7), 3183−3203.
(38) Hill, J.; Crich, D. The N,N,O-Trisubstituted Hydroxylamine Isostere and Its Influence on Lipophilicity and Related Parameters. *ACS Med. Chem. Lett.* **2022**, *13* (5), 799−806.
(39) Goodreid, J. D.; Duspara, P. A.; Bosch, C.; Batey, R. A. Amidation Reactions from the Direct Coupling of Metal Carboxylate Salts with Amines. *J. Org. Chem.* **2014**, *79* (3), 943−954.
(40) Friesner, R. A.; Murphy, R. B.; Repasky, M. P.; Frye, L. L.; Greenwood, J. R.; Halgren, T. A.; Sanschagrin, P. C.; Mainz, D. T. Extra Precision Glide: Docking and Scoring Incorporating a Model of Hydrophobic Enclosure for Protein-Ligand Complexes. *J. Med. Chem.* **2006**, *49* (21), 6177−6196.
(41) Ramírez, D.; Caballero, J. Is It Reliable to Use Common Molecular Docking Methods for Comparing the Binding Affinities of Enantiomer Pairs for Their Protein Target? *Int. J. Mol. Sci.* **2016**, *17* (4), 525.
(42) Liu, J.; Yu, Y.; Kelly, J.; Sha, D.; Alhassan, A. B.; Yu, W.; Maletic, M. M.; Duffy, J. L.; Klein, D. J.; Holloway, M. K.; Carroll, S.; Howell, B. J.; Barnard, R. J. O.; Wolkenberg, S.; Kozlowski, J. A. Discovery of Highly Selective and Potent HDAC3 Inhibitors Based on a 2-Substituted Benzamide Zinc Binding Group. *ACS Med. Chem. Lett.* **2020**, *11* (12), 2476−2483.
(43) Osko, J. D.; Christianson, D. W. Methods for the Expression, Purification, and Crystallization of Histone Deacetylase 6-Inhibitor Complexes. *Methods Enzymol.* **2019**, *626*, 447−474.
(44) Hai, Y.; Christianson, D. W. Histone Deacetylase 6 Structure and Molecular Basis of Catalysis and Inhibition. *Nat. Chem. Biol.* **2016**, *12* (9), 741−747.
(45) Oikonomou, A.; Valsecchi, L.; Quadri, M.; Watrin, T.; Scharov, K.; Procopio, S.; Tu, J. W.; Vogt, M.; Savino, A. M.; Silvestri, D.; Valsecchi, M. G.; Biondi, A.; Borkhardt, A.; Bhatia, S.; Cazzaniga, G.; Fazio, G.; Bardini, M.; Palmi, C. High-Throughput Screening as a Drug Repurposing Strategy for Poor Outcome Subgroups of Pediatric B-Cell Precursor Acute Lymphoblastic Leukemia. *Biochem. Pharmacol.* **2023**, *217* (May), 115809.
(46) Yadav, B.; Pemovska, T.; Szwajda, A.; Kulesskiy, E.; Kontro, M.; Karjalainen, R.; Majumder, M. M.; Malani, D.; Murumägi, A.; Knowles, J.; Porkka, K.; Heckman, C.; Kallioniemi, O.; Wennerberg, K.; Aittokallio, T. Quantitative Scoring of Differential Drug Sensitivity for Individually Optimized Anticancer Therapies. *Sci. Rep.* **2014**, *4*, 5193.
(47) Nalawansha, D. A.; Gomes, I. D.; Wambua, M. K.; Pflum, M. K. H. HDAC Inhibitor-Induced Mitotic Arrest Is Mediated by Eg5/KIF11 Acetylation. *Cell Chem. Biol.* **2017**, *24* (4), 481−492.e5.
(48) Stockhammer, P.; Okumus, O. ·.; Hegedus, L.; Rittler, D.; Ploenes, T.; Herold, T.; Kalbourtzis, S.; Bankfalvi, A.; Sucker, A.; Kimmig, R.; Aigner, C.; Hegedus, B. HDAC Inhibition Induces Cell Cycle Arrest and Mesenchymal-Epithelial Transition in a Novel Pleural-Effusion Derived Uterine Carcinosarcoma Cell Line. *Pathol. Oncol. Res.* **2021**, *27* (March), 1−10.
(49) Caserta, T. M.; Smith, A. N.; Gultice, A. D.; Reedy, M. A.; Brown, T. L. Q-VD-OPh, a Broad Spectrum Caspase Inhibitor with Potent Antiapoptotic Properties. *Apoptosis* **2003**, *8* (4), 345−352.
(50) Kalac, M.; Scotto, L.; Marchi, E.; Amengual, J.; Seshan, V. E.; Bhagat, G.; Ulahannan, N.; Leshchenko, V. V.; Temkin, A. M.; Parekh, S.; Tycko, B.; O'Connor, O. A. HDAC Inhibitors and Decitabine Are Highly Synergistic and Associated with Unique Gene-Expression and Epigenetic Profiles in Models of DLBCL. *Blood* **2011**, *118* (20), 5506−5516.
(51) Blagitko-Dorfs, N.; Schlosser, P.; Greve, G.; Pfeifer, D.; Meier, R.; Baude, A.; Brocks, D.; Plass, C.; Lübbert, M. Combination Treatment of Acute Myeloid Leukemia Cells with DNMT and HDAC Inhibitors: Predominant Synergistic Gene Downregulation Associated with Gene Body Demethylation. *Leukemia* **2019**, *33* (4), 945−956.
(52) Tretbar, M.; Schliehe-Diecks, J.; von Bredow, L.; Tan, K.; Roatsch, M.; Tu, J. W.; Kemkes, M.; Sönnichsen, M.; Schöler, A.; Borkhardt, A.; Bhatia, S.; Hansen, F. K. Preferential HDAC6 Inhibitors Derived from HPOB Exhibit Synergistic Antileukemia Activity in Combination with Decitabine. *Eur. J. Med. Chem.* **2024**, *272* (April), 116447.
(53) Kirschbaum, M.; Gojo, I.; Goldberg, S. L.; Bredeson, C.; Kujawski, L. A.; Yang, A.; Marks, P.; Frankel, P.; Sun, X.; Tosolini, A.; Eid, J. E.; Lubiniecki, G. M.; Issa, J. P. A Phase 1 Clinical Trial of Vorinostat in Combination with Decitabine in Patients with Acute Myeloid Leukaemia or Myelodysplastic Syndrome. *Br. J. Hamaetol.* **2014**, *167* (2), 185−193.
(54) How, J.; Minden, M. D.; Brian, L.; Chen, E. X.; Brandwein, J.; Schuh, A. C.; Schimmer, A. D.; Gupta, V.; Webster, S.; Degelder, T.; Haines, P.; Stayner, L. A.; McGill, S.; Wang, L.; Piekarz, R.; Wong, T.; Siu, L. L.; Espinoza-Delgado, I.; Holleran, J. L.; Egorin, M. J.; Yee, K. W. L. A Phase i Trial of Two Sequence-Specific Schedules of Decitabine and Vorinostat in Patients with Acute Myeloid Leukemia. *Leuk. Lymphoma* **2015**, *56* (10), 2793−2802.
(55) Jones, P. L.; Veenstra, G. J. C.; Wade, P. A.; Vermaak, D.; Kass, S. U.; Landsberger, N.; Strouboulis, J.; Wolffe, A. P. Methylated DNA and MeCP2 Recruit Histone Deacetylase to Repress Transcription. *Nat. Genet.* **1998**, *19* (2), 187−191.
(56) Cameron, E. E.; Bachman, K. E.; Myöhänen, S.; Herman, J. G.; Baylin, S. B. Synergy of Demethylation and Histone Deacetylase

Inhibition in the Re- Expression of Genes Silenced in Cancer. *Nat. Genet.* **1999**, *21* (1), 103−107.
(57) Gkotzamanidou, M.; Terpou, E.; Kentepozidis, N.; Terpos, E. Targeting the Interplay between Hdacs and Dna Damage Repair for Myeloma Therapy. *Int. J. Mol. Sci.* **2021**, *22* (19), 10406.
(58) Di, L.; Kerns, E. H. Profiling Drug-like Properties in Discovery Research. *Curr. Opin. Chem. Biol.* **2003**, *7* (3), 402−408.
(59) Markovic, M.; Zur, M.; Fine-Shamir, N.; Haimov, E.; González-Álvarez, I.; Dahan, A. Segmental-Dependent Solubility and Permeability as Key Factors Guiding Controlled Release Drug Product Development. *Pharmaceutics* **2020**, *12* (3), 295.
(60) Gangnus, T.; Burckhardt, B. B. Low-Volume LC-MS/MS Method for the Pharmacokinetic Investigation of Carvedilol, Enalapril and Their Metabolites in Whole Blood and Plasma: Application to a Paediatric Clinical Trial. *Drug Test. Anal.* **2021**, *13* (3), 694−708.
(61) Nation, R. L.; Theuretzbacher, U.; Tsuji, B. T. Concentration-Dependent Plasma Protein Binding: Expect the Unexpected. *Eur. J. Pharm. Sci.* **2018**, *122* (May), 341−346.
(62) Schafer-Korting, M.; Korting, H. C.; Amann, F.; Peuser, R.; Lukacs, A. Influence of Albumin on Itraconazole and Ketoconazole Antifungal Activity: Results of a Dynamic in Vitro Study. *Antimicrob. Agents Chemother.* **1991**, *35* (10), 2053−2056.
(63) Konsoula, R.; Jung, M. In Vitro Plasma Stability, Permeability and Solubility of Mercaptoacetamide Histone Deacetylase Inhibitors. *Int. J. Pharm.* **2008**, *361* (1−2), 19−25.
(64) Europe, Middle East, and Africa. *Withdrawal Assessment Report Vorinostat MSD 100 Mg Hard Capsules (Vorinostat)*, 2009.
(65) 021991s000_Zolinza_ClinPharmR.Pdf.
(66) Venkatesh, P. R.; Goh, E.; Zeng, P.; New, L. S.; Xin, L.; Pasha, M. K.; Sangthongpitag, K.; Yeo, P.; Kantharaj, E. In Vitro Phase I Cytochrome P450 Metabolism, Permeability and Pharmacokinetics of SB639, a Novel Histone Deacetylase Inhibitor in Preclinical Species. *Biol. Pharm. Bull.* **2007**, *30* (5), 1021−1024.
(67) Yeo, P.; Xin, L.; Goh, E.; New, L. S.; Zeng, P.; Wu, X.; Venkatesh, P.; Kantharaj, E. Development and Validation of High-performance Liquid Chromatography-Tandem Mass Spectrometry Assay for 6-(3-benzoyl-ureido)-hexanoic Acid Hydroxyamide, a Novel HDAC Inhibitor, in Mouse Plasma for Pharmacokinetic Studies. *Biomed. Chromatogr.* **2007**, *21* (2), 184−189.
(68) Hiriyan, J.; Shivarudraiah, P.; Gavara, G.; Annamalai, P.; Natesan, S.; Sambasivam, G.; Sukumaran, S. K. Discovery of PAT-1102, a Novel, Potent and Orally Active Histone Deacetylase Inhibitor with Antitumor Activity in Cancer Mouse Models. *Anticancer Res.* **2015**, *35* (1), 229−238.
(69) Hull, E. E.; Montgomery, M. R.; Leyva, K. J. HDAC Inhibitors as Epigenetic Regulators of the Immune System: Impacts on Cancer Therapy and Inflammatory Diseases. *Biomed. Res. Int.* **2016**, *2016*, 1−15.
(70) Mopin, A.; Driss, V.; Brinster, C. A Detailed Protocol for Characterizing the Murine C1498 Cell Line and Its Associated Leukemia Mouse Model. *J. Visualized Exp.* **2016**, No. 116, 54270.
(71) Avelar, L. A. A.; Held, J.; Engel, J. A.; Sureechatchaiyan, P.; Hansen, F. K.; Hamacher, A.; Kassack, M. U.; Mordmüller, B.; Andrews, K. T.; Kurz, T. Design and Synthesis of Novel Anti-Plasmodial Histone Deacetylase Inhibitors Containing an Alkoxyamide Connecting Unit. *Arch. Pharm.* **2017**, *350* (3−4), 1600347.
(72) Vogt, M.; Dienstbier, N.; Schliehe-Diecks, J.; Scharov, K.; Tu, J. W.; Gebing, P.; Hogenkamp, J.; Bilen, B. S.; Furlan, S.; Picard, D.; Remke, M.; Yasin, L.; Bickel, D.; Kalia, M.; Iacoangeli, A.; Lenz, T.; Stühler, K.; Pandyra, A. A.; Hauer, J.; Fischer, U.; Wagener, R.; Borkhardt, A.; Bhatia, S. Co-Targeting HSP90 Alpha and CDK7 Overcomes Resistance against HSP90 Inhibitors in BCR-ABL1+ Leukemia Cells. *Cell Death Dis.* **2023**, *14* (12), 799.
(73) Bottomley, M. J.; Surdo, P. L.; Giovine, P. D.; Cirillo, A.; Scarpelli, R.; Ferrigno, F.; Jones, P.; Neddermann, P.; De Francesco, R.; Steinkühler, C.; Gallinari, P.; Carfí, A.; Carfí, A. Structural and Functional Analysis of the Human HDAC4 Catalytic Domain Reveals a Regulatory Structural Zinc-Binding Domain. *J. Biol. Chem.* **2008**, *283* (39), 26694−26704.
(74) Somoza, J. R.; Skene, R. J.; Katz, B. A.; Mol, C.; Ho, J. D.; Jennings, A. J.; Luong, C.; Arvai, A.; Buggy, J. J.; Chi, E.; Tang, J.; Sang, B. C.; Verner, E.; Wynands, R.; Leahy, E. M.; Dougan, D. R.; Snell, G.; Navre, M.; Knuth, M. W.; Swanson, R. V.; McRee, D. E.; Tari, L. W. Structural Snapshots of Human HDAC8 Provide Insights into the Class I Histone Deacetylases. *Structure* **2004**, *12* (7), 1325−1334.
(75) Olsson, M. H. M.; Søndergaard, C. R.; Rostkowski, M.; Jensen, J. H. PROPKA3: Consistent Treatment of Internal and Surface Residues in Empirical p K a Predictions. *J. Chem. Theory Comput.* **2011**, *7* (2), 525−537.
(76) Li, J.; Abel, R.; Zhu, K.; Cao, Y.; Zhao, S.; Friesner, R. A. The VSGB 2.0 Model: A next Generation Energy Model for High Resolution Protein Structure Modeling. *Proteins: Struct., Funct., Bioinf.* **2011**, *79* (10), 2794−2812.
(77) Porter, N. J.; Mahendran, A.; Breslow, R.; Christianson, D. W. Unusual Zinc-Binding Mode of HDAC6-Selective Hydroxamate Inhibitors. *Proc. Natl. Acad. Sci. U.S.A.* **2017**, *114* (51), 13459−13464.
(78) Von Stetten, D.; Carpentier, P.; Flot, D.; Beteva, A.; Caserotto, H.; Dobias, F.; Guijarro, M.; Giraud, T.; Lentini, M.; McSweeney, S.; Royant, A.; Petitdemange, S.; Sinoir, J.; Surr, J.; Svensson, O.; Theveneau, P.; Leonard, G. A.; Mueller-Dieckmann, C. ID30A-3 (MASSIF-3) - A Beamline for Macromolecular Crystallography at the ESRF with a Small Intense Beam. *J. Synchrotron Radiat.* **2020**, *27*, 844−851.
(79) Theveneau, P.; Baker, R.; Barrett, R.; Beteva, A.; Bowler, M. W.; Carpentier, P.; Caserotto, H.; Sanctis, D. d.; Dobias, F.; Flot, D.; Guijarro, M.; Giraud, T.; Lentini, M.; Leonard, G. A.; Mattenet, M.; McCarthy, A. A.; McSweeney, S. M.; Morawe, C.; Nanao, M.; Nurizzo, D.; Ohlsson, S.; Pernot, P.; Popov, A. N.; Round, A.; Royant, A.; Schmid, W.; Snigirev, A.; Surr, J.; Mueller-Dieckmann, C. The Upgrade Programme for the Structural Biology Beamlines at the European Synchrotron Radiation Facility-High Throughput Sample Evaluation and Automation. *J. Phys.: Conf. Ser.* **2013**, *425* (1), 012001.
(80) Kabsch, W. *XDS. Acta Crystallogr., Sect. D: Biol. Crystallogr.* **2010**, *66*, 125−132.
(81) Winn, M. D.; Ballard, C. C.; Cowtan, K. D.; Dodson, E. J.; Emsley, P.; Evans, P. R.; Keegan, R. M.; Krissinel, E. B.; Leslie, A. G. W.; McCoy, A.; McNicholas, S. J.; Murshudov, G. N.; Pannu, N. S.; Potterton, E. A.; Powell, H. R.; Read, R. J.; Vagin, A.; Wilson, K. S. Overview of the CCP4 Suite and Current Developments. *Acta Crystallogr., Sect. D: Biol. Crystallogr.* **2011**, *67* (4), 235−242.
(82) Evans, P. R.; Murshudov, G. N. How Good Are My Data and What Is the Resolution? *Acta Crystallogr., Sect. D: Biol. Crystallogr.* **2013**, *69* (7), 1204−1214.
(83) McCoy, A. J.; Grosse-Kunstleve, R. W.; Adams, P. D.; Winn, M. D.; Storoni, L. C.; Read, R. J. Phaser Crystallographic Software. *J. Appl. Crystallogr.* **2007**, *40* (4), 658−674.
(84) Emsley, P.; Lohkamp, B.; Scott, W. G.; Cowtan, K. Features and Development of Coot. *Acta Crystallogr., Sect. D: Biol. Crystallogr.* **2010**, *66* (4), 486−501.
(85) Murshudov, G. N.; Vagin, A. A.; Dodson, E. J. Refinement of Macromolecular Structures by the Maximum-Likelihood Method. *Acta Crystallogr., Sect. D: Biol. Crystallogr.* **1997**, *53* (3), 240−255.
(86) Schrodinger LLC. *The PyMOL Molecular Graphics System*. version 3.0, 2015.
(87) Andrés, A.; Rosés, M.; Ràfols, C.; Bosch, E.; Espinosa, S.; Segarra, V.; Huerta, J. M. Setup and Validation of Shake-Flask Procedures for the Determination of Partition Coefficients (Log D) from Low Drug Amounts. *Eur. J. Pharm. Sci.* **2015**, *76*, 181−191.
(88) Yu, S.; Li, S.; Yang, H.; Lee, F.; Wu, J. T.; Qian, M. G. A Novel Liquid Chromatography/Tandem Mass Spectrometry Based Depletion Method for Measuring Red Blood Cell Partitioning of Pharmaceutical Compounds in Drug Discovery. *Rapid Commun. Mass Spectrom.* **2005**, *19* (2), 250−254.

https://doi.org/10.1021/acs.jmedchem.4c02024
J. Med. Chem. 2024, 67, 21223−21250

(89) Hinderling, P. H. Red Blood Cells: A Neglected Compartment in Pharmacokinetics and Pharmacodynamics. *Pharmacol. Rev.* **1997**, *49* (3), 279−295.
(90) Banker, M. J.; Clark, T. H.; Williams, J. A. Development and Validation of a 96-Well Equilibrium Dialysis Apparatus for Measuring Plasma Protein Binding. *J. Pharm. Sci.* **2003**, *92* (5), 967−974.
(91) Riccardi, K.; Cawley, S.; Yates, P. D.; Chang, C.; Funk, C.; Niosi, M.; Lin, J.; Di, L. Plasma Protein Binding of Challenging Compounds. *J. Pharm. Sci.* **2015**, *104* (8), 2627−2636.
(92) Rocha, F. G. *Liver Blood Flow: Physiology, Measurement, and Clinical Relevance*, 5th ed; Elsevier Inc., 2012..
(93) Bhatia, S.; Diedrich, D.; Frieg, B.; Ahlert, H.; Stein, S.; Bopp, B.; Lang, F.; Zang, T.; Kröger, T.; Ernst, T.; Kögler, G.; Krieg, A.; Lüdeke, S.; Kunkel, H.; Rodrigues Moita, A. J.; Kassack, M. U.; Marquardt, V.; Opitz, F. V.; Oldenburg, M.; Remke, M.; Babor, F.; Grez, M.; Hochhaus, A.; Borkhardt, A.; Groth, G.; Nagel-Steger, L.; Jose, J.; Kurz, T.; Gohlke, H.; Hansen, F. K.; Hauer, J. Targeting HSP90 Dimerization via the C Terminus Is Effective in Imatinib-Resistant CML and Lacks the Heat Shock Response. *Blood* **2018**, *132* (3), 307−320.

https://doi.org/10.1021/acs.jmedchem.4c02024
J. Med. Chem. 2024, 67, 21223−21250